Chapter 19
Radiation Effects in Metals: Void Swelling and Irradiation Creep

19.1 INTRODUCTION

Until about 1967 the most detrimental radiation effect expected to be suffered by the stainless-steel cladding of the fuel elements of the projected liquid-metal-cooled fast breeder reactor (LMFBR) was embrittlement due to excessive hardening at low temperatures or helium agglomeration at grain boundaries at high temperatures. These problems, however, were at least qualitatively understood, and sufficient experimental data had been amassed to permit embrittlement to be circumvented by careful design. Since that time a number of unexpected phenomena have been uncovered by microscopic examination of fuel elements and structural components that had been irradiated in a fast reactor environment for long periods. In addition to the chemical attack of the inside of the cladding by the fuel (Chap. 12), steels irradiated to large fast-neutron fluences exhibited dramatic density decreases. Using transmission electron microscopy, Cawthorne and Fulton[1] demonstrated that this swelling was due to the formation of small cavities within the grains of the metal. These voids, which did not contain sufficient gas (if any) to be classed as bubbles, ranged in size from the smallest observable to greater than 1000 Å. Further research has shown that voids form in stainless steel only at temperatures between ~350 to 600°C. Unfortunately, this range falls squarely within the temperature zone in which the cladding of LMFBR fuel pins is designed to operate (Table 10.2).

Void formation is not unique to stainless steel; in fact, steel is one of the alloys most resistant to this phenomenon. Nearly all metals swell by this mechanism over a temperature band from 0.3 to 0.55 of the absolute melting temperature.

The severity of metal swelling under irradiation also depends on the fast-neutron exposure (and to a much smaller extent on the fast-neutron flux). There appears to be an incubation period up to a fast fluence of $\sim 10^{22}$ neutrons/cm^2 in which no observable swelling of steel occurs. Thereafter swelling (measured, as in the case of fuel swelling by fission gases, as $\Delta V/V$) increases as $(\Phi t)^n$, where the exponent n is greater than unity. Very few data at fluences above 10^{23} neutrons/cm^2 exist, and, because of the many variables controlling swelling, extrapolation of the dose dependence to the design fluence of the LMFBR ($\sim 3 \times 10^{23}$ neutrons/cm^2) is very insecure. Consequently, there has been intense activity in developing theoretical models that can accurately predict swelling at large fluences and in devising experimental techniques other than neutron irradiation to produce voids in metals in short times. Of special interest is the fluence to which the power law $\Delta V/V \sim (\Phi t)^n$ extends and if and at what fluence the swelling saturates. Leveling off of the swelling curve has not yet been observed in reactor-irradiated steel, but high-energy ion bombardment (Sec. 17.9) has shown[2] that swelling of stainless steel saturates at fluences approaching 10^{24} neutrons/cm^2. The high equivalent neutron-fluence ion-irradiation studies, taken with extrapolation of low-fluence neutron-irradiation data, suggest that type 316 stainless steel, which is the most likely LMFBR cladding, will swell by 5 to 10% in a commercial reactor. The ramifications of volume increases of this magnitude on fuel-element design are profound, and the remedies are costly. Some of the undesirable side effects of swelling can be alleviated by the related phenomenon of irradiation creep. The effects of swelling and irradiation creep on core design are discussed in Chap. 21.

The origins of void swelling of metals are qualitatively understood. Collision of fast neutrons with lattice atoms produces large numbers of vacancy–interstitial pairs (see Chap. 17). Most of these point defects eventually recombine with each other or migrate to sinks in the solid where the point defects lose their identity. The most effective sinks are dislocations, either those which are part of the natural dislocation network of the metal or dislocation loops created by condensation of radiation-produced interstitials. Precipitates and grain boundaries also act to remove point defects from the medium. The dynamic balance between the point-defect creation and removal processes during irradiation sustains concentrations of vacancies and interstitials far in excess of thermal equilibrium (see Fig. 13.17).

Nucleation of segregated clusters of interstitials and vacancies can take place provided that the temperature is high enough so that both interstitials and vacancies are

mobile in the solid, but not so high that the point defects are removed by recombination or migration to sinks so quickly that high supersaturation cannot be maintained. The type of cluster formed by interstitials is invariably a dislocation loop. Vacancies, however, can agglomerate either into platelets, which collapse into dislocation loops, or into three-dimensional clusters, which are termed voids. The atomic structures of interstitial and vacancy loops are shown in Fig. 18.4.

The collection of interstitial atoms as extra planes in the lattice causes the solid to swell. If the vacancies condensed into analogous vacancy loops, the lattice contraction around these loops would cause shrinkage of the surrounding solid by an amount that just counterbalances the swelling due to interstitial loops. However, when the vacancies agglomerate into voids, no lattice contraction is available to cancel the dilatation due to the interstitial loops, and a net volume increase of the solid ensues. In irradiated zirconium, for example, large vacancy loops, but no voids and hence no swelling, are observed.

The relative stability of voids and vacancy loops can be assessed by comparing the energy difference between the particular cluster containing m vacancies and the perfect lattice. For the void this difference is just the energy required to form the surface of the void:

$$E_{void} = 4\pi R^2 \gamma \tag{19.1}$$

where γ is the surface tension of the solid (approximately 500 dynes/cm for stainless steel) and R is the radius of the void, which is related to the number of vacancies in the cavity by

$$m = \frac{4\pi R^3}{3\Omega} \tag{19.2}$$

where Ω is the atomic volume, or the volume contributed by each vacancy to the void. The energy of the void is thus

$$E_{void} = 4\pi\gamma \left(\frac{3\Omega m}{4\pi}\right)^{2/3} \tag{19.3}$$

The energy of a faulted dislocation loop composed of m vacancies in a disk of radius R_l is

$$E_{loop} = (2\pi R_l)\tau_d + \pi R_l^2 \gamma_{sf} \tag{19.4}$$

where τ_d is the energy per unit length (i.e., the line tension) of the dislocation comprising the periphery of the loop. According to Eq. 8.10 τ_d is $\sim Gb^2$, where b is the Burgers vector of the faulted loop.

The term γ_{sf} is the energy per unit area of the stacking fault enclosed by the loop. As shown in Sec. 3.6, the sequence of close-packed (111) planes in the fcc structure is ordered 123123.... When part of one of these planes is removed or a section of another (111) plane is inserted, the stacking sequence is disturbed, but the atoms surrounding the stacking fault are surrounded by the same number (12) of nearest neighbors as in the perfect lattice. However, the configuration of the next-nearest neighbors is slightly altered, and the stacking-fault configuration is somewhat more energetic than the perfect lattice. This energy difference is manifest as the stacking-fault energy. Because the energy difference is due to second-order atomic arrangements, γ_{sf} is small, typical values being ~10 dynes/cm.

In fcc metals dislocation loops form on the close-packed (111) planes in which the area per atom is $3^{1/2} a_o^2/4$, where a_o is the lattice constant. The radius of a vacancy loop created by removal of m atoms from (or the condensation of m vacancies on) a (111) plane is

$$R_l = \left(\frac{3^{1/2}\Omega m}{\pi a_o}\right)^{1/2} \tag{19.5}$$

where $\Omega = a_o^3/4$ is the atomic volume in the fcc structure. The energy of the faulted vacancy loop is therefore

$$E_{loop} = 2\pi Gb^2 \left(\frac{3^{1/2}\Omega m}{\pi a_o}\right)^{1/2} + \frac{3^{1/2}\Omega\gamma_{sf} m}{a_o} \tag{19.6}$$

If the loop is unfaulted (i.e., the stacking fault is removed), the second term on the right of Eq. 19.6 is absent, but the resulting reduction in energy is partially compensated by the larger Burgers vector of the perfect loop compared to that of the faulted loop.

The void and loop energies given by Eqs. 19.3 and 19.6 are rather close to each other, and conclusions concerning the relative stability of the two types of vacancy clusters are uncertain because important parameters, such as the dislocation line tension, are not accurately known. It appears that the void is the stable form for small clusters (small m), but, as m increases, the loop becomes the energetically favored configuration. If the presence of the stacking-fault term in Eq. 19.6 is ignored temporarily, the energy of the void increases more rapidly with m than that of the loop, and the energy balance tips in favor of the loop at void radii of several tens of angstroms. However, collapse of the embryo void into a vacancy loop is probably impeded by the presence of small quantities of helium gas in the void, and thus voids may survive and grow. Equation 19.6 also indicates that loops rather than voids are favored in metals in which the stacking-fault energy is low. Gold, for example, has a very low stacking-fault energy, and irradiation-produced voids have not been observed in this metal. On the other hand, voids are easily produced in nickel, for which γ_{sf} is large. The stacking-fault energy in stainless steel lies between these two extremes, and voids can be produced in this alloy but only at much higher fluences than that required for void formation in nickel. This observation is consistent with the preceding discussion of the effect of stacking-fault energy on the relative stability of voids and vacancy loops, but many other factors influence the relative resistances to void formation of a complex alloy, such as steel, and of pure metals, such as gold or nickel.

Granted that, given a choice between forming loops or voids, vacancies will condense as the latter, there remains the question of why the irradiation-produced point defects form separate interstitial loops and voids in the first place. Since vacancies and interstitials are formed in equal numbers by fast-neutron bombardment, one would expect that point defects of both types would diffuse to voids at equal rates and hence produce no net growth of the voids. Inasmuch as the voids represent accumulated excess vacancies, the interstitials must be preferentially absorbed elsewhere in the solid. The preferential interstitial sink is

undoubtedly the dislocations, either those belonging to the original network in the metal or the interstitial loops. It was noted in Sec. 13.9 that dislocations exhibit a slightly larger capture radius for interstitials than for vacancies, and it is this fact which fundamentally provides the mechanism for void formation. The preference of dislocations for interstitials is due to the interaction of the strain field around the dislocation with the strain field established by the misfit of an interstitial atom in the lattice (the strain field around a vacancy is much smaller than that around an interstitial). This strain-field interaction causes an attraction of interstitials for dislocations when the two are in proximity. Ham[3] has shown that the directed drift of interstitials toward dislocations can be incorporated into a diffusional model of the transport process if the dislocation line is assigned a somewhat larger capture radius for interstitials than for vacancies (see problem 13.7). The preferred migration of interstitials to dislocations leaves the matrix of the metal slightly depleted in interstitials relative to vacancies; so nonpreferential sinks, such as voids, absorb vacancies at a somewhat greater rate than interstitials and growth results.

In summary, the conditions necessary for void swelling are:

1. Both interstitials and vacancies must be mobile in the solid. This requirement is easily met by interstitials, which can migrate in metals at very low temperatures. If the vacancies are not mobile as well, they will simply be annihilated by the cloud of moving interstitials.

2. Point defects must be capable of being removed at sinks provided by structural defects in the solid in addition to being destroyed by recombination. Moreover, one of the sinks must have a preference for the interstitials in order to permit establishment of the excess vacancy population necessary for voids to form.

3. The supersaturation of vacancies must be large enough to permit voids and dislocation loops to be nucleated, either homogeneously or heterogeneously, and to grow. At temperatures sufficiently high that the thermal equilibrium concentration of vacancies at the void surface is comparable to that sustained in the matrix by irradiation, void nucleation and growth cease. At high temperatures voids thermally emit vacancies as fast as the irradiation-produced vacancies arrive from the bulk of the solid.

4. Trace quantities of insoluble gases must be present to stabilize the embryo voids and prevent collapse to vacancy loops. Transmutation helium provides the necessary gas content in neutron-irradiated metals, although other gaseous impurities (oxygen, nitrogen, and hydrogen) present in most metals can perform the same function. Although some helium gas is undoubtedly present in voids, there is definitely not enough to class these cavities as equilibrium bubbles.

19.2 OBSERVED CHARACTERISTICS OF VOIDS

Excellent summaries of the experimental observations of voids in metals have been presented by Bement[4] and by Norris.[5] In addition, the papers in two conferences devoted to voids[6,7] contain much detailed information pertinent to the experimental and theoretical status of the subject. Emphasis here is placed on voids formed in neutron-irradiated stainless steel. Void formation in the potential cladding materials nickel and its alloys vanadium and molybdenum will not be considered in detail. In addition to fast-neutron irradiation, voids may be formed by bombarding metals with heavy ions (e.g., protons, carbon, and self-ions) or with electrons. The results of these investigations are summarized in Refs. 4 and 5.

The bulk of the information on void formation in metals has been obtained by transmission electron microscopy (Sec. 18.1). This technique permits the *void distribution function*, $N(R)\,dR$ = number of voids/cm^3 with radii between R and R + dR, to be measured. Often, only the total void number density,

$$N = \int_0^\infty N(R)\,dR \tag{19.7}$$

the average void size,

$$\bar{R} = \frac{1}{N}\int_0^\infty R\,N(R)\,dR \tag{19.8}$$

or the void swelling,

$$\frac{\Delta V}{V} = \frac{4}{3}\pi\int_0^\infty R^3\,N(R)\,dR \tag{19.9}$$

are reported. If the void distribution is narrow, the swelling may be expressed by

$$\frac{\Delta V}{V} = \left(\frac{4}{3}\pi\bar{R}^3\ N\right) \tag{19.10}$$

Most theoretical treatments are content to predict the average void size, assuming that the void density is a specified number rather than the complete void distribution function.

Swelling can also be experimentally determined by immersing a sample of known weight in a fluid to measure the solid volume. However, only the electron microscope can provide data on void size and density. In addition, this tool can provide information on the evolution of the dislocation structure of the irradiated metal. This information consists of:

1. The density of network dislocations (i.e., dislocations other than those comprising the loops).

2. The total dislocation line length of the loops, which is determined by the average diameter of the loops and the number density of the loops.

19.2.1 The Void Distribution Function

Figure 19.1 shows the void-size distributions for stainless steel irradiated at different temperatures but to the same fluence. The distributions at low temperatures are approximately Gaussian, with the peak shifted to the larger void sizes as the temperature is increased. The very narrow distributions at low temperatures indicate that, although void nucleation has occurred, the low growth rate prevents voids from attaining large sizes in the allotted irradiation time. At high temperatures the distribution function is very broad and contains some very large voids and a small proportion of little ones. This type of distribution suggests

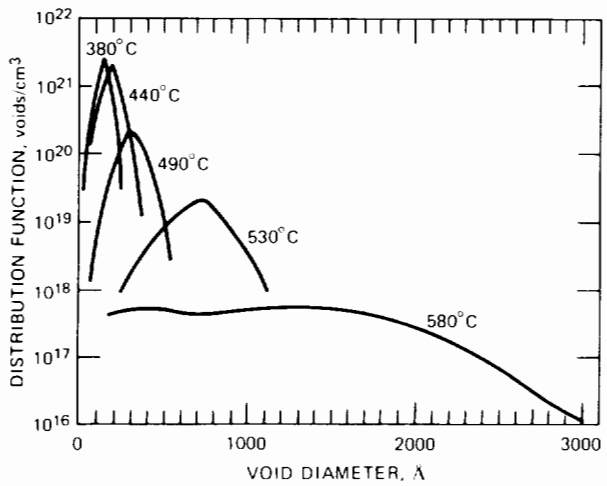

Fig. 19.1 Void-size distribution N(R) in type 316 stainless steel irradiated to a fluence of 6×10^{22} neutrons/cm^2 at various temperatures. (After J. I. Bramman et al., p. 125, Ref. 6.)

that nucleation has ceased and a constant density of voids is in the process of growing.

19.2.2 Void Size and Density

The zeroth and first moments of the void distribution function, which represent the void number density and average void size, respectively, are shown in the three-dimensional representations of Fig. 19.2. Figure 19.2(a) indicates a rapid increase in void size at low temperatures and a smaller rate of increase at high temperatures. Similar nonlinear behavior is seen along the fluence axis. Figure 19.2(b) shows that the void number density decreases with increasing temperature and increases with fluence. Observed void densities range from 10^{13} to 10^{16} voids/cm^3.

19.2.3 Void Swelling

According to Eq. 19.10, the dependence of volume swelling on temperature and fluence could be constructed by multiplying the cube of the surface heights of Fig. 19.2(a) by the surface heights in Fig. 19.2(b). Cuts through this three-dimensional representation of volume swelling are shown in Figs. 19.3 and 19.4. Figure 19.3 shows the restriction of swelling to the temperature band 350 to 600°C with peak swelling occurring at ~500°C. Figure 19.4 indicates a power-law increase of void swelling with neutron fluence. The fluence dependence is of the form

$$\frac{\Delta V}{V} \propto (\Phi t)^n \qquad (19.11)$$

where the exponent n is about unity at 400°C and increases to about 2 at high temperatures. Other functional forms have been suggested for the fluence dependence of swelling. Because of the scatter of the data, swelling can equally well be fitted to a linear equation with an incubation period during which voids are absent:[8]

$$\frac{\Delta V}{V} \propto \Phi t - (\Phi t)_0 \qquad (19.12)$$

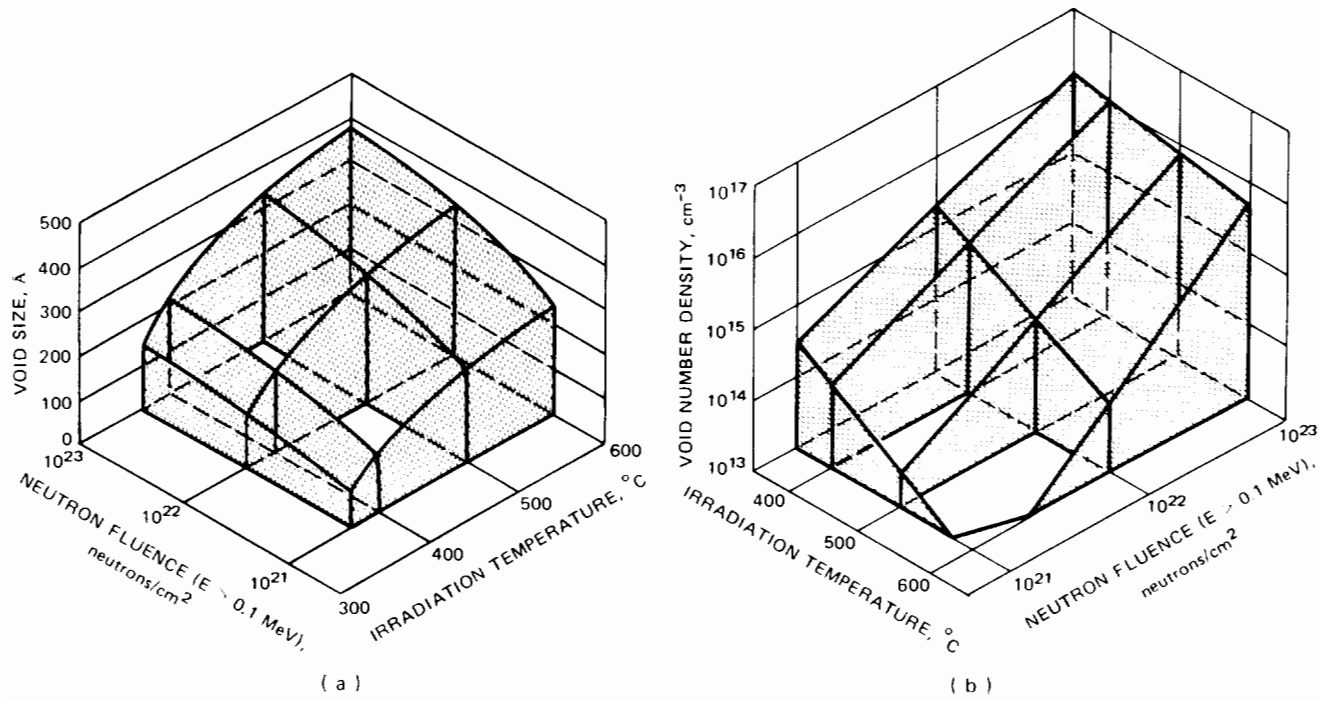

Fig. 19.2 Void size (a) and number density (b) in fast reactor irradiated austenitic stainless steel as a function of fast-neutron fluence and irradiation temperature. [After T. T. Claudson, R. W. Barker, and R. L. Fish, *Nucl. Appl. Technol.*, 9: 10(1970).]

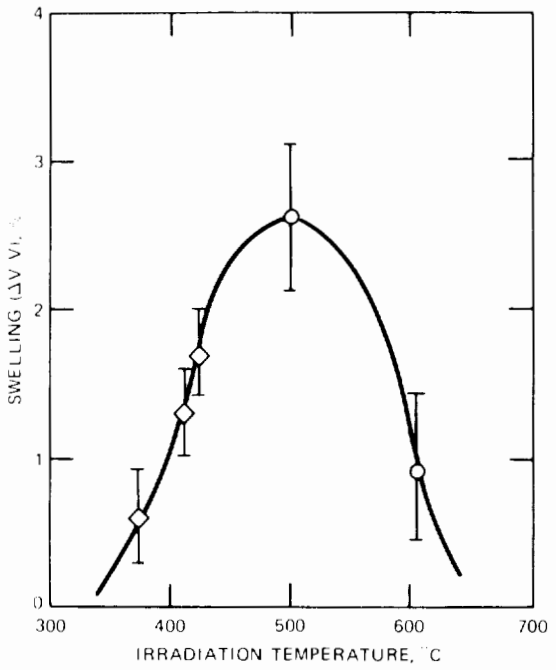

Fig. 19.3 Effect of irradiation temperature on swelling of type 304 stainless steel at a fluence of 5×10^{22} neutrons/cm^2. ●, transmission electron microscopy. ○, immersion density. [After S. D. Harkness and Che-Yu Li, *Met. Trans.*, 2: 1457 (1971).]

The incubation period, $(\Phi t)_0$, is of the order of 10^{22} neutrons/cm^2 and is believed to represent the neutron dose needed to produce enough helium to permit void nucleation to proceed. The induction period may also be required to build up a sufficient density of interstitial loops to allow the preferential absorption of interstitials by dislocations to sufficiently bias the point-defect population in the metal in favor of vacancies so as to permit vacancy agglomeration into voids.

Neither of the above empirical formulations of the fluence dependence of void swelling indicates saturation (i.e., leveling off) of this phenomenon.

19.2.4 The Effect of Cold Work

Cold work, which increases the density of network dislocations, has a significant effect on the swelling characteristics of austenitic steels. Up to a point, cold working improves the resistance of steel to swelling, as is shown by the smaller swelling of 20% cold worked type 316 stainless steel compared with the solution-treated (i.e., annealed) material (Fig. 19.5). Excessive cold work may not be beneficial, as indicated by the curve for type 304 stainless steel in Fig. 19.5. For this steel, two swelling peaks are observed. The low-temperature hump is associated with normal void formation in a metal of constant microstructure. The high-temperature peak is probably due to the instability of the dislocation network introduced by cold work. Above 600°C extensive recovery and recrystallization occur in the steel, and large segments of the microstructure are free from dislocations. Voids easily form in these zones and are responsible for the second hump in the swelling curve for type 304 stainless steel. The dislocation structure introduced by cold working of type 316 stainless steel appears to be more stable. The major difference between these two steels is the 2 to 3% molybdenum addition to type 316 stainless steel. This alloying element can sufficiently reduce the mobility of dislocations (by pinning) to diminish the recovery process.

19.2.5 Effect of Precipitates

The effect of alloy composition is even more dramatically exhibited in the swelling behavior of nickel and the high-nickel-content alloy Inconel (Fig. 19.6). Nickel with 0.4% impurities swells considerably less than high-purity nickel, and Inconel actually densifies during irradiation. The excellent swelling resistance of Inconel is probably due to the fine Ni_3Nb precipitate that is present in this material. This precipitate particle is coherent, which means that its lattice constant is close to that of the matrix, and the precipitate–matrix interface is continuously bonded. It will be shown later that coherent precipitates act as

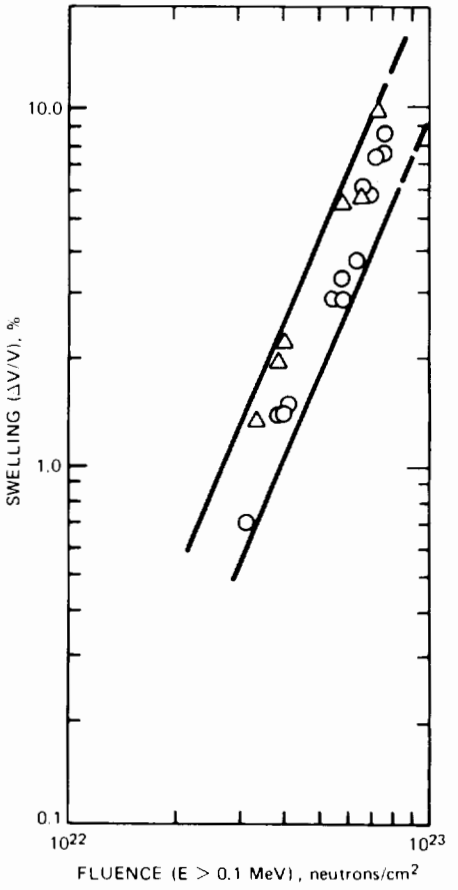

Fig. 19.4 Effect of fast-neutron fluence on swelling in type 316 (○) and in type 347 (△) stainless steels. Irradiation temperatures were between 470 and 540°C. (After W. K. Appleby et al., p. 156, Ref. 6.)

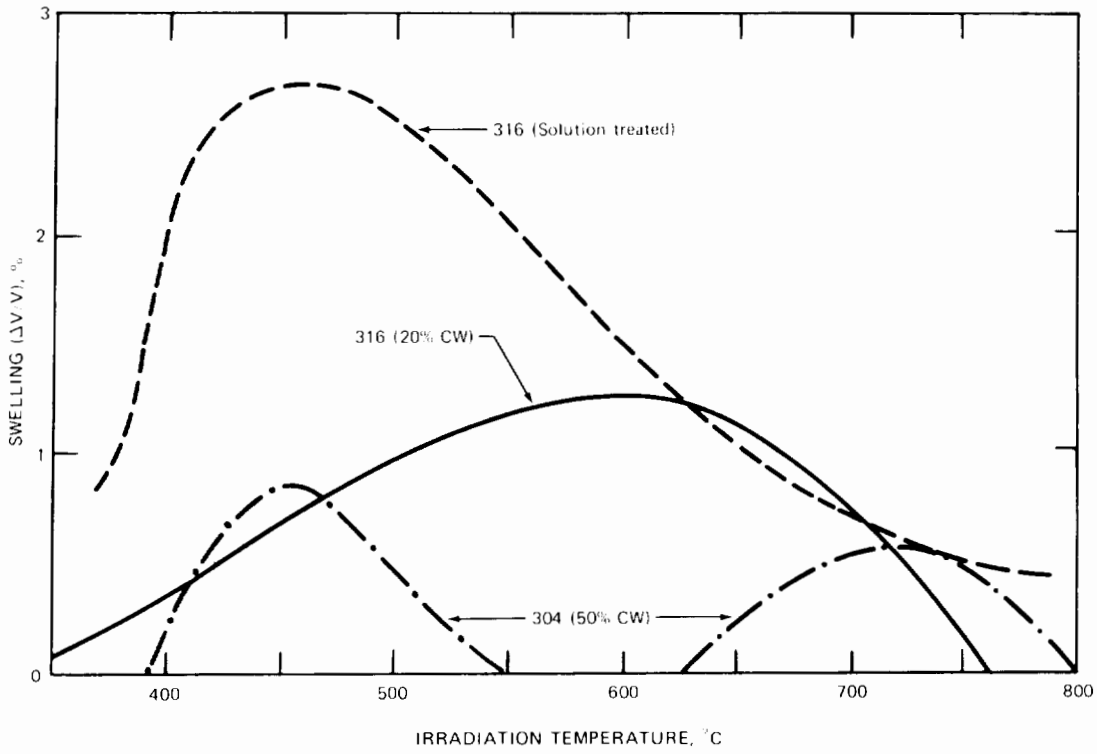

Fig. 19.5 Effect of cold work (CW) on the swelling behavior of austenitic stainless steels. The curves for type 316 stainless steel are plots of Eqs. 19.12a and 19.12b for a fluence of 5×10^{22} neutrons/cm^2. The curve for 50% CW type 304 stainless steel is for a fluence of 24×10^{22} neutrons/cm^2. (After Straalsund et al., p. 142, Ref. 6.)

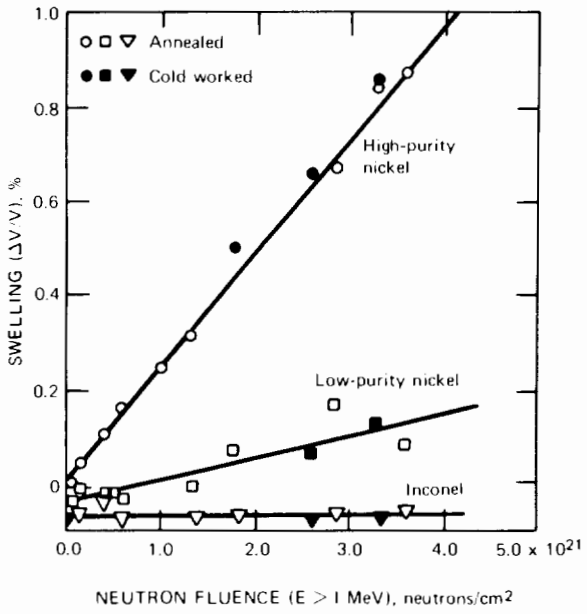

Fig. 19.6 Swelling of high-purity nickel, nickel of 99.6% purity, and Inconel (73% Ni–17% Cr–8% Fe) at 425°C. [After J. J. Holmes, *Trans. Amer. Nucl. Soc.*, 12: 117 (1969).]

recombination sites for vacancies and interstitials and thus contribute to reducing swelling. Another way that a dispersion of fine precipitate particles in an alloy reduces swelling is by impeding dislocation climb (i.e., they act in a manner similar to molybdenum in type 316 stainless steel). Another nickel-based alloy whose microstructure contains a fine dispersion of coherent precipitates is Nimonic PE16. Titanium and aluminum are added in equal amounts to this alloy, and the precipitates have the composition $Ni_3(TiAl)$. This alloy shows less swelling than does type 316 stainless steel at high fluences.

19.2.6 Empirical Void Swelling Formulas

In view of the rudimentary state of the theory of void formation in alloys, empirical equations are used to account for the effects of void swelling in fuel-element performance estimates. The equations used in current core-design studies reflect the influence of the primary variables of temperature and fluence and the degree of cold work of the alloy. For type 316 stainless steel,[9] the swelling equation for solution-treated steel is

$$\frac{\Delta V}{V}(\%) = (\Phi t \times 10^{-22})^{(2.05 - 27/\theta + 78/\theta^2)}[(T - 40)10^{-10}] \exp(32.6 - 5100/T - 0.015T) \quad (19.12a)$$

and for 20% cold-worked steel is

$$\frac{\Delta V}{V}(\%) = 9.0 + 10^{-3.5}(\phi t)^{1.5}\,[4.028 - 3.712 \times 10^{-2} \times (T - 273) + 1.0145 \times 10^{-4}(T - 273)^2 - 7.879 \times 10^{-8}(T - 273)^3] \qquad (19.12b)$$

where $\theta = T - 623^\circ K$.

19.2.7 Interstitial Loops

The qualitative model of swelling described earlier in this section, the quantitative theories discussed later in this chapter, and electron-microscope observations of irradiated steels all indicate that the nucleation and growth of interstitial dislocation loops accompanies and may even precede void formation. In the fcc structure of austenitic stainless steel, the loops that form first are faulted and lie on {111} planes in the lattice [Figs. 18.4(c) and (d) and Fig. 18.5(a)]. Unfaulting occurs when the faulted loop grows to a size at which it is unstable with respect to a perfect loop (the critical loop size for unfaulting is given by equating Eq. 19.6 for faulted loops with $b = a_o/3^{1/2}$ to the similar equation for perfect loops, wherein $b = a_o/2^{1/2}$ and $\gamma_{sf} = 0$). Unfaulting is very slow at temperatures below ~550°C but may be assisted by the passage of glide dislocations over the fault or by interaction of the growing faulted loops with each other. The unfaulted loops [shown in Fig. 18.5(b)] are capable of conservative motion along their glide cylinders and soon become indistinguishable from (and augment the density of) the original dislocation network of the alloy. At low temperatures (~500°C), loop densities are approximately ten times greater than void densities, and the loop diameters are about two to five times the average void diameter.

For type 316 stainless steel, Brager and Straalsund[10] give the empirical formulas:

$$\rho_l + \rho_N = 10^9\,(\Phi t \times 10^{-22})^{F(T)} \exp[G(T)] \qquad (19.13)$$

where

$$F(T) = 31.07 - 0.0145T - \frac{13750}{T} \qquad (19.14a)$$

$$G(T) = -47.7 + 0.0193T + \frac{25970}{T} \qquad (19.14b)$$

The fraction of the total dislocation density which consists of network dislocations is

$$\frac{\rho_N}{\rho_l + \rho_N} = \{1 + \exp[0.11(715 - T)]\}^{-1} \qquad (19.15)$$

In these formulas, ρ_l and ρ_N denote the dislocation densities (in centimeters of dislocation line per cubic centimeter of solid) as faulted loops and network dislocations, respectively; ρ_N includes the contribution of perfect loops, and T is the temperature in °K.

Equations 19.13 and 19.15 are plotted in Fig. 19.7. For $T < 500^\circ C$ the dislocation population is dominated by faulted loops, but above 500°C the faulted loops rapidly disappear and only network dislocations remain. The network dislocation density decreases with increasing temperature because of recovery of the dislocation structure (i.e., mutual annihilation of dislocations of opposite sign or glide out of the specimen).

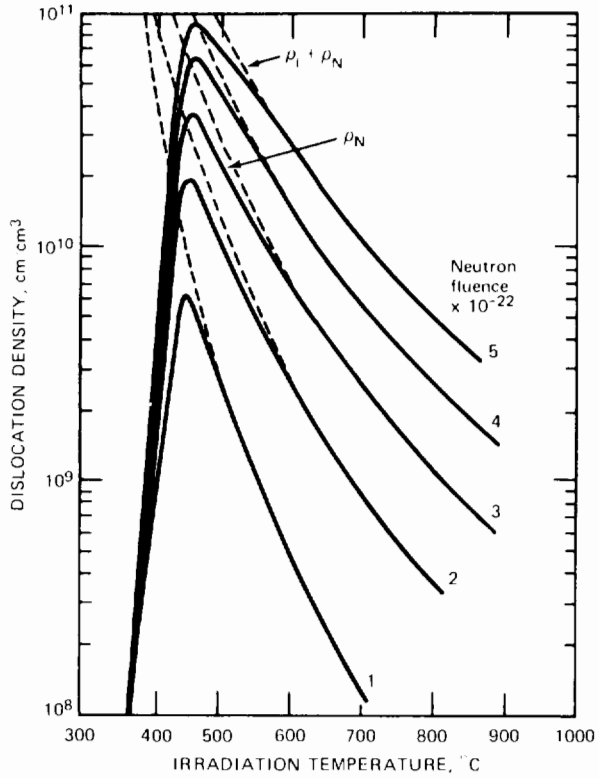

Fig. 19.7 Dislocation density in solution-treated type 316 stainless steel. [After Ref. 10.]

The average diameter of the faulted loops is correlated by

$$\bar{R}_l = \frac{1}{2}(\Phi t \times 10^{-22})^{H(T)} \exp[J(T)] \quad Å \qquad (19.16)$$

where

$$H(T) = -6.31 + 0.00262T + \frac{3060}{T} \qquad (19.17a)$$

$$J(T) = 23.89 - 0.0071T - \frac{9040}{T} \qquad (19.17b)$$

The faulted-loop number density is given by

$$N_l = 10^{15}\,(\Phi t \times 10^{-22})^{0.53} \exp[L(T)] \qquad (19.18)$$

where

$$L(T) = -203.5 + 0.116T + \frac{85900}{T} \qquad (19.19)$$

The loop characteristics according to Eqs. 19.16 and 19.18 are shown in Fig. 19.8.

The preceding recitation of the experimental observations pertaining to void and loop formation in stainless steel illustrates the many different and often poorly defined factors affecting the void-swelling process. It is entirely possible that not all of the variables have been discovered. Consequently, it is unlikely that an accurate and comprehensive theoretical model of this process will be developed,

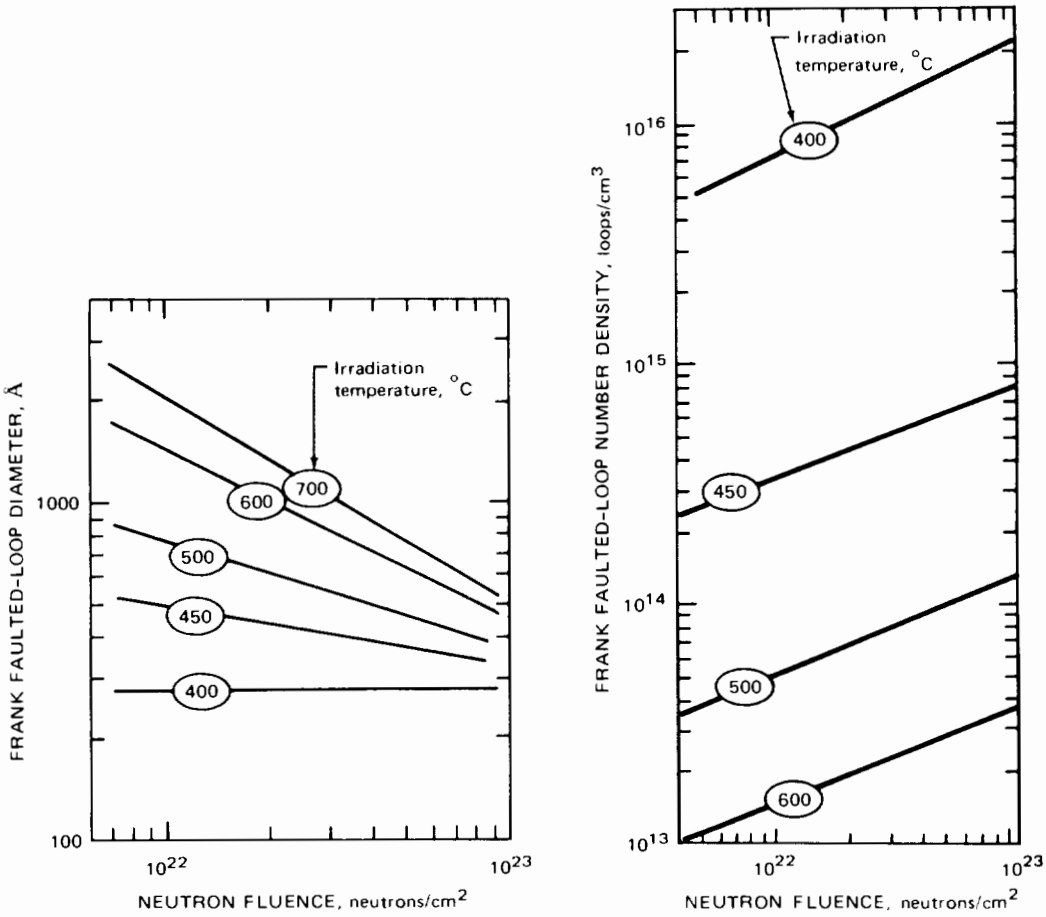

Fig. 19.8 Graphs of equations correlating the size and density of the faulted interstitial loops in type 316 stainless steel for various temperatures and neutron fluences. (After Ref. 10.)

and fuel-element performance predictions will be forced to rely on empirical correlations for LMFBR design. However, theoretical models of the process are valuable because they offer guidance for experiments and elucidate the factors that may prevent or at least retard void growth in cladding materials.

Void-formation theories usually divide the overall process into distinct nucleation and growth phases, models for which are presented in the following two sections. Prediction of the evolution of the loop and void distribution functions with irradiation time requires coupling the basic nucleation and growth laws into point defect, loop, and void conservation statements. Progress in this aspect of void swelling theory is reviewed in Sec. 19.6.

19.3 NUCLEATION OF VOIDS

Nucleation of voids refers to the rate at which tiny embryos of these defect clusters appear in the solid. Once nucleated, the embryos tend to grow and are safe from destruction. Nucleation and growth are often treated as sequential steps in the overall process of void formation. Supersaturation of the solid with point defects is a prerequisite to both nucleation and growth, but a higher supersaturation is required to force nucleation than to continue growth of existing embryos.

The most common example of nucleation is the condensation of water vapor in air. If the partial pressure of water in dust-free air is slowly increased beyond the equilibrium vapor pressure, nothing happens until the supersaturation (i.e., the ratio of the partial pressure to the vapor pressure) attains a value of about 5 to 6. At this point a fog, which corresponds to nucleation of small liquid droplets, appears. The supersaturation of the gas phase falls abruptly at the onset of nucleation, and the newly born droplets consume the remaining excess water vapor at a purely diffusion-limited rate until the equilibrium vapor pressure in the gas phase is attained. Formation of voids and loops in solids may not be as clearly divisible into nucleation and growth phases because in this case generation of point defects acts to maintain the supersaturation. Nucleation of new voids and loops may proceed in parallel with the growth of existing ones.

Nonetheless, nucleation and growth processes can be analyzed as individual phenomena, the rates of which are functions of the point-defect supersaturations, the helium content of the solid, and the temperature. After the basic rate equations have been derived, simultaneous operation of

the growth and nucleation processes can be treated by use of the appropriate conservation statements for voids, loops, and point defects in the solid. When nucleation precedes growth, the conservation equations are considerably simplified, and most theories of void formation in metals have adopted the nucleation-followed-by-growth approach.

As with the condensation of water, nucleation of voids and loops in metals can be classed either as homogeneous or heterogeneous. Homogeneous nucleation refers to the buildup of small clusters by chance encounters of individual point defects executing random walks in the solid. The stability of these clusters relative to the individual point defects of which they are composed (i.e., voids contain vacancies and perhaps gas atoms whereas loops contain interstitials) is the driving force for nucleation. None of the structural features of the solid are needed to cause agglomeration of the point defects.

Heterogeneous nucleation refers to the appearance of voids on distinct structural features of the solid. In water condensation, for example, dust particles provide heterogeneous nucleation sites. In metals the heterogeneities that may accelerate void nucleation include preexisting gas bubbles (containing either impurity gases in the as-fabricated metal or irradiation-produced helium or hydrogen which has precipitated into equilibrium bubbles prior to nucleation of voids), incoherent precipitate particles, and dislocations. The depleted zones created in the collision cascades (Sec. 17.10) can also act as heterogeneous nucleation sites for void formation.

There is no general consensus on the predominant void nucleation mechanism. The importance of homogeneous nucleation vis-a-vis heterogeneous nucleation has been debated since irradiation-produced voids in metals were first discovered (Refs. 4, 5, 11, and 12).

Nucleation of voids in the depleted zones formed in the collision cascade is unlikely because of the rapid thermal annealing (and resulting low concentration) of these zones at the peak swelling temperatures in stainless steel (see Sec. 18.5). Furthermore, irradiation of metals by electrons results in copious void formation, even though depleted zones are not formed by this type of bombarding particle (Sec. 18.5).

It has not been possible to unequivocally determine the conditions under which heterogeneous nucleation of voids on second-phase particles is important. Bloom[11] has found that when the void concentration is low (either by combination of low fluence at low temperature or high fluence at high temperature) the voids are often associated with dislocations or precipitates. At constant fluence Brager and Straalsund[10] observed what appears to be homogeneous nucleation at low temperatures, whereas at high temperatures the voids were fewer in number and attached to precipitates. Nevertheless, the idea that a fixed number of heterogeneous sites is responsible for all void nucleation is unacceptable on two counts. The concept predicts that the void concentration should be (1) limited by the number density of nucleation sites in the metal and (2) independent of irradiation temperature. Neither of these expectations is satisfied by void formation in stainless steel.

All studies of void nucleation in irradiated metals agree that the presence of helium in the solid profoundly affects the nucleation process, although helium is not a prerequisite for nucleation. Neutron-irradiation and ion-bombardment experiments in which helium gas is expressly preinjected into the sample show a larger density of voids than experiments in which helium is totally absent (ion bombardment) or builds up continuously during irradiation (neutron irradiation). The incubation fluence of $\sim 10^{22}$ neutrons cm^{-2} (Eq. 19.12) may be the time needed for sufficient transmutation helium to be produced by irradiation to cause void nucleation. Although the void density is markedly increased by the presence of helium, the total swelling of the metal is unaffected.[13] Typically, ~0.1% of the free vacancies produced by the displacement process in a fast-neutron flux end up in voids (see problem 19.1 at the end of this chapter). The remaining 99.9% either recombine or are removed at sinks. The presence of helium does not alter this partitioning of the vacancies. According to Eq. 19.10, if $\Delta V/V$ is to remain constant even though N increases, the average void size must decrease. The explanation for this observation is that the high void densities in experiments with preinjected helium provide more effective traps for vacancy capture, thereby reducing the vacancy supersaturation and slowing down the rate of growth of the embryos.

In neutron irradiation there is no way of turning off the helium production as a means of controlling void formation. One can at best hope to understand the mechanism by which helium influences void nucleation in order to be able to predict void behavior at fluences as yet unattainable by neutron-irradiation tests.

The details of the processes by which helium affects void nucleation are not known. The mechanism may simply be a matter of stabilizing embryo voids that have nucleated without the aid of gas atoms and preventing collapse of the embryos to vacancy loops. If such collapse occurs, the fate of the loop is determined—because of the preferential bias of dislocations of any sort for interstitials, the vacancy loop will collect more interstitials than vacancies and will be destroyed. However, it is more likely that helium is intimately involved in the nucleation process, probably by precipitating simultaneously with vacancies and interstitials to form embryo voids that are partially gas filled. Whether or not this role of helium converts a homogeneous nucleation process to a heterogeneous one is a matter of semantics. If, however, the helium first migrates to and is trapped by imperfections in the solid (e.g., precipitates) and then small voids form by accretion of vacancies to these bubbles, the nucleation process is clearly heterogeneous.

Although void nucleation probably occurs by a mixture of homogeneous or heterogeneous processes, each assisted by helium, only homogeneous nucleation has been treated quantitatively. Homogeneous nucleation of voids in metals is not simply a matter of applying classical nucleation theory to a new system. Classical theory, which was developed to explain liquid-droplet formation from supersaturated vapor of condensible gases, has been applied to many precipitation processes occurring in solids. However, in all nucleation problems that have been treated by classical theory, growth or shrinkage of small clusters occurs by exchange of a single species between the embryos and the supersaturated medium. Void nucleation, however,

involves the exchange of at least two species, namely, the vacancy and its antiparticle the interstitial, between the clusters and the lattice. A void can grow either by adding a vacancy or by releasing an interstitial; it can shrink by adding an interstitial or by emitting a vacancy. Moreover, if helium is involved in the nucleation process, three species must be considered in the shrinkage and enlargement processes which contribute to homogeneous nucleation.

In the remainder of this section, homogeneous nucleation of voids from a matrix containing arbitrary supersaturations of both vacancies and interstitials is described. Progress in incorporating helium into the nucleation process is considered briefly; nucleation of interstitial loops is treated in Sec. 19.4. The bulk concentration of vacancies and interstitials, which drives the nucleation processes, is assumed to be determined by point-defect balances that consider all sources and sinks of point defects in the solid, as shown in Sec. 19.5.

19.3.1 Homogeneous Nucleation of Voids

Homogeneous nucleation theory begins by deducing the equilibrium void distribution function, $N^{eq}(m)$ (where m is the number of vacancies in a void), which is developed by a supersaturation $S_v = C_v/C_v^{eq}$ of vacancies in the solid. The theory then considers the nonequilibrium situation of arbitrary vacancy and interstitial supersaturations in which there is a net flux, I, of voids from one size to the next larger size. The resulting equation for I (which is the desired nucleation rate) is solved with the aid of the equilibrium distribution, from which certain coefficients appearing in the nonequilibrium equation are obtained. The theory of homogeneous nucleation of voids in the absence of gas atoms was developed simultaneously and independently by Katz and Wiedersich[14] and by Russell.[15]

19.3.2 The Equilibrium Void Distribution Function

When there is no vacancy supersaturation ($S_v = 1$), the equilibrium concentration of vacancies in the solid is given by

$$C_v^{eq} = N_s \exp\left(-\frac{\epsilon_v}{kT}\right) \tag{19.20}$$

where $N_s = 1/\Omega$ and is the number of atom sites in a unit volume of solid and ϵ_v is the energy of formation of a vacancy. Even in this situation there are some small voids (i.e., clusters containing more than one vacancy). The equilibrium fraction of divacancies, for example, was derived in Sec. 6.4 and is given by Eq. 6.22. Similar calculations can be used to determine the concentrations of voids containing three or more vacancies. For the particular case of unit supersaturation, the equilibrium concentration of clusters decreases rapidly as the cluster size increases; i.e., for $S_v = 1$, $N^{eq}(m)$ is a rapidly decreasing function of m.

When the vacancy concentration is maintained at a value greater than C_v^{eq} (e.g., by irradiation), it is also possible to compute an equilibrium void distribution function. For $S_v > 1$, however, $N^{eq}(m)$ is not a monotonically decreasing function of m. Rather, it passes through a minimum at some cluster size and thereafter increases rapidly with m. This equilibrium distribution cannot be attained in practice because it implies large concentrations of large voids. In spite of this practical difficulty, the equilibrium distribution is useful because it permits estimation of certain properties of void growth and shrinkage which are needed for analysis of the actual nonequilibrium case.

We therefore determine the hypothetical void distribution function $N^{eq}(m)$ arising from a supersaturation S_v of vacancies. The vacancies are in equilibrium with the entire void population, or in the language of chemical thermodynamics, the reaction

$$mv \rightleftharpoons v_m \tag{19.21}$$

is at equilibrium for all values of m. Here v denotes a vacancy and v_m is a void composed of m vacancies.

Since a situation of total thermodynamic equilibrium is envisaged, the interstitials present in the solid must also be in equilibrium with the vacancies according to the reaction

$$v + i \rightleftharpoons \text{null} \tag{19.22}$$

where i denotes an interstitial and null means an atom on a normal lattice site. The equilibrium concentration of interstitials in a solid wherein the vacancies are also at equilibrium is

$$C_i^{eq} = N_s \exp\left(-\frac{\epsilon_i}{kT}\right) \tag{19.23}$$

where ϵ_i is the energy of formation of an interstitial. Equation 19.22 requires that the product $C_v C_i$ be a constant, and this constant must be equal to $C_v^{eq} C_i^{eq}$. Or, the concentration of interstitials in equilibrium with a supersaturated solution of vacancies is given by

$$C_i = \frac{C_v^{eq} C_i^{eq}}{C_v} = \frac{N_s}{S_v} \exp\left(-\frac{\epsilon_i}{kT}\right) \tag{19.24}$$

The interstitials are undersaturated by an amount equal to the vacancy supersaturation S_v. Because of this fact and because of the high formation energy of interstitials, the interstitial concentration in the matrix containing a supersaturation of vacancies is negligibly small.

The distribution function $N^{eq}(m)$ is obtained by applying the criterion of chemical equilibrium to reaction 19.21. Specifically, Eq. 5.14 becomes

$$m\mu_v = \mu_m \tag{19.25}$$

where μ_v is the chemical potential of a vacancy and μ_m is the chemical potential of a void of size m. The chemical potentials are related to the total Gibbs free energy of the system by Eq. 5.50:

$$\mu_m = \frac{\partial G}{\partial N^{eq}(m)} \tag{19.26}$$

where the partial derivative is taken with temperature, total pressure, and concentration of clusters of sizes different from m held constant. By analogy to the cases of monovacancies (Eq. 6.11) or divacancies (Eq. 6.16), the total Gibbs free energy of a system containing a distribution $N^{eq}(m)$ of clusters is given by

$$G = G_0 + \sum_m N^{eq}(m)\, g_m - kT \sum_m \ln W_m \qquad (19.27)$$

where G_0 is the free energy of the perfect lattice and g_m is the Gibbs free energy, or reversible work, required to form a void of size m, which is

$$g_m = h_m - Ts_m = \epsilon_m + pv_m - Ts_m$$

Here ϵ_m is the energy required to form a void of m vacancies, s_m is the excess entropy associated with this process, and v_m is the volume change due to introduction of a void in the solid ($v_m = m\Omega$ if local contraction around an isolated vacancy in the lattice is neglected); p is the hydrostatic stress in the solid. Following the usual simplifications in dealing with point-defect equilibria, the last two terms on the right are neglected, and g_m reduces to ϵ_m. However, it should be noted that the presence of the term pv_m in the above expression provides a means whereby the state of stress of the solid can influence the nucleation rate.

For large m, the energy of the void is assumed to be adequately represented by the surface energy, which may be obtained by combining Eqs. 19.1 and 19.2:

$$g_m \simeq \epsilon_m \simeq (36\pi\Omega^2)^{1/3}\, \gamma m^{2/3} \qquad (19.28)$$

Equation 19.28 represents the capillarity model of homogeneous nucleation, in which the energy of a cluster is related to a macroscopic parameter, namely, the surface tension. Equation 19.28 has no meaning for clusters of one or two vacancies. The energy required to create a monovacancy, is the vacancy formation energy ϵ_v, and not the right side of Eq. 19.28 with m = 1. This inability to accurately describe the energy of clusters too small to be treated as droplike entities but too large to be considered in atomic terms is common to all applications of nucleation theory, including the present one.

The last term in Eq. 19.27 is the temperature times the configurational entropy (or entropy of mixing). It can be obtained by calculating the number of ways in which voids can be distributed in a crystal containing N_s lattice sites per unit volume. To perform this computation, we make the assumption that the solution is dilute in voids and vacancies, so the combinatorial numbers W_m can be calculated independently of each other. This problem has already been treated in Sec. 6.4 for the particular case of divancies (m = 2), and similar methods are applied here. However, the problem is simplified by requiring that the clusters be spherical, which eliminates the orientation factors that entered into the divacancy calculation. We begin with a unit volume of perfect lattice and withdraw voids of size m sequentially until there are $N^{eq}(m)$ of these holes in the solid. The size m is fixed during this process. The center of the first void can be removed from any of the N_s available sites, which leaves $N_s - m$ sites from which the second void may be withdrawn. The third void is removed from the $N_s - 2m$ remaining sites, etc. The product of each of these factors gives the number of different ways of removing $N^{eq}(m)$ voids of size m from the solid, or

$$W_m = \frac{N_s(N_s - m)\,(N_s - 2m) \cdots \{N_s - [N^{eq}(m) - 1]m\}}{[N^{eq}(m)]!}$$

where the denominator serves to eliminate permutations among the identical voids (changing the order in which particular voids are removed does not produce a distinguishable state). The quantity $m^{N^{eq}(m)}$ is factored from the numerator of the above equation, and the top and bottom are multiplied by $[(N_s/m) - N^{eq}(m)]!$,

$$W_m = \frac{m^{N^{eq}(m)}\,(N_s/m)!}{[(N_s/m) - N^{eq}(m)]!\,[N^{eq}(m)]!} \qquad (19.29)$$

Substituting Eq. 19.29 into Eq. 19.27, using Stirling's formula for the factorial term, and taking the derivative as required by Eq. 19.26 yields

$$\mu_m = \epsilon_m + kT \ln\left[\frac{N^{eq}(m)}{N_s}\right] \qquad (19.30)$$

In obtaining this result, we have neglected $mN^{eq}(m)$ compared to N_s because the void concentration is low. For monovacancies (m = 1), Eq. 19.30 reduces to

$$\mu_v = \epsilon_v + kT \ln\left(\frac{C_v}{N_s}\right) \qquad (19.31)$$

The vacancy-formation energy is eliminated from Eq. 19.31 by Eq. 19.20. This procedure leads to

$$\mu_v = kT \ln\left(\frac{C_v}{C_v^{eq}}\right) = kT \ln S_v \qquad (19.32)$$

Having determined μ_m and μ_v in terms of the distribution function $N^{eq}(m)$ and the vacancy supersaturation S_v, we determine $N^{eq}(m)$ by substituting Eqs. 19.30 and 19.32 into the criterion of chemical equilibrium, Eq. 19.25, and relating ϵ_m to m by Eq. 19.28. The equilibrium void distribution function is found to be

$$N^{eq}(m) = N_s \exp(m \ln S_v - \xi m^{2/3}) \qquad (19.33)$$

where

$$\xi = (36\pi\Omega^2)^{1/3}\frac{\gamma}{kT} \qquad (19.34)$$

is dimensionless and of magnitude between 10 and 30.

Equation 19.33 is the result of purely thermodynamic arguments and is independent of the mechanism by which the equilibrium void distribution is established. Mechanistic information of the nucleation process can be extracted from Eq. 19.33 if the distribution is regarded as a dynamic balance of the rates of vacancy capture by a cluster and vacancy emission from the cluster. At equilibrium the rates of these two processes are equal, and, since the rate constant for the forward (capture) process is known, the rate constant of the reverse process can be determined from Eq. 19.33.* Equilibrium is attained if the rate at which clusters of m vacancies capture single vacancies is equal to the rate at which clusters of size m + 1 emit vacancies, or

$$\beta_v(m)\, N^{eq}(m) = \alpha_v\,(m + 1)\, N^{eq}(m + 1) \qquad (19.35)$$

*This procedure is an example of the application of the principle of detailed balancing, which has previously been invoked to determine the climb velocity of an edge dislocation (Eqs. 16.51 and 16.52) and to calculate the rate of condensation of UO_2 on the cold side of a pore (Eqs. 14.14 and 14.15).

where $\beta_v(m)$ is the rate of vacancy capture by a size m cluster and $\alpha_v(m)$ is the rate of vacancy emission from a size m cluster.

A formula similar to Eq. 19.35 applies to interstitial capture and emission from a cluster, but, because of the very small interstitial concentration at equilibrium, this relation is unnecessary. The ratio $N^{eq}(m)/N^{eq}(m+1)$ is obtained from Eq. 19.33:

$$\frac{N^{eq}(m)}{N^{eq}(m+1)} = \frac{1}{S_v} \exp\left(\frac{2}{3}\xi m^{-1/3}\right) \qquad (19.36)$$

In deriving Eq. 19.36, the approximation $[1 + (1/m)]^{2/3} \sim 1 + (2/3m)$ has been made.

If the clusters are assumed to be spherical, the vacancy-capture rate is expressed by the rate constant for point-defect absorption by spherical sinks derived in Secs. 13.4 and 13.5. Specifically, $\beta_v(m)$ is given by the product of the rate constant k of Eq. 13.96 and the bulk vacancy concentration C_v. In the present application the void embryos are so small that the capture rate is of the mixed control type in which both diffusion and reaction-rate limitations are of comparable magnitude. Thus

$$\beta_v(m) = \frac{4\pi R D_v C_v}{1 + (a_0/R)} \qquad (19.37)$$

where a_0 is the lattice constant and D_v is the vacancy diffusion coefficient. If unity in the denominator is neglected (which corresponds to complete reaction-rate control of the capture kinetics), Eq. 19.37 reduces to the formulas used in Refs. 14 and 15. However, Eq. 19.37 is preferable to the reaction-rate-limited form since a_0/R is never larger than unity. In either case, R in Eq. 19.37 is related to the cluster size m by Eq. 19.7, and an approximate expression for $\beta_v(m)$ for $a_0/R < 1$ is

$$\beta_v(m) \simeq a_0 D_v C_v m^{1/3} \qquad (19.38)$$

Using Eqs. 19.36 and 19.38 in Eq. 19.35 gives the emission rate constant

$$\alpha_v(m+1) \simeq a_0 D_v C_v^{eq} m^{1/3} \exp\left(\frac{2}{3}\xi m^{-1/3}\right) \qquad (19.39)$$

The preceding formulas show that the vacancy-capture rate increases with cluster size, whereas the vacancy-emission rate decreases with m. Once a cluster has managed to reach a certain minimum size, its propensity to grow outweighs its tendency to shrink, and continued existence and development of the embryo into a full-fledged void is assured. Determination of the critical size beyond which growth is favored is the next task for homogeneous nucleation theory.

19.3.3 The Nonequilibrium Void Distribution Function, the Nucleation Rate, and the Critical Cluster Size

The nucleation current I represents a rate of flow of voids in the phase space of cluster size (as opposed to real space, wherein the flux would be denoted by J). The current I is the net rate at which clusters of size m grow to clusters of size m + 1 per unit volume. It is analogous to the slowing-down density in nuclear reactor analysis, which represents the rate at which neutrons pass a particular energy (i.e., the flux of neutrons in energy space). Since small void clusters grow by capturing vacancies and shrink either by capturing interstitials or emitting vacancies, the nucleation current is the difference between the rate at which clusters pass from size m to size m + 1 and the rate at which clusters of size m + 1 are reduced to size m:

$$I = \beta v(m)\, N(m) - \alpha_v(m+1)\, N(m+1) - \beta_i(m+1)\, N(m+1) \qquad (19.40)$$

where N(m) is the void distribution function for the nonequilibrium but steady-state case. The vacancies and interstitials are supersaturated to arbitrary extents; thus C_v and C_i are not related by a mass action formula such as Eq. 19.24. In addition, the void population represented by the distribution N(m) is not in equilibrium with either the vacancies or the interstitials in the solid. Therefore, N(m) can only be determined by kinetic arguments.

Equation 19.40 is applied to the case in which the same number of voids pass from size m to size m + 1 per unit volume no matter how large m is. To maintain the situation implied by this requirement, one imagines that some mechanism is available for destroying large voids and returning their component vacancies to the metal lattice. In practice, we need not worry about the artificiality of this device for maintaining the steady state; nucleation theory is used solely to determine the ratio at which voids pass the critical size that assures their continued existence. Thereafter, the fate of the voids is determined by growth models, which are formulated independently of the nucleation model and provide the sources and sinks necessary to establish the vacancy and interstitial supersaturations used in the nucleation analysis.

The capture rates are assumed to be the same as those used in determining the equilibrium distribution; $\beta_v(m)$ is given by Eq. 19.37 or 19.38. The rate at which a void absorbs interstitials, $\beta_i(m)$, is given by either of these equations with the subscript v replaced by i. The nucleation rate depends on the ratio of the capture rates of interstitials and vacancies by the voids, or by

$$\frac{\beta_i}{\beta_v} = \frac{D_i C_i}{D_v C_v} \qquad (19.41)$$

The above ratio is called the *arrival-rate ratio* and is independent of void size. It depends on the rates of point-defect production and removal in the bulk solid. These balances are considered in the section on growth. For the moment, we assume that β_i/β_v is a specified constant that is just a bit smaller than unity.

The vacancy-emission rate constant α_v is assumed to be the same as the one deduced for the equilibrium void population, Eq. 19.39. The term in Eq. 19.40 representing interstitial emission from a void has been neglected owing to the very large formation energy of interstitials, which renders C_i^{eq} very small. Therefore, a formula of the type given by Eq. 19.39 for interstitials would show $\alpha_i \simeq 0$.

Elimination of $\alpha_v(m+1)$ from Eq. 19.40 by use of Eq. 19.35 yields

$$I = \beta_v(m) \left\{ N(m) - N(m+1) \left[\frac{N^{eq}(m)}{N^{eq}(m+1)} + \frac{\beta_i}{\beta_v} \right] \right\} \qquad (19.42)$$

where the ratio $\beta_i(m+1)/\beta_v(m)$ has been approximated by $\beta_i(m)/\beta_v(m)$, which is a constant. We now define a function h(m) by

$$\frac{h(m)}{h(m+1)} = \frac{N^{eq}(m)}{N^{eq}(m+1)} + \frac{\beta_i}{\beta_v} \tag{19.43}$$

which is determined by Eq. 19.36 in conjunction with the specified constant value of the arrival-rate ratio. The solution of Eq. 19.43 is (see problem 19.2 at the end of this chapter)

$$\ln\left[\frac{h(m)}{N_s}\right] = -\sum_{m'=0}^{m-1} \ln\left[\frac{N^{eq}(m')}{N^{eq}(m'+1)} + \frac{\beta_i}{\beta_v}\right] \tag{19.44}$$

Equation 19.44 is plotted in Fig. 19.9 for various arrival-rate ratios and for irradiation conditions appropriate to fast reactor cladding. The properties of nickel were used in

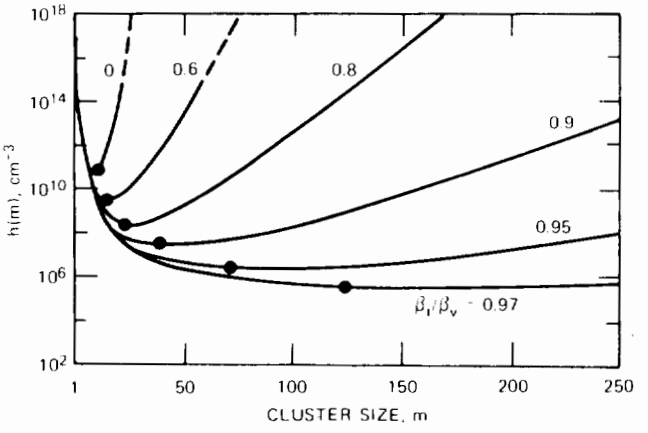

Fig. 19.9 The function h(m) calculated from Eqs. 19.44 and 19.36 for various values of the arrival-rate ratio β_i/β_v. Physical properties for determining ξ from Eq. 19.34 are for nickel at 900°K. The vacancy supersaturation S_v is 430. The dots indicate the location of the minima of h(m). (After Ref. 14.)

preparing the plots, on the grounds that this pure metal resembles stainless steel. The curve for $\beta_i/\beta_v = 0$ corresponds to the equilibrium distribution given by Eq. 19.33.

Using Eq. 19.43, we find that Eq. 19.42 becomes

$$I = \beta_v(m)\, h(m)\left[\frac{N(m)}{h(m)} - \frac{N(m+1)}{h(m+1)}\right]$$

For sufficiently large values of m (i.e., $m > 2$ is sufficient), the difference in the brackets of the above formula can be approximated by a derivative, and

$$I = -\beta_v h \frac{d(N/h)}{dm} \tag{19.45}$$

Solution of Eq. 19.45 requires one boundary condition, but an additional condition is needed if the heretofore unknown nucleation rate I is to be determined as well as the distribution function N(m).

The first requirement on the distribution function is that it approach the equilibrium distribution function $N^{eq}(m)$ at small m. This condition is based on the supposition that very tiny voids capture and shed vacancies so rapidly that they remain in equilibrium with the vacancy supersaturation despite the net drain caused by the nucleation current I. Since it can be shown from Eq. 19.44 that $h \to N^{eq}$ as $m \to 1$, the first condition is

$$\frac{N}{h} \to 1 \text{ as } m \to 1 \tag{19.46a}$$

The second condition requires that there be no very large voids in the system or that

$$\frac{N}{h} \to 0 \text{ as } m \to \infty \tag{19.46b}$$

Integration of Eq. 19.45 between these limits yields

$$-I\int_1^{\infty} \frac{dm}{\beta_v h} = \int_{(N/h)_1}^{(N/h)_\infty} d\left(\frac{N}{h}\right) = -1$$

or

$$I = \left[\int_1^{\infty} \frac{dm}{\beta_v(m)\, h(m)}\right]^{-1} \tag{19.47}$$

This equation can be simplified by noting that the function h(m) has a very sharp minimum at a cluster size m_c (shown as dots in Fig. 19.9). The minimum becomes broader as $\beta_i/\beta_v \to 1$, but, in view of the 16 order-of-magnitude range of the ordinate of Fig. 19.9, the minimum is still quite distinct. The integral in Eq. 19.45 is determined primarily by the behavior of h(m) near this minimum. Consequently, $\beta_v(m)$, which is a slowly varying function of m, is evaluated at m_c and removed from the integral and ln h(m) is expanded in a Taylor series about the minimum:

$$\ln h(m) = \ln |h(m_c)| + \frac{1}{2}\left(\frac{d^2 \ln h}{dm^2}\right)_{m_c} (m - m_c)^2$$

where m_c is defined by

$$\left(\frac{d \ln h}{dm}\right)_{m_c} = 0$$

Substituting the series into Eq. 19.47 and integrating yields

$$I = \left[\frac{1}{2\pi}\left(\frac{d^2 \ln h}{dm^2}\right)_{m_c}\right]^{1/2} \beta_v(m_c)\, h(m_c) \tag{19.48}$$

The first factor on the right of Eq. 19.48 is called the Zeldovich factor.

The void-nucleation rate is therefore determined by the vacancy-capture rate of a critical-size void and the properties of the function h(m) near its minimum. The complete void distribution function N(m) can be determined, but it is of no utility since only the nucleation rate is desired.

Nucleation rates calculated from Eq. 19.48 are plotted in Fig. 19.10. The curves for $\beta_i/\beta_v = 0$ correspond to classical nucleation theory applied to a single-component system. It can be seen that inclusion of interstitials

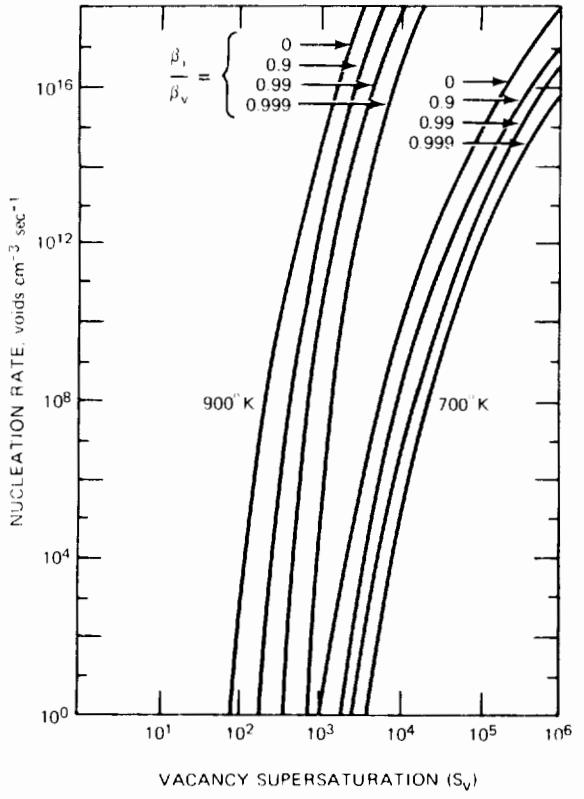

Fig. 19.10 Nucleation rate as a function of vacancy supersaturation for various arrival-rate ratios. (After Ref. 14.)

drastically reduces the nucleation rate. Increasing the arrival-rate ratio from 0 to 0.98 reduces the nucleation rate by six orders of magnitude. If $\beta_i/\beta_v = 1$, nucleation is impossible because interstitials arrive at a void embryo as fast as vacancies. The supersaturations on the abscissa of Fig. 19.10 are obtained from the point-defect balances, which will be considered in Sec. 19.5. An example of the vacancy and interstitial concentrations expected in fast reactor cladding is shown in Fig. 13.17. Although at a fixed S_v the nucleation rate increases with temperature, the supersaturation at high temperature is greatly reduced from what can be maintained at low temperature. At T = 700°K, which is somewhat below the peak swelling temperature of stainless steel, Fig. 13.17(a) shows that it is quite possible to sustain a vacancy supersaturation of 10^4, and Fig. 19.10 gives for this condition a nucleation rate of 10^8 voids cm^{-3} sec^{-1}. Cladding examined after a year (10^7 sec) in-pile would be expected to show a void density of $\sim 10^{15}$ cm^{-3}, which is of the correct order of magnitude. However, the nucleation computation is highly sensitive to poorly known parameters, such as the arrival-rate ratio β_i/β_v, and properties, such as the surface tension of the solid. In addition, the supersaturation is determined by the densities and efficiencies of point-defect sinks, which are difficult to estimate and in any case change during irradiation. In general, homogeneous nucleation theory as outlined does not predict as many voids as are in fact observed in irradiated cladding, nor is it able to account for the cluster incubation period that is also observed experimentally.* In fact, the theory would suggest that voids should be nucleated early in irradiation while the supersaturation is high. The vacancy concentration decreases during irradiation because of the growth of interstitial loops (loop nucleation appears to precede void nucleation). The loops augment the number of point-defect sinks in the solid and, in so doing, reduce the supersaturation of both vacancies and interstitials (i.e., during irradiation, the vacancy concentration drops from one of the solid curves in Fig. 13.17(a) to the corresponding dashed curve). It is believed that the reason for the incubation period observed in swelling experiments is associated with the time required to build up sufficient helium in the matrix.

19.3.4 Nucleation in the Presence of Helium

The preceding theory of void nucleation in a solid supersaturated with vacancies and interstitials was based on the assumption that point defects were capable of readily moving between voids and the bulk solid. Extensions of void nucleation theory to account for helium in the metal have been advanced by Katz and Wiedersich[16] and by Russell.[17]

Helium generated in the solid is much less mobile than vacancies and interstitials at the temperatures where void formation is important. Moreover, once a helium atom has been trapped by a void embryo, return to the matrix is very difficult. Consequently, nucleation in the presence of helium need not involve the simultaneous equilibration of all three species (vacancies, interstitials, and helium atoms) between the void embryos and the bulk solid. A simpler analysis of the effect of helium on void nucleation may be constructed by regarding the helium atoms as immobile nucleation sites to which vacancies and interstitials can migrate to form void clusters. We visualize point defects quickly moving to and from a distribution of embryo voids which contains a fixed number of gas atoms.

The solid is also supposed to contain a distribution of gas-atom clusters, M_j, which is the number of gas-atom clusters per unit volume composed of j helium atoms. The total helium concentration in the solid

$$M = \sum_{j=1} jM_j \qquad (19.49)$$

at any time during irradiation is determined by the helium production rates discussed in Sec. 18.10. It is assumed that nucleation of voids proceeds independently and concurrently on each of the gas-atom cluster populations characterized by M_j nucleation sites per unit volume. All these parallel nucleation processes are driven by the prevailing vacancy and interstitial supersaturations. In addition to the heterogeneous nucleation paths provided by the helium clusters in the metal, the homogeneous nucleation mechanism described earlier in this section still occurs on the N_s lattice sites in the solid. The total nucleation rate is the sum of the contributions of the

*There is an incubation period inherent in the theory, but it is not as long as the incubation time for observed void swelling in stainless steel (see Ref. 15).

parallel processes of homogeneous and heterogeneous nucleation:

$$I = I_{homo} + \sum_{j=1} I_j \qquad (19.50)$$

where I_{homo} is given by Eq. 19.48 with h(m) given by Eq. 19.44 and $N^{eq}(m)$ by Eq. 19.33. Thus, we need only to determine the heterogeneous nucleation rate I_j on the M_j helium-atom clusters (each containing j helium atoms) per unit volume. Each of the voids formed on these M_j sites contains the fixed number j of gas atoms but a variable number m of vacancies. The void embryos that form on the gas-atom clusters are described by the equilibrium distribution functions:

$N_j^{eq}(m)$ = number of embryos per unit volume that contain m vacancies and j gas atoms

Equation 19.33 gives the equilibrium distribution of voids that contain no gas atoms (j = 0).

The equilibrium reactions that establish the distribution $N_j^{eq}(m)$ are

$$mv \rightleftharpoons v_{mj}$$

where v_{mj} denotes a void consisting of m vacancies and j gas atoms. In accord with the assumption that the helium is immobile, no chemical reaction expressing equilibration of gas atoms between the voids and the bulk is written. The criterion of chemical equilibrium for the above reactions is

$$m\mu_v = \mu_{mj} \qquad (19.51)$$

where μ_v is the chemical potential of a vacancy (Eq. 19.32) and μ_{mj} is the chemical potential of a void with m vacancies and j gas atoms. The latter is given by

$$\mu_{mj} = \frac{\partial G}{\partial N_j^{eq}(m)} \qquad (19.52)$$

where the total Gibbs free energy depends on both the vacancy and helium-atom content of the voids:

$$G = G_0 + \sum_j \sum_m [N_j^{eq}(m)\, g_{mj} - kT \ln W_{mj}] \qquad (19.53)$$

where g_{mj} is the reversible work required to form a cluster containing m vacancies and j helium atoms and $k \ln W_{mj}$ is the configuration entropy due to this class of clusters. The effect of helium on the nucleation rate is entirely contained in these two terms.

Following arguments similar to those applied to homogeneous nucleation on all lattice sites, the number of ways of arranging $N_j^{eq}(m)$ voids on M_j sites is found to be

$$W_{mj} = \frac{M_j (M_j - 1) \ldots \{M_j - [N_j^{eq}(m) - 1]\}}{[N_j^{eq}(m)]!} = \frac{M_j!}{[M_j - N_j^{eq}(m)]!\,[N_j^{eq}(m)]!}$$

Expressing W_{mj} by the above equation and using Eq. 19.53 in Eq. 19.52 yields:

$$\mu_{mj} = g_{mj} + kT \ln \left[\frac{N_j^{eq}(m)}{M_j}\right] \qquad (19.54)$$

Next we determine g_{mj}, the reversible work of forming the vacancy gas-atom cluster from a solid which has no vacancies but contains the j gas-atom clusters embedded in the otherwise perfect lattice. The term g_{mj} consists of two terms. The first is the work required to create a gas-free void in the solid, which is given by Eq. 19.28. The second represents the work required to move the helium from the solid to the space inside the void. Since helium is nearly insoluble in the metal, it has a natural tendency to escape from the solid to the gas space of the void. Thus, we expect that work can be recovered by reversibly transferring helium from the solid to the void, or that this step reduces the work requirement of void formation and consequently facilitates nucleation. The helium transfer operation is performed in three stages to determine the free-energy change:

1. Helium is withdrawn from solution to a gas container at the equilibrium helium pressure corresponding to the temperature and the total helium concentration of the solid. This pressure is denoted by p_{eq}.
2. The gas is expanded isothermally and reversibly to the pressure at which the helium exists in the void.
3. The helium is transferred to the void.

Consider the free-energy changes that accompany each of the above steps.

The first step, which is analogous to vaporization of a liquid at its vapor pressure, involves no change in free energy. Isothermal, reversible expansion of j atoms of an ideal gas from pressure p_{eq} to pressure p provides a release of free energy of the amount

$$jkT \ln \left(\frac{p_{eq}}{p}\right)$$

The third step involves no work and hence contributes nothing to the free-energy change.

Assuming that the helium in the void obeys the ideal gas law, we find the pressure p is given by

$$p(m\Omega) = jkT \qquad (19.55)$$

where $m\Omega$ is the volume of a void made up of m vacancies each of which contributes a volume Ω.

Determination of the equilibrium helium pressure, p_{eq}, requires more information. Although helium is nearly insoluble in metals, it is not completely so. The solubility of a gas in a metal can be analyzed by statistical mechanical methods, as shown in Chap. 5 (see problem 5.9). Briefly, the chemical potential of gas-phase helium is equated to the chemical potential of dissolved helium (which is assumed to be monatomically dispersed in the lattice). The partition of gas-phase helium needed to compute the chemical potential in the gas is due to translation only. The partition function of dissolved helium is obtained by assuming that helium in the lattice behaves as a three-dimensional oscillator. This procedure yields

$$p_{eq} = M \frac{kT}{N_s} \left(\frac{h\nu}{kT}\right)^3 \left(\frac{2\pi m_{He} kT}{h^3}\right)^{3/2} \exp\left(\frac{\epsilon_g}{kT}\right) \qquad (19.56)$$

where M/N_s is the total atom fraction of helium in the metal and ϵ_g is the energy difference between an atom of gaseous helium and one in the lattice (i.e., the heat of solution). If it is assumed that helium occupies

substitutional positions in the metal lattice, ϵ_g very closely represents the energy required to remove a metal atom from a lattice and place it on the surface. This step provides the opening into which a helium atom can fit. The bonding between helium and the surrounding metal atoms is quite small; so the entire energy requirement in the process is consumed in removing the metal atom. Consequently, ϵ_g should be approximately equal to the formation energy of a vacancy in the metal, or $\epsilon_g \simeq \epsilon_v$. The vibration frequency ν in Eq. 19.56 is that of a helium atom on a lattice site and is approximately 10^{13} sec^{-1}, m_{He} is the mass of a helium atom, and h is Planck's constant.

Because ϵ_g is positive and large compared to kT, the ratio p_{eq}/M is also large. For the parts-per-million helium concentrations encountered in LMFBR fuel-element cladding, p_{eq} may be as large as 10^9 atm. It should be emphasized that the helium in the cladding never exists as a gas at the pressure p_{eq}; it is either in the metal at concentration M or in the void at pressure p. The equilibrium pressure given by Eq. 19.56 appears solely as a result of computing the work that could be extracted from the process of transferring helium from the lattice to the void if it were done reversibly.

Accounting for the stabilizing effect of helium, the reversible work to form a void embryo of m vacancies and j gas atoms is

$$g_{mj} = 4\pi\left(\frac{3\Omega}{4\pi}\right)^{2/3}\gamma m^{2/3} - jkT \ln\left(\frac{HMm\Omega}{jkT}\right) \quad (19.57)$$

where H is the coefficient of M in Eq. 19.56 (i.e., H is the Henry's law constant for the dissolution of helium in the metal). It is a function of temperature only.

We now substitute Eq. 19.57 into Eq. 19.54 to determine μ_{mj} and use the resulting equation and Eq. 19.32 for μ_v in Eq. 19.51. Solving for the equilibrium distribution, we find

$$N_j^{eq}(m) = M_j \exp\left[m \ln S_v - \xi m^{2/3} + jkT \ln\left(\frac{HMm\Omega}{jkT}\right)\right] \quad (19.58)$$

where ξ is given by Eq. 19.34. When $j = 0$, $M_j = N_s$ and Eq. 19.58 reduces to the equilibrium distribution for gas-free voids, given by Eq. 19.33. Figure 19.11 shows the negative of the argument of the exponential in Eq. 19.58

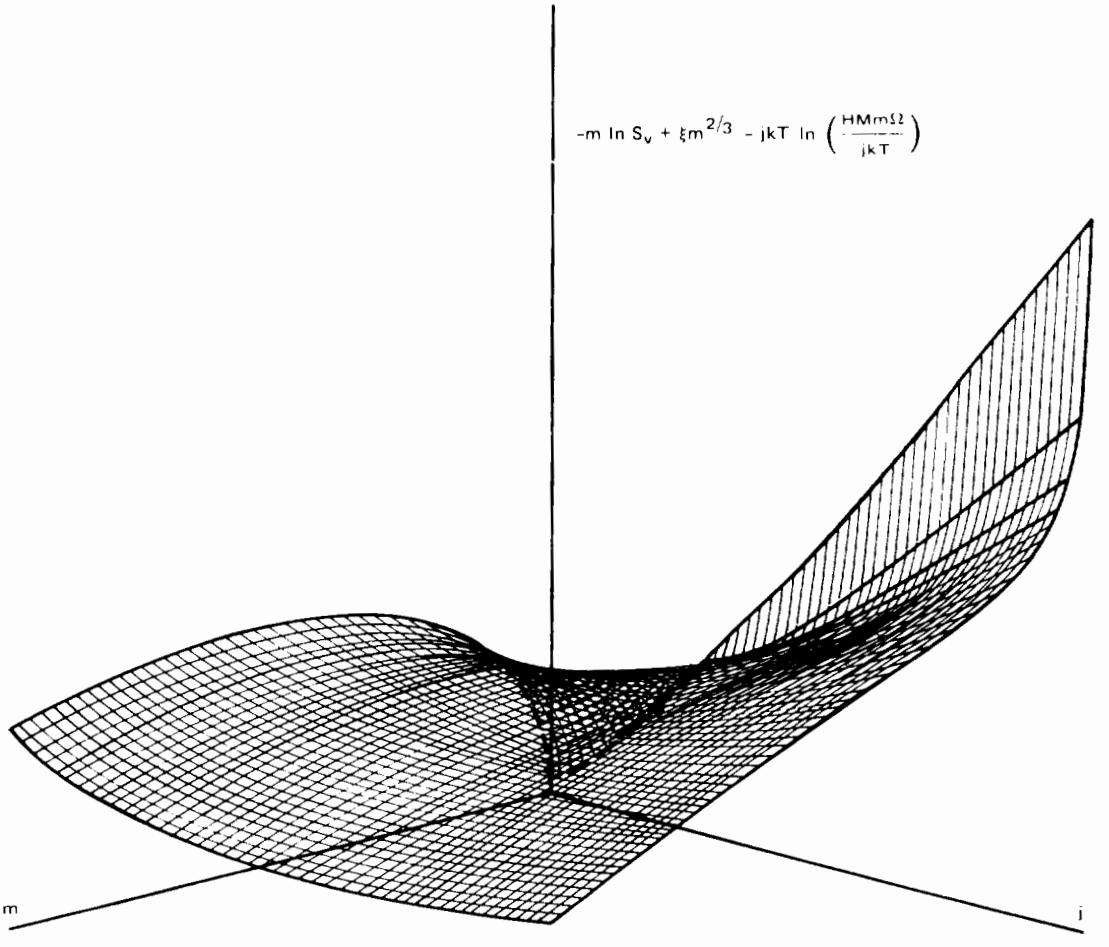

Fig. 19.11 Plot of the free energy of void formation as a function of the number of vacancies (m) and the number of gas atoms (j) in the void. Conditions: $S_v = 600$, $p_{eq} = 5000$ atm, $T = 500°C$, $\gamma = 1000$ dynes/cm. (After Ref. 17.)

(which is sometimes called the free energy of void formation) plotted as a function of m and j. The intercept of this surface at j = 0 (no gas) corresponds to the $\beta_i/\beta_v = 0$ curve in Fig. 19.9. Gas atoms in the void reduce the energy barrier for nucleation below the value characteristic of gas-free voids. The saddle point on the surface shown in Fig. 19.11 occurs at m = 11 and j = 6. This plot, however, does not consider interstitials, which are included in the analysis in exactly the same manner as in the case of homogeneous nucleation in the absence of gas.

The remaining analysis is straightforward. The arrival rates β_v and β_i and the vacancy emission rate α_v are independent of the presence of gas atoms in the void. As long as the helium is immobile and does not move among the voids, Eq. 19.40 is valid if the subscript j is appended to both I and N in this formula. Only the function h(m), which depends on the equilibrium void distribution function, changes explicitly. In place of Eq. 19.43, we write for gas-containing voids

$$\ln\left[\frac{h_j(m)}{M_j}\right] = -\sum_{m'=0}^{m-1} \ln\left[\frac{N_j^{eq}(m')}{N_j^{eq}(m'+1)} + \frac{\beta_i}{\beta_v}\right] \quad (19.59)$$

For a specified value of j, the minimum of the function $h_j(m)$ occurs at m_{cj} vacancies, and the nucleation rate on the population of j helium-atom clusters is given by the analog of Eq. 19.48:

$$I_j = \left[\frac{1}{2\pi}\left(\frac{d^2 \ln h_j}{dm^2}\right)_{m_{cj}}\right]^{1/2} \beta_v(m_{cj})\, h_j(m_{cj}) \quad (19.60)$$

To evaluate the nucleation rate on the gas-atom clusters in the metal, we must estimate the distribution of the available gas (M atoms/cm^3) among the various cluster sizes. In principle, the distribution M_j could be obtained by considering independently the problem of helium-atom agglomeration in the cladding in much the same way that fission-gas precipitation into bubbles in the fuel was analyzed in Chap. 13. However, for simplicity, the distribution

$$M_j = M_1^{-(j+1)/2}$$

is assumed. The distribution must also satisfy Eq. 19.49. Figure 19.12 shows the results of calculations based on Eqs. 19.60 and 19.61 for M equivalent to 10 ppm helium (which is the concentration that would be formed in stainless-steel cladding following irradiation to a fluence of $\sim 5 \times 10^{22}$ neutrons/cm^2). The vacancy supersaturation scale is divided into regimes expected in a reactor and in an ion-bombardment experiment. It can be seen from the graph that, for all supersaturations expected in-pile, heterogeneous nucleation on helium-atom clusters far outweighs homogeneous nucleation. This behavior constitutes theoretical confirmation of the often observed enhancement of void nucleation by helium. The relative importance of homogeneous and heterogeneous nucleation shifts according to the helium concentration because $h_{homo}(m)$ is proportional to N_s, whereas $h_j(m)$ is proportional to M_j. At low fluence homogeneous nucleation is dominant because there is not enough helium

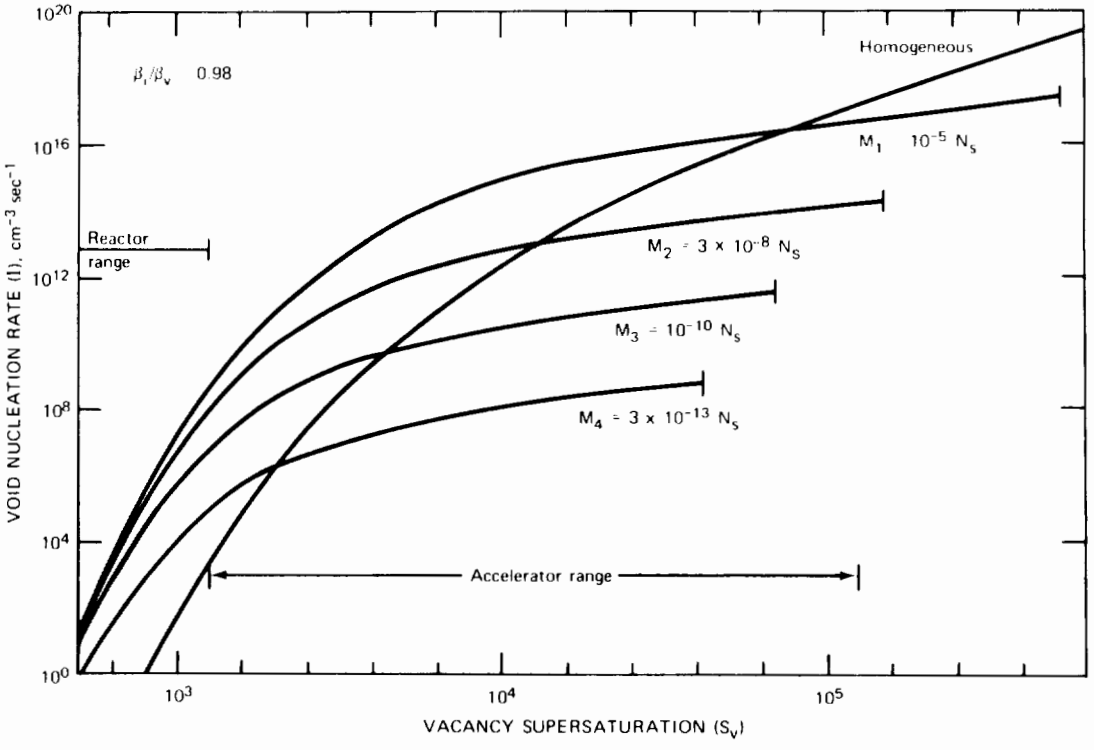

Fig. 19.12 Void-nucleation rates (I_j) on helium-atom clusters and the homogeneous nucleation rate (I_{homo}) as functions of vacancy supersaturation at 500°C. Total helium content of 10 ppm. (After Ref. 16.)

to drive heterogeneous nucleation. However, since I_{homo} is quite low, no voids are observed until sufficient helium has been generated by transmutation reactions to give the high heterogeneous nucleation rates shown in Fig. 19.12. This incubation period is equivalent to a fluence of $\sim 10^{22}$ neutrons/cm^2 for stainless steel.

19.4 NUCLEATION OF INTERSTITIAL DISLOCATION LOOPS

The microstructure of irradiated steel is found to contain a high concentration of interstitial dislocation loops in addition to voids. In Sec. 19.3, it was shown that void nucleation is driven by the supersaturation S_v of vacancies aided by a slightly greater rate of vacancy than interstitial absorption by the voids, which is expressed as $(\beta_i/\beta_v)_{voids} < 1$. Nucleation of loops because of interstitial supersaturation S_i is possible because more interstitials than vacancies arrive at all dislocations in the solid, or $(\beta_v/\beta_i)_{loops} < 1$. The fact that the relative vacancy and interstitial arrival rates are inverted for voids and loops is a consequence of the small but extremely important preference of dislocations for interstitials. Formally, interstitial loop nucleation can be treated in precisely the same manner as void nucleation, but the very large formation energy of interstitials ($\epsilon_i \simeq 4$ eV) compared to that for vacancies ($\epsilon_v \simeq 1$ eV) profoundly alters the quantitative aspects of the nucleation process. Another important difference between void and loop nucleation is that the latter is not subject to enhancement by helium in the solid. Growing loops are not sinks for inert gas atoms, as are voids.

19.4.1 Loop Nucleation by Classical Theory

The methods applied to predict void-nucleation rates in the preceding section can be utilized in toto for loop nucleation simply by exchanging the subscripts i and v in all of the formulas and by replacing the void energy given by Eq. 19.3 by the energy of a faulted loop, Eq. 19.6. Such a calculation has been performed by Russell and Powell.[18] They found that the critical cluster for loop nucleation contains only two or three interstitials, even in the presence of vacancies. The reason for this result can be explained as follows. The equilibrium cluster distribution (i.e., the distribution for which clusters, vacancies, and interstitials are all in equilibrium) is given by the analog of Eq. 19.33:

$$N^{eq}(m) = N_s \exp\left(m \ln S_i - \frac{\epsilon_m}{kT}\right) \qquad (19.61)$$

where $N^{eq}(m)$ is the number of loops per unit volume comprised of m interstitials; S_i is the interstitial supersaturation

$$S_i = \frac{C_i}{C_i^{eq}} = \Omega C_i \exp\left(\frac{\epsilon_i}{kT}\right) \qquad (19.62)$$

and ϵ_m is the work required to form a loop of size m from a perfect solid. Application of the principle of detailed balancing to the interstitial-capture and -emission rates for a loop leads to a formula similar to Eq. 19.35:

$$\beta_i(m)\, N^{eq}(m) = \alpha_i(m+1)\, N^{eq}(m+1) \qquad (19.63)$$

where $\beta_i(m)$ is the rate at which a loop of size m captures interstitials and $\alpha_i(m)$ is the rate at which the loop emits interstitials. With the aid of Eq. 19.61, 19.63 can be solved for the interstitial-emission rate

$$\alpha_i(m+1) = \frac{\beta_i(m)}{S_i} \exp\left(\frac{\epsilon_{m+1} - \epsilon_m}{kT}\right) \qquad (19.64)$$

The interstitial-capture rate $\beta_i(m)$ is a slowly varying function of m, and the primary size dependence of the emission rate is contained in the exponential term in Eq. 19.64. In estimating ϵ_m, Russell and Powell[18] neglect the stacking-fault energy in Eq. 19.6 and use a slightly different formula for the strain energy of the loop (i.e., the first term on the right of Eq. 19.6). The loop energy they used is given by

$$\epsilon_m = 500\, m^{1/2} \text{ kJ/mole} \qquad (19.65)$$

for $m > 1$ and $\epsilon_1 = \epsilon_i = 420$ kJ/mole for the formation energy of a single interstitial. Using this energy formula and a typical interstitial supersaturation of 10^{17}, we find the emission rates from di- and tri-interstitials to be

$$\alpha_i(2) \simeq 3 \times 10^4\, \beta_i(1)$$

$$\alpha_i(3) \simeq 6 \times 10^5\, \beta_i(2)$$

Since $\beta_i(1) \simeq \beta_i(2)$, $\alpha_i(2)$ is some 9 orders of magnitude larger than $\alpha_i(3)$. In other words, the triinterstitial has virtually no tendency to shed interstitials and is therefore the critical cluster for loop nucleation.

Application of classical nucleation theory (even when modified to account for point defects of the opposite sign) is of dubious validity when the critical cluster contains only two or three particles. First, the use of a cluster energy formula based on the strain energy of a circular dislocation loop as calculated from elasticity theory hardly seems appropriate for di- and triinterstitials. Second, approximation of finite differences by differentials, as is required to obtain Eq. 19.45 from the preceding formula, and the subsequent manipulation of the integrals is of questionable accuracy when the sums involved contain only two or three terms. Consequently, loop nucleation is best analyzed by a method that views the nucleation process as the result of homogeneous reactions between the point defects and small clusters.

19.4.2 Loop Nucleation by Chemical Reaction-Rate Theory

The kinetics of point-defect annealing are commonly treated by methods analogous to those employed in homogeneous chemical kinetics.[19] This method has been used in Sec. 13.8 to calculate nucleation rates of fission-gas bubbles in fuel. Hayns[20] has treated interstitial loop nucleation in a similar manner.

1. The vacancy and interstitial supersaturations are independent of the loop-nucleation process. For void nucleation, S_v and S_i are assumed to be specified by point-defect balances that consider all sinks in the solid.
2. Vacancies and interstitials are mobile.
3. Di- and triinterstitials are immobile.

4. Destruction of the clusters by radiation (i.e., by dynamic resolution due to the energetic recoils in the irradiated metal) is neglected.

Conditions 1 and 2 are quite appropriate for cladding under fast reactor conditions. The third assumption is probably not valid, but inasmuch as interstitial cluster migration is not considered either in void-nucleation theory (Sec. 19.3) or in void- and loop-growth theory (Sec. 19.5), we shall not introduce it at this point. The effect of re-solution on loop nucleation rates is treated in problem 19.7 at the end of this chapter.

To visualize the process of loop nucleation in an irradiated solid clearly, we first examine the simpler situation in which the metal contains a supersaturation of interstitials S_i but no vacancies. Interstitial cluster nucleation is assumed to be governed by the reactions

$$i + i \rightleftharpoons i_2 \qquad [1]$$

$$i + i_2 \rightarrow i_3 \qquad [2]$$

The physical justification for this mechanism is that the rates of formation and decomposition of diinterstitials according to reaction 1 are very rapid compared to the rate of formation of triinterstitials; so the small drain on the diinterstitial population caused by reaction 2 does not appreciably disturb the equilibrium of reaction 1. The triinterstitials do not decompose, because of the very low value of $\alpha_i(3)$.

In Sec. 13.4 the forward rate of reaction 1 has been determined for the case of vacancies. For interstitials, the rate R_{1f} is expressed by

$$R_{1f} = k_{1f} C_i^2 \qquad (19.66)$$

where, by analogy to Eq. 13.39,

$$k_{1f} = \frac{z_{1i} \Omega D_i}{a_o^2} \qquad (19.67)$$

where z_{1i} is the combinatorial number that includes the number of sites from which a diinterstitial can be formed in a single jump of one interstitial atom to an adjacent one. For the vacancy–vacancy reaction in fcc metals, this coefficient was found to be 84, but the rate must be multiplied by a factor of 2 to account for the mobility of both partners of the reaction. Thus the combinatorial number z_{1i} is probably between 100 and 200. Instead of the rate constants k, nucleation theory uses arrival rates β; thus the forward rate of reaction 1 can also be written as

$$R_{1f} = \beta_i(1)\, C_i \qquad (19.68)$$

where

$$\beta_i(1) = k_{1f} C_i = \frac{z_{1i} \Omega D_i C_i}{a_o^2} \qquad (19.69)$$

and is the arrival rate of interstitials at a cluster of size 1 (i.e., another interstitial).

The rate of the reverse of reaction 1 is

$$R_{1r} = \alpha_i(2)\, N_2 \qquad (19.70)$$

where N_2 is the volumetric concentration of diinterstitials and $\alpha_i(2)$ is given by Eq. 19.64 with m = 1. In chemical rate theory, the formation energy of a diinterstitial is not approximated by the strain energy of a dislocation loop of two interstitials as it is in classical nucleation theory. Instead, ϵ_2 is related to the binding energy of the diinterstitial by the analog of Eq. 6.15:

$$\epsilon_2 = 2\epsilon_i - B \qquad (19.71)$$

where B is the energy required to separate a diinterstitial into two isolated interstitials. If B were 125 kJ/mole in stainless steel, ϵ_2 calculated from Eq. 19.71 would be identical to the value obtained by setting m = 2 in Eq. 19.65. Substituting Eqs. 19.69 and 19.71 into Eq. 19.64, setting $\epsilon_1 = \epsilon_i$, and replacing C_i with S_i by use of Eq. 19.62 produces the result

$$\alpha_i(2) = \frac{z_{1i} D_i}{a_o^2} \exp\left(-\frac{B}{kT}\right) \qquad (19.72)$$

Because reaction 1 is assumed to be at equilibrium, we can set $R_{1f} = R_{1r}$, or $\beta_i(1)\, C_i = \alpha_i(2)\, N_2$. Using Eq. 19.69 for $\beta_i(1)$ and Eq. 19.72 for $\alpha_i(2)$ yields

$$N_2 = \Omega \exp\left(\frac{B}{kT}\right) C_i^2 \qquad (19.73)$$

The rate of reaction 2 is

$$R_2 = \beta_i(2)\, N_2 \qquad (19.74)$$

Assuming the diinterstitial to be immobile, we find the arrival rate of interstitials at diinterstitials to be given by

$$\beta_i(2) = \frac{z_{2i} \Omega D_i C_i}{a_o^2} \qquad (19.75)$$

where z_{2i} is the number of sites surrounding a diinterstitial from which a single interstitial can jump to form a triinterstitial. Once the latter is formed, it cannot be destroyed; so the rate of nucleation of interstitial loops is equal to the rate of formation of triinterstitials:

$$I^*_{loop} = R_2 = \beta_i(2)\, N_2 \qquad (19.76)$$

where the asterisk denotes nucleation in the absence of vacancies. Substitution of Eqs. 19.73 and 19.75 into Eq. 19.76 yields the nucleation rate:

$$I^*_{loop} = \frac{z_{2i} \Omega^2 D_i C_i^3}{a_o^2} \exp\left(\frac{B}{kT}\right) \qquad (19.77)$$

or, in terms of the interstitial supersaturation expressed by Eq. 19.62,

$$I^*_{loop} = \frac{z_{2i} D_i}{a_o^2 \Omega} S_i^3 \exp\left[-\frac{(3\epsilon_i - B)}{kT}\right] \qquad (19.78)$$

To apply loop-nucleation theory to irradiated metals, we must consider the role of vacancies. To do so, the preceding analysis is modified to include reactions between vacancies and di- and triinterstitials in addition to reactions 1 and 2. The additional reactions are

$$v + i_2 \rightarrow i \qquad [3]$$

$$v + i_3 \rightarrow i_2 \qquad [4]$$

for which the rates are

$$R_3 = \beta_v(2)\, N_2 \qquad (19.79)$$

$$R_4 = \beta_v(3)\, N_3 \qquad (19.80)$$

where $\beta_v(m)$ denotes the rate at which an interstitial cluster of size m captures vacancies:

$$\beta_v(m) = \frac{z_{vm}\Omega D_v C_v}{a_o^2} \qquad (19.81)$$

z_{vm} being the number of locations surrounding a size m interstitial cluster from which a vacancy can jump and reduce the cluster size by one.

Reactions 1 to 4 are depicted schematically in Fig. 19.13. The nucleation current I_m is the net rate at which clusters of size m grow to clusters of size m + 1. Balances on di- and triinterstitials can be expressed in terms of the nucleation currents by

$$\frac{dN_2}{dt} = I_1 - I_2 \qquad (19.82)$$

$$\frac{dN_3}{dt} = I_2 - I_3 \qquad (19.83)$$

As indicated in Fig. 19.13, the nucleation currents are related to the reaction rates by

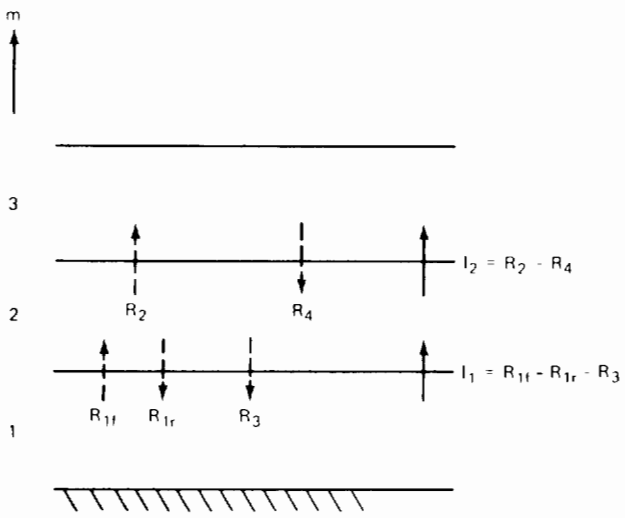

Fig. 19.13 Relations between nucleation currents and the rates of elementary reactions between point defects and interstitial clusters.

$$I_1 = R_{1f} - R_{1r} - R_3$$
$$= \beta_i(1)\, C_i - \alpha_i(2)\, N_2 - \beta_v(2)\, N_2 \qquad (19.84)$$

$$I_2 = R_2 - R_4 = \beta_i(2)\, N_2 - \beta_v(3)\, N_3 \qquad (19.85)$$

It will be recalled that steady-state nucleation refers to the condition in which $I_1 = I_2 = I_3 = \ldots = I_{loop}$. Application of this constraint to Eq. 19.82 and use of Eqs. 19.84 and 19.85 show that

$$\beta_i C_i = [\alpha_i(2) + \beta_i + \beta_v]\, N_2 - \beta_v N_3 \qquad (19.86)$$

Because the arrival rates $\beta_i(m)$ and $\beta_v(m)$ are very weakly dependent on m, the arguments denoting the cluster-size dependence of these coefficients have been deleted in Eq. 19.86; β_i and β_v are considered as known constants which depend only on the vacancy and interstitial supersaturations.

Under irradiation, the ratio β_v/β_i at loops is just slightly less than unity; thus β_i and β_v are of comparable magnitudes. However, it was shown earlier in this section that $\alpha_i(2)$ is $\sim 10^4$ times larger than β_i (or β_v). Consequently, the last two terms in the brackets of Eq. 19.86 can be neglected. By the same token, since N_3 is no greater than N_2, the last term on the right is also negligibly small. Therefore, when steady-state nucleation has been attained, $\beta_i C_i = \alpha_i(2)\, N_2$, or the equilibrium of reaction 1 is not significantly perturbed by the introduction of vacancies into the system. Therefore, N_2 is given by Eq. 19.73, whether or not vacancies are present along with interstitials.

At steady state, Eq. 19.83 and analogous balances for m = 4, . . . reduce to

$$(\beta_i + \beta_v)N_3 = \beta_i N_2 + \beta_v N_4$$

$$(\beta_i + \beta_v)N_4 = \beta_i N_3 + \beta_v N_5 \qquad (19.87)$$

.

.

.

Since the vacancy and interstitial arrival rates are approximately equal, the above equations are satisfied by

$$N_2 \simeq N_3 \simeq N_4 \simeq \ldots \qquad (19.88)$$

The nucleation rate is equal to any of the I_m. Using m = 2,

$$I_{loop} = I_2 = R_2 - R_4 = \beta_i N_2 - \beta_v N_3 \qquad (19.89)$$

or, taking into account the equality of N_2 and N_3,

$$I_{loop} = (\beta_i - \beta_v)N_2 = \left(1 - \frac{\beta_v}{\beta_i}\right)\beta_i N_2$$

$$= \left(1 - \frac{\beta_v}{\beta_i}\right) I^*_{loop} \qquad (19.90)$$

Inasmuch as N_2 is given by Eq. 19.73, the product $\beta_i N_2$ in the above expression for I_{loop} is the nucleation rate in the absence of vacancies. The vacancy supersaturation of

the metal under irradiation reduces the loop-nucleation rate by the factor $|1 - (\beta_v/\beta_i)|$. The point-defect balances developed in Sec. 19.5 suggest that $0.99 < \beta_v/\beta_i < 0.999$ at loops; so loop nucleation under irradiation is reduced by factors ranging from 10^{-2} to 10^{-3} owing to vacancy arrival at the critical nucleus (the triinterstitial).

In the fcc lattice, $z_{2i} \simeq 20$ (the same combinatorial number was assumed for fission-gas-atom capture on two-atom clusters in the bubble-nucleation calculation of Sec. 13.8). The interstitial diffusion coefficient can be approximated by

$$D_i = a_o^2 \nu \exp\left(-\frac{\epsilon_i^*}{kT}\right) \tag{19.91}$$

where ϵ_i^* is the activation energy for interstitial migration. In stainless steel, ϵ_i^* is believed to be about 13 kJ/mole. The other parameters in the nucleation rate are

$$\Omega = 12\ \text{Å}^3$$

$$\epsilon_i = 420\ \text{kJ/mole}$$

The binding energy of a diinterstitial in stainless steel is not known, but the value obtained by the loop strain-energy approximation of Eq. 19.65 is 125 kJ/mole. Taking $\nu \simeq 10^{13}\ \text{sec}^{-1}$, Eqs. 19.78 and 19.90 together yield

$$I_{loop} \simeq 2 \times 10^{-37}\left(1 - \frac{\beta_v}{\beta_i}\right) S_i^3 \exp\left[-\frac{1150}{R(T/10^3)}\right] \tag{19.92}$$

For a typical LMFBR fuel cladding $S_i = 10^{18}$, $\beta_v/\beta_i = 0.98$, and $T = 500°C$. Using these values in Eq. 19.92 gives $I_{loop} = 10^{12}\ \text{cm}^{-3}\ \text{sec}^{-1}$. Thus, a loop concentration of $10^{16}\ \text{cm}^{-3}$ is established after about 3 hr of irradiation. This time is considerably shorter than the incubation time needed for void nucleation, which is about 1 year. The observation that loop nucleation precedes void nucleation is thus theoretically justifiable. However, the substantial uncertainty in properties such as the binding energy of the diinterstitial in stainless steel renders the accuracy of the calculated nucleation rates no better than a factor of 100.

19.5 POINT-DEFECT BALANCES AND THE VOID-GROWTH LAW

Having determined the rate at which embryo voids and dislocation loops are introduced into the solid by nucleation, we next develop the theory for calculating the rates at which these defect clusters grow. Point-defect balances provide the means of computing the vacancy and void supersaturations (S_v and S_i, or, equivalently, C_v and C_i) which drive both the nucleation and growth processes. The effects of applied stress and internal gas pressure on the growth law are considered later in this section. The present analysis is restricted to gas-free voids and unstressed solids.

The concentrations of vacancies and interstitials in the irradiated solid are determined by equating the rate of production of point defects to the rate of removal by all mechanisms. The treatment is quasi-stationary because the time derivatives dC_v/dt and dC_i/dt are neglected. This approximation is justifiable on the grounds that changes in the sink strengths (and hence the rates of point-defect removal) due to the evolution of the microstructure of the metal during irradiation are very slow compared with the time required for the point-defect population to respond to such changes.

The spatial gradients in the point-defect population are also neglected because both the rates of production and removal are assumed to be uniform throughout the metal. The calculations are thus of the infinite-medium type. Very strong concentration gradients do exist in the immediate vicinity of the microstructural features of the solid which are responsible for point-defect absorption. This complication is removed from the point-defect balances by homogenizing the sinks. That is, the discrete sinks in the solid are replaced by spatially uniform absorbers of point defects. The strength of the homogenized sinks, however, must be determined by solving the point-defect diffusion equations in the immediate vicinity of the discrete sinks. These calculations have been reviewed in Sec. 13.5. The approach is similar to that applied to nuclear reactor analysis before the advent of extensive computer facilities; properties such as resonance capture or thermal utilization were determined by analysis of the spatial distribution of neutrons in a cell containing representative quantities of fuel and moderator in a geometry appropriate to the actual fuel-element configuration. This analysis provided the infinite multiplication factor, which could then be used (without further reference to the inhomogeneities in the internal configuration of the core) to compute the critical size of the reactor from neutron diffusion theory in which the system was regarded as homogeneous.

Point-defect balance equations have been developed by Harkness, Tesk, and Li;[21] Wiedersich;[22] and Brailsford and Bullough.[23] These three analyses are equivalent in approach but differ in detail. Wiedersich's method was developed in Sec. 13.10 for use in determining the growth rate of nonequilibrium gas bubbles in the fuel. In this section the theory of Brailsford and Bullough is used, since their treatment of vacancy emission from the vacancy sinks in the metal is superior to that used in the earlier theories.

19.5.1 Point-Defect Production Rates

Vacancies and interstitials are created in the collision cascade caused by the scattering of fast neutrons from lattice atoms. Each collision creates a primary knock-on atom (PKA), which in turn produces free interstitials, free vacancies, and clusters of interstitials and vacancies which are the debris of the displacement spike (Sec. 17.10). If the defect clusters are thermally stable, the number of free vacancies and free interstitials created by a PKA need not be equal, although the total number of vacancies (free plus in clusters) must be the same as the total number of interstitials. Section 18.5 treats a case in which more free interstitials than free vacancies are formed, the remainder of the latter appearing as a depleted zone. This calculation showed that the depleted zones were not thermally stable (i.e., they tended to evaporate) at temperatures above ~350°C, which is the lower temperature limit for void formation. For $T > 350°C$, the defect clusters formed in the collision cascade proper are very quickly destroyed, either by dissociation into their component point defects

by thermal evaporation or by annihilation by point defects of the opposite kind. For the purposes of void-growth analysis, we may assume that equal numbers, ν, of vacancies and interstitials are produced by each fast-neutron scattering collision with a lattice atom. The volumetric production rate of point defects is

Rate of production of vacancies

$$= \text{rate of production of interstitials} = \nu\Sigma_s\Phi \text{ cm}^{-3} \text{ sec}^{-1} \quad (19.93)$$

The number of displacements per PKA, ν, is considerably smaller than that predicted by isolated cascade theory (Sec. 17.7), owing primarily to recombination during cascade formation or shortly thereafter as the point defects move away from the spike. For stainless steel, the best estimate of ν in a fast-neutron spectrum is

$$\nu = 30 \text{ Frenkel pairs per neutron collision} \quad (19.94)$$

This number may not be applicable below ~350°C (Ref. 21).

The macroscopic scattering cross section for the metal is Σ_s. It is the product of the microscopic scattering cross section and the density of metal atoms. For stainless steel, $\Sigma_s \approx 0.2 \text{ cm}^{-1}$; Φ is the total fast-neutron flux (with neutron energies >0.1 MeV).

19.5.2 Bulk Recombination

Recombination of vacancies and interstitials to reform an atom on a normal lattice site occurs in the bulk of the metal at a rate equal to $k_{vi}C_vC_i \text{ cm}^{-3} \text{ sec}^{-1}$, where k_{vi} is the rate constant for recombination (Eq. 13.42).

19.5.3 Removal at Microstructural Sinks

Natural and radiation-produced microstructural features in the metal capture point defects of both types. These sinks can be divided into three categories:[2,3]

1. Unbiased (neutral) sinks. This type of sink shows no preference for capturing one type of defect over the other type. The rate of absorption is proportional to the product of the diffusion coefficient of the point defect and the difference in the concentrations of the point defect in the bulk metal and at the sink surface. Included in this category are (1) voids, (2) incoherent precipitates, and (3) grain boundaries.

2. Biased sinks. Any dislocation in the solid exhibits a preferential attraction for interstitials compared with vacancies. This bias is due to the nonrandom drift of interstitials down the stress gradient near the dislocation core. Vacancies do not exhibit stress-induced migration when near the dislocation. The effect may be incorporated into ordinary diffusion calculations by making the effective radius of the dislocation core slightly larger for interstitials than for vacancies. Dislocations are unsaturable sinks for point defects because they can climb as a result of absorbing a vacancy or an interstitial (provided that climb is not impeded by pinning of the line). The dislocations in the solid are divided into two classes: (1) network dislocations present in the unirradiated metal and augmented by unfaulting of the Frank dislocation loops and (2) dislocation loops formed by agglomeration of interstitials.

The only difference between loops and network dislocations is the concentration of vacancies which is maintained at the core. Both types of dislocations exhibit the same bias toward interstitial absorption.

3. Coherent precipitates. If a point defect is captured by a sink but does not lose its identity on absorption, it can only wait at the sink surface to be annihilated by point defects of the opposite type. Such sinks act as recombination centers of limited capacity. The most important example of this type of sink is the coherent precipitate.

19.5.4 Point-Defect Absorption by Voids

The diffusion-controlled rate of absorption of vacancies by all of the voids in a unit volume of solid is given by

$$Q_v^{void} = 4\pi RND_v\left[C_v - C_v^{eq}\exp\left(\frac{2\gamma\Omega}{RkT}\right)\right] \quad (19.95)$$

where R is the average radius of the void population and N is the total concentration of voids in the solid. The vacancy concentration at the void surface (the second term in the brackets of Eq. 19.95) has been taken as that corresponding to thermodynamic equilibrium in a solid under a negative hydrostatic stress $2\gamma/R$. This tensile stress arises from the surface tension of the solid, which pulls the surface inward.

The analogous formula for interstitial absorption by voids is

$$Q_i^{void} = 4\pi RND_iC_i \quad (19.96)$$

The interstitial concentration at the void surface is effectively zero.

19.5.5 Incoherent Precipitates

Equations 19.95 and 19.96 apply to incoherent precipitates if R and N are interpreted as the average radius and concentration, respectively, of the precipitate particles.

19.5.6 Grain Boundaries

For simplicity, grain-boundary absorption of point defects is not included in the analysis presented here. It is, however, covered in problem 19.9 at the end of this chapter. The strength of grain-boundary sinks has been estimated in Refs. 21 and 24. The latter study showed that for grain sizes larger than ~10 μm, grain-boundary absorption of point defects is small compared to the effects of the other sinks in the metal.

19.5.7 Network Dislocations

Network dislocations maintain the equilibrium vacancy concentration at the core radius. The rate of diffusion-controlled absorption of vacancies by the ρ_N cm of network dislocations per cm^3 of solid is given by

$$Q_v^N = \frac{2\pi}{\ln(\mathcal{R}/R_{dv})} D_v\rho_N (C_v - C_v^{eq}) \quad (19.97)$$

where $\mathscr{R}$ is approximately one-half the distance between dislocations (Eq. 13.79) and R_{dv} is the radius of the dislocation core for vacancies.

For interstitials the absorption rate by network dislocations is

$$Q_i^N = \frac{2\pi}{\ln(\mathscr{R}/R_{di})} D_i \rho_N C_i \tag{19.98}$$

where R_{di} is the core radius for interstitials. Setting

$$Z_v = \frac{2\pi}{\ln(\mathscr{R}/R_{dv})} \tag{19.99}$$

and

$$Z_i = \frac{2\pi}{\ln(\mathscr{R}/R_{di})} \tag{19.100}$$

Eqs. 19.97 and 19.98 can be written as

$$Q_v^N = Z_v D_v \rho_N (C_v - C_v^{eq}) \tag{19.101}$$

and

$$Q_i^N = Z_i D_i \rho_N C_i \tag{19.102}$$

Inasmuch as $R_{di} > R_{dv}$, $Z_i > Z_v$. The ratio $(Z_i - Z_v)/Z_v$ is estimated to be between 0.01 and 0.02.

19.5.8 Dislocation Loops

The only difference between network dislocations and interstitial dislocation loops is the equilibrium vacancy concentration at the core. When a dislocation loop emits a vacancy or absorbs an interstitial atom, the area of the stacking fault enclosed by the loop and the perimeter of the loop increase. According to Eq. 19.6, energy is required for this expansion to occur, and so vacancy emission or interstitial absorption by interstitial loops is less favorable than network dislocations. The latter, if unpinned, are free to climb without changing their length and so are not subject to the energy restraint that affects loop expansion. This phenomenon is taken into account by expressing the rates at which loops absorb vacancies and interstitials by the equations

$$Q_v^l = Z_v D_v \rho_l (C_v - C_v^l) \tag{19.103}$$

$$Q_i^l = Z_i D_i \rho_l (C_i - C_i^l) \tag{19.104}$$

The coefficients Z_v and Z_i are the same as they are for network dislocations since the stress fields around a dislocation are the same for the two types. The point-defect concentrations at the dislocation core, however, are different for network dislocations and loops; C_v^l and C_i^l are determined by thermodynamic arguments.

In a solid containing equilibrium concentrations of vacancies and interstitials, interstitial loops cannot (thermodynamically) exist; the system could reduce its Gibbs free energy by dissolving the loops. However, if the point-defect concentrations are altered in such a way that the vacancies and interstitials are always in equilibrium (i.e., $C_i C_v = C_i^{eq} C_v^{eq}$), it is possible for an interstitial loop of a particular size to exist in equilibrium with the point-defect environment provided that $C_i > C_i^{eq}$. Conversely, a stable vacancy loop could form in a solid in which $C_v > C_v^{eq}$. Here we compute the size of an interstitial loop which exists in equilibrium with a specified vacancy concentration C_v^l and the corresponding equilibrium interstitial concentration C_i^l.

The Gibbs free energy of a piece of metal containing n_v vacancies, n_i interstitials (at concentrations C_v^l and C_i^l, respectively), and one interstitial dislocation loop containing m_i interstitials is

$$G = G_0 + \epsilon(m_i) + n_v \mu_v + n_i \mu_i \tag{19.105}$$

where μ_v and μ_i are the chemical potentials of the vacancies and the interstitials, respectively, $\epsilon(m_i)$ is the energy of the loop, and G_0 is the reference free energy of the piece of metal without the loop and with point-defect concentrations C_v^{eq} and C_i^{eq}.

We now perturb the system by transferring point defects between the bulk solid and the loop. The criterion of chemical equilibrium states that for the system at equilibrium the free-energy change, δG, for this process is zero. Thus, taking the differential of Eq. 19.105,

$$\delta G = \left(\frac{d\epsilon}{dm_i}\right) \delta m_i + \mu_v \delta n_v + \mu_i \delta n_i = 0$$

The number of interstitial atoms in the loop can be changed only at the expense of the point defects in the bulk, so the perturbations are related by

$$\delta m_i = \delta n_v - \delta n_i$$

Eliminating δm_i from the preceding equations yields

$$\left(\frac{d\epsilon}{dm_i}\right) \delta n_v - \left(\frac{d\epsilon}{dm_i}\right) \delta n_i + \mu_v \delta n_v + \mu_i \delta n_i = 0$$

The changes δn_v and δn_i are arbitrary and independent of each other; thus the coefficients of both these perturbations must independently be set equal to zero. This requirement leads to two relations:

$$\frac{d\epsilon}{dm_i} + \mu_v = 0 \tag{19.106a}$$

and

$$\frac{d\epsilon}{dm_i} - \mu_i = 0 \tag{19.106b}$$

The chemical potential of vacancies in a solid with a concentration C_v^l of this species is given by Eq. 19.32:

$$\mu_v = kT \ln \left(\frac{C_v^l}{C_v^{eq}}\right) \tag{19.107a}$$

For interstitials the formula is

$$\mu_i = kT \ln \left(\frac{C_i^l}{C_i^{eq}}\right) \tag{19.107b}$$

When the vacancies and interstitials are in equilibrium with each other, $C_i^l C_v^l = C_i^{eq} C_v^{eq}$, which is equivalent to

$$\mu_i = -\mu_v \tag{19.108}$$

applies. Therefore, Eqs. 19.106a and 19.106b are equivalent. Using the former in conjunction with Eq. 19.107a gives

$$C_v^l = C_v^{eq} \exp\left(-\frac{d\epsilon/dm_i}{kT}\right)$$

The loop energy $\epsilon(m_i)$ is given by Eq. 19.6. If the coefficient of $m^{1/2}$ in this formula is symbolized by K and the stacking-fault term is neglected (because it is small compared to the line-tension term), $d\epsilon/dm_i$ can be computed, and the above equation can be written

$$C_v^l = C_i^{eq} \exp\left(-\frac{K}{2(m_i)^{1/2}\,kT}\right) \tag{19.109}$$

Had Eqs. 19.106b and 19.107b been used, the result would be

$$C_i^l = C_i^{eq} \exp\left(\frac{K}{2(m_i)^{1/2}kT}\right) \tag{19.110}$$

According to Eq. 19.65, K = 500 kJ/mole in stainless steel.

Equation 19.109 shows that the vacancy concentration in equilibrium with an interstitial dislocation loop is less than the equilibrium concentration in the loop-free solid. Simultaneously, C_i^l is greater than C_i^{eq} in order to maintain the loop.

Although the above analysis applies to a strictly thermodynamic situation, the results can be employed in the nonequilibrium environment created by irradiation of the solid. To do so, it is assumed that the concentrations of point defects in the solid immediately adjacent to the core of the dislocation line comprising the interstitial loop are given by Eqs. 19.109 and 19.110. The concentrations in the bulk of the solid far from the loop are C_v and C_i, which are not in equilibrium with the loop (nor with each other). The assumption of interfacial equilibrium is commonly used in analyses of many chemical engineering mass-transfer operations. With this assumption the rates of vacancy and interstitial absorption by the loops in the solid are determined using Eq. 19.109 in Eq. 19.103 and Eq. 19.110 in Eq. 19.104. For application in the point-defect balance equations, m_i in Eqs. 19.109 and 19.110 can be approximated by the size of the average loop in the solid, and the point-defect absorption rates by loops become

$$Q_v^l = Z_v D_v \rho_l \left[C_v - C_v^{eq} \exp\left(-\frac{K}{2(\bar{m}_i)^{1/2}\,RT}\right)\right] \tag{19.111}$$

and

$$Q_i^l = Z_i D_i \rho_l \left[C_i - C_i^{eq} \exp\left(\frac{K}{2(\bar{m}_i)^{1/2}\,RT}\right)\right] \tag{19.112}$$

Thus the loop components of the total dislocation density of the solid do not exhibit quite so large a bias for interstitials as do the network dislocations, for which Q_v^N and Q_i^N are given by Eqs. 19.101 and 19.102. The alterations in the driving forces due to the last terms in the brackets of the above formulas tend to reduce the bias toward interstitials introduced by the inequality of the coefficients $Z_i > Z_v$. However, if the loops are large and/or the temperature is high, the exponential terms in Eqs. 19.111 and 19.112 approach unity, and the dislocation network and the dislocation loops behave in an identical manner toward the point defects in the solid.

19.5.9 Coherent Precipitates

Brailsford and Bullough[2,3] assign the recombination function of coherent precipitates to the plane of matrix atoms adjacent to the second-phase particle. This plane, or interface, is endowed with the capacity to strongly bind or trap point defects that hop into it from the adjacent matrix. Figure 19.14 shows a cross section through the precipitate–matrix interface. Vacancies and interstitials that are trapped at the interface are assumed to be unable to escape; removal of trapped point defects occurs only by annihilation with point defects of the opposite type which impinge on the interface or by recombination of trapped vacancies and interstitials. The coherent precipitate is distinguished from the other microstructural defects in the solid by the absence of thermal emission of point defects (which appears in the terms involving C_v^{eq} in Eq. 19.95 for voids, in Eq. 19.97 for network dislocations, and in Eq. 19.111 for loops).* We will summarize the function of these sinks in the manner visualized in Ref. 23.

Although the interface between a coherent precipitate particle and the matrix does not release point defects, the fact that it is of limited capacity means that the concentrations of vacancies and interstitials at the surface of the particle are not reduced to zero as they would be at the surface of a totally black sink. Figure 19.15 shows schematically the concentration profiles of point defects near a coherent precipitate–matrix interface. The rates at which vacancies and interstitials flow to the interface can be divided into two steps, which proceed in series. Between the bulk of the solid and the interface, the flow of point defects is governed by ordinary diffusion to a spherical sink. The driving force for this step is the concentration difference $C_v - C_v^*$ for vacancies and $C_i - C_i^*$ for interstitials. For diffusion-controlled absorption by a spherical

*This unique property means that coherent precipitates are capable of removing point defects from a solid in which the point-defect concentrations are at the equilibrium values C_v^{eq} and C_i^{eq}. Or these supposedly thermodynamic quantities are determined by Eqs. 19.20 and 19.23 only in solids that contain no coherent precipitates. If coherent precipitate particles are added to a solid that initially contained its equilibrium complement of point defects, the precipitates would augment the homogeneous recombination process and thereby depress the concentrations of vacancies and interstitials below the equilibrium value. The extent of the decrease would depend on the number of precipitate particles and the density of network dislocations in the solid. The latter are the principal suppliers or removers of point defects when the equilibrium concentrations are perturbed by the introduction of sources (e.g., by irradiation) or sinks (in the case of coherent precipitates). Despite the unpalatable theoretical consequences of the lack of thermal emission of point defects from coherent precipitates in a solid, the practical effect on C_v^{eq} is negligible (see problem 19.11 at the end of this chapter).

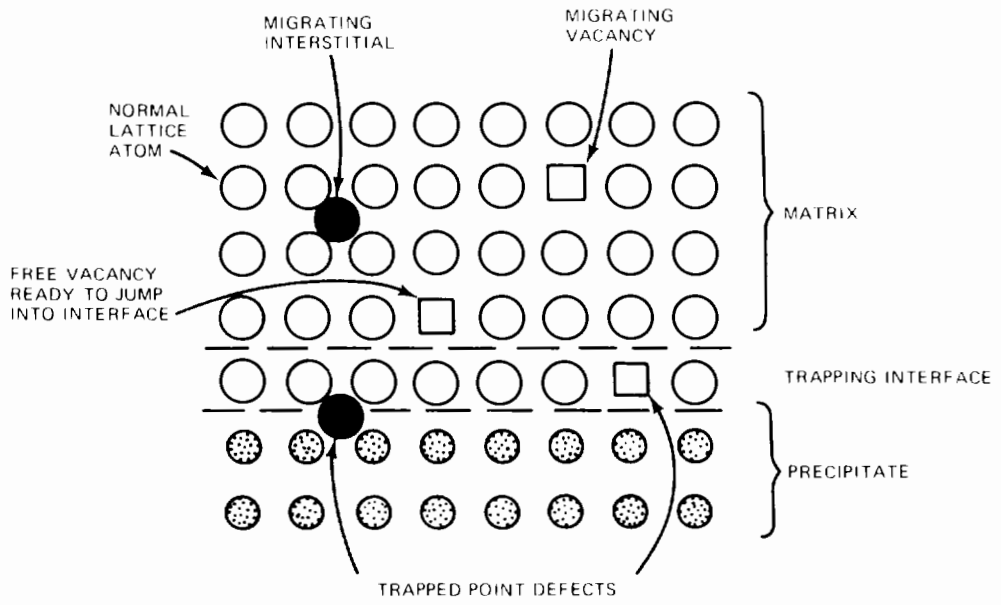

Fig. 19.14 Schematic diagram of the interface between a coherent precipitate particle and the host matrix. (After Ref. 23.)

body in which the concentrations at $r = R_p$ (the particle radius) and $r = \infty$ (the bulk solid) are specified, the fluxes are given by Eq. 13.65:

$$J_v = \frac{D_v}{R_p}(C_v - C_v^*) \tag{19.113}$$

and

$$J_i = \frac{D_i}{R_p}(C_i - C_i^*) \tag{19.114}$$

where J_v and J_i are the number of point defects reaching a unit area of precipitate per unit time. Because there is no net accumulation of either type of point defect at the interface, the fluxes must obey

$$J_v = J_i \tag{19.115}$$

The concentrations C_v^* and C_i^* refer to the matrix adjacent to the trapping interface. In order to evaluate these concentrations, we must consider the second step in the series, that of point-defect attachment to the interface. We first determine the rate at which point defects impinge on the trapping interface from the adjacent matrix when the vacancy and interstitial concentrations here are C_v^* and C_i^*, respectively. Consider the case of vacancies. The plane of matrix atoms above the interface plane contains $1/a_o^2$ lattice sites per unit area from which a vacancy can hop toward the interface. The fraction of lattice sites that are occupied by vacancies in the matrix at this point is $C_v^*\Omega = C_v^* a_o^3$, where Ω is the atomic volume and a_o is the lattice parameter. Therefore, a total of $(a_o^{-2})(C_v^* a_o^3) = a_o C_v^*$ vacancies per unit area can potentially reach the trapping interface in one jump. The frequency with which a vacancy jumps in any one direction in the matrix is w_v (Sec. 7.2). For the fcc lattice, w_v is related to the vacancy diffusion coefficient by Eq. 7.29. Thus the rate at which vacancies impinge on a unit area of trapping surface is given by

$$\text{Vacancy impingement rate} = (a_o C_v^*) w_v = (a_o C_v^*)\left(\frac{D_v}{a_o^2}\right) = \frac{D_v C_v^*}{a_o}$$

Similarly, the interstitial impingement rate on the interface from the adjacent matrix is $D_i C_i^*/a_o$. These impingement rates can be regarded as the solid-state analogs of the rate at which molecules from a gas strike a unit area of surface. To determine whether the impinging vacancies and interstitials stick or are reflected back to the matrix, we need to calculate the fraction of the available sites on the trapping interface which are occupied by the two types of point defects. To do this, imagine the trapping interface to be a simple square grid that binds vacancies at the mesh points and interstitials in the open spaces. The mesh-point sites may either be occupied by a trapped vacancy or empty (i.e., occupied by an atom). Similarly, the interstitial trapping sites may either be occupied by a trapped interstitial atom or empty. Let θ_v = fraction of vacancy trapping sites on the interface occupied by vacancies and θ_i = fraction of interstitial trapping sites on the interface occupied by interstitials. A vacancy is trapped only if it jumps into an unoccupied site; the probability of so doing is $1 - \theta_v$. The rate at which vacancies are trapped on the interface is the product of the impingement rate and the fraction of unoccupied sites. Since the process of diffusion from the bulk to the interface is in series with the process of attachment to the interface, we equate the rates of diffusion and trapping,* or

*Equating the rates of sequential processes is also used in analyzing series resistances in heat-transfer processes.

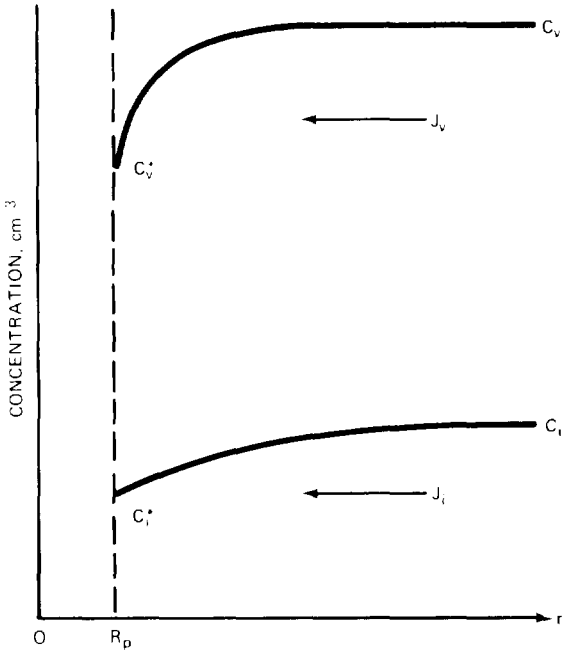

Fig. 19.15 Vacancy- and interstitial-concentration profiles next to a coherent precipitate particle.

$$J_v = \frac{D_v}{R_p}(C_v - C_v^*) = \frac{D_v C_v^*}{a_o}(1 - \theta_v) \qquad (19.116)$$

For interstitials, the analogous formula is

$$J_i = \frac{D_i}{R_p}(C_i - C_i^*) = \frac{D_i C_i^*}{a_o}(1 - \theta_i) \qquad (19.117)$$

To deduce the connection between the point-defect occupation of the trapping interface (the θ's) and the point-defect concentration in the matrix adjacent to the trapping interface (the C*'s), we must specify the details of the interaction between the free point defects and the trapped ones. Many models of this interaction can be constructed; here we will investigate a primitive model similar to that invoked by Brailsford and Bullough[23] in their analysis of the same phenomenon (the present model differs from theirs in that recombination reactions between trapped point defects are not considered here). Three possible fates of a vacancy impinging on the trapping interface are depicted in Fig. 19.16. The impinging vacancy may:

(a) Strike a site already occupied by a vacancy, in which case the impinging vacancy is returned to the matrix.

(b) Enter an unoccupied site that is adjacent to a trapped interstitial. The probability of this event is $z\theta_i$, where z is the number of vacancy sites surrounding a trapped interstitial which result in certain recombination when jointly occupied (for the simple square interfacial structure, z = 4).

(c) Enter an unoccupied site that is not adjacent to a trapped interstitial. The probability of such a jump is $1 - \theta_v - z\theta_i$.

The consequences of interstitial atom impingement on the interface are obtained from processes (a) to (c) by interchanging the subscripts i and v.

We now construct a balance equation for the trapped vacancies and interstitials. Because the system is at steady state, θ_v and θ_i are time independent, or the rate at which point defects become incorporated into the interface by process (c) must be equal to the rate at which they are removed by process (b). Note that process (b) removes a point defect of the opposite type from that which process (c) adds to the interface. Conservation of trapped vacancies is expressed by

$$\frac{D_v C_v^*}{a_o}(1 - \theta_v - z\theta_i) = \frac{D_i C_i^*}{a_o}\theta_v \qquad (19.118)$$

where the left side is the input due to the fraction of impinging vacancies that strike an unoccupied site that is not adjacent to a trapped interstitial and the right side is the rate of removal of trapped vacancies by impinging interstitials from the nearby matrix. The balance on trapped interstitials yields

$$\frac{D_i C_i^*}{a_o}(1 - \theta_i - z\theta_v) = \frac{D_v C_v^*}{a_o}\theta_i \qquad (19.119)$$

Subtracting Eq. 19.119 from Eq. 19.118 yields

$$D_i C_i^*(1 - \theta_i) = D_v C_v^*(1 - \theta_v)$$

which, when compared with Eqs. 19.116 and 19.117, simply confirms the fact that the fluxes of the two types of point defects from the bulk to the coherent precipitate are equal no matter which step of the two back-to-back processes is considered.

Equations 19.118 and 19.119 can be solved for θ_v and θ_i to yield

$$\theta_v = \frac{\gamma^*[1 + (\gamma^* - 1)z]}{\gamma^{*2}z + \gamma^* + z} \qquad (19.120)$$

$$\theta_i = \frac{\gamma^* + z - \gamma^* z}{\gamma^{*2}z + \gamma^* + z} \qquad (19.121)$$

where

$$\gamma^* = \frac{D_v C_v^*}{D_i C_i^*} \qquad (19.122)$$

In Fig. 19.17 θ_v and θ_i are shown as functions of the parameter γ^* for a fixed value of z (e.g., z = 4). Equations 19.120 and 19.121 apply only in the range

$$\frac{z-1}{z} \leq \gamma^* \leq \frac{z}{z-1} \qquad (19.123)$$

Beyond this range, either θ_i or θ_v is zero, and the other is given by the formulas shown on the graph. When $\gamma^* = 1$, θ_i and θ_v are both equal to $(1 + 2z)^{-1}$.

The trapping and recombination efficiency of the interface has been analyzed with the aid of a particular model of what goes on at the boundary separating the precipitate particle and the host matrix. Other models of these interactions are certainly possible, but they will all lead to relations between the θ's and γ's of the type shown

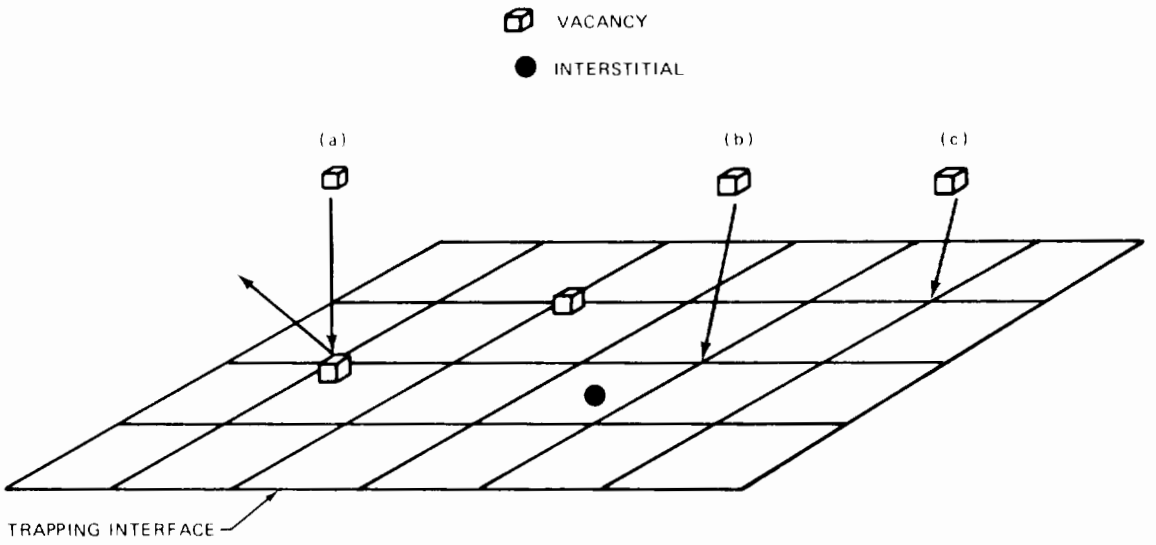

Fig. 19.16 Consequences of vacancy impingement on a coherent precipitate particle. See text for a discussion of the processes labeled a, b, and c.

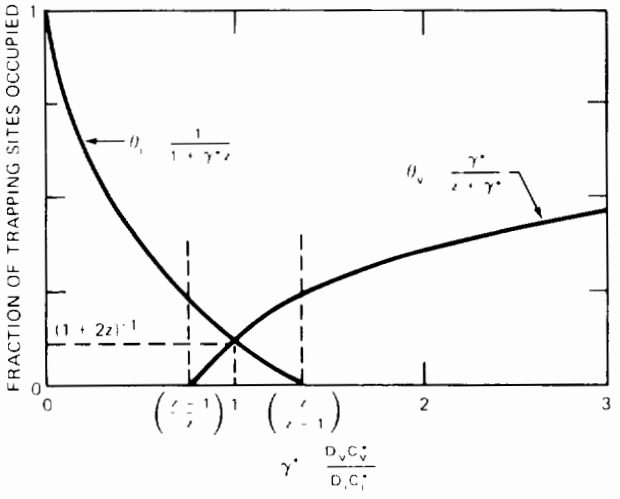

Fig. 19.17 Point-defect occupation probabilities of the trapping interface for a simple model.

in Fig. 19.17. Although this aspect of the theory is dependent on the model chosen, the development up to Eq. 19.117 and what follows from now on are applicable to any mechanism of trapping.

If we use the second equalities of Eqs. 19.116 and 19.117, C_v^*/C_v and C_i^*/C_i can be expressed as functions of θ_v and θ_i:

$$\frac{C_v^*}{C_v} = \left[1 + \frac{R_p}{a_o}(1-\theta_v)\right]^{-1} \tag{19.124}$$

$$\frac{C_i^*}{C_i} = \left[1 + \frac{R_p}{a_o}(1-\theta_i)\right]^{-1} \tag{19.125}$$

Now J_v and J_i are set equal to each other and the C^*'s are expressed in terms of the θ's by the above formulas. These manipulations lead to

$$\left(\frac{D_vC_v}{D_iC_i}\right)\frac{(1-\theta_v)}{(a_o/R_p)+(1-\theta_v)} = \frac{(1-\theta_i)}{(a_o/R_p)+(1-\theta_i)} \tag{19.126}$$

According to Eqs. 19.120 and 19.121, θ_v and θ_i are functions of the single parameter γ^* (assuming z is a specified constant). Inserting these equations into Eq. 19.126 determines γ^* as a function of D_vC_v/D_iC_i, which is specified by the bulk concentration of point defects. Once γ^* is determined, θ_v and θ_i are obtained from Eqs. 19.120 and 19.121, and C_v^*/C_v and C_i^*/C_i, from Eqs. 19.124 and 19.125. The desired fluxes of vacancies and interstitial atoms to the coherent precipitates are then obtained by eliminating C_v^* and C_i^* from the fluxes given by Eqs. 19.113 and 19.114. Multiplying J_v and J_i by $4\pi R_p^2 N_p$ (where N_p is the number of precipitate particles per unit volume of solid) yields Q_v^p and Q_i^p, the removal rates of vacancies and interstitials per unit volume of metal by the coherent precipitates. Following the procedure described above yields

$$Q_v^p = 4\pi R_p N_p D_v C_v Y_v \tag{19.127}$$

$$Q_i^p = 4\pi R_p N_p D_i C_i Y_i \tag{19.128}$$

where

$$Y_v = \frac{(1-\theta_v)}{(a_o/R_p)+(1-\theta_v)} \tag{19.129}$$

$$Y_i = \frac{(1-\theta_i)}{(a_o/R_p)+(1-\theta_i)} \tag{19.130}$$

and θ_v and θ_i are known functions of the ratio D_vC_v/D_iC_i determined by the method outlined above. The coefficients Y_v and Y_i represent the biasing of point-defect fluxes to the coherent precipitates. They are analogous to the coefficients Z_v and Z_i which established the preference of dislocations for interstitials. For coherent precipitates,

however, the biasing coefficients Y_v and Y_i depend on D_vC_v/D_iC_i, which is in turn established by the strengths of the other point defects in the system. Thus, the biased absorption properties of coherent precipitates depend on the environment in which the precipitates are situated, which is not the case for the fixed-bias dislocations. The manner in which the coherent precipitates function can be illustrated qualitatively as follows. Because $Z_i > Z_v$ by a percent or so, D_vC_v/D_iC_i is greater than unity by a comparable amount (otherwise voids would not nucleate or grow). Since $D_vC_v/D_iC_i > 1$, Eq. 19.126 shows that $\theta_v > \theta_i$ or, according to Eqs. 19.129 and 19.130, $Y_i > Y_v$. The requirement that there be no net accumulation of point defects at the coherent precipitates (as expressed by Eq. 19.126) leads to

$$Y_i = \left(\frac{D_vC_v}{D_iC_i}\right)Y_v \tag{19.131}$$

so the problem is reduced to one of finding the magnitude of Y_v (or of Y_i). If the precipitate radius, R_p, is reasonably large (say several hundreds of angstroms), the ratio a_o/R_p is small ($\sim 10^{-2}$). If, in addition, the ratio D_vC_v/D_iC_i is close to unity, then the parameter γ^* will also be close to unity, and Fig. 19.17 shows that θ_v and θ_i are equal to $\sim(2z + 1)^{-1} \sim 10^{-1}$. For this situation, Eqs. 19.129 and 19.130 show that Y_v and Y_i are both close to unity. We may make the approximation

$$\begin{aligned} Y_v &\simeq 1 \\ Y_i &\simeq \frac{D_vC_v}{D_iC_i} \end{aligned} \tag{19.132}$$

and Eqs. 19.127 and 19.128 reduce to

$$Q_v^p = Q_i^p = 4\pi R_p N_p D_v C_v \tag{19.133}$$

This equation adequately describes the strength of coherent precipitate sinks in irradiated metals.

19.5.10 Point-Defect Balances

Having determined the rate of production of vacancies and interstitials from fast-neutron collisions with lattice atoms and the rates at which the point defects are consumed by various processes involving the large defects in the solid, we can write the steady-state point-defect balances as

$$\nu\Sigma_s\Phi = Q_v^{void} + Q_v^N + Q_v^L + Q_v^p + \text{homo. recomb.} \tag{19.134}$$

for vacancies, and

$$\nu\Sigma_s\Phi = Q_i^{void} + Q_i^N + Q_i^L + Q_i^p + \text{homo. recomb.} \tag{19.135}$$

for interstitials.

The vacancy-removal rates per unit volume of solid, Q_v^{void}, Q_v^N, and Q_v^L, are given by Eqs. 19.95, 19.101, and 19.111. The corresponding terms for interstitial removal are given by Eqs. 19.96, 19.102, and 19.112 (the thermal emission term in the last of these formulas can be neglected). The rate of absorption of both types of point defects by coherent precipitates is given by Eq. 19.133. The rate of homogeneous recombination is $k_{iv}C_vC_i$, where k_{iv} is given by Eq. 13.42. With these sink strengths, Eqs. 19.134 and 19.135 become

$$\begin{aligned} \nu\Sigma_s\Phi = {} & 4\pi RND_v\left[C_v - C_v^{eq}\exp\left(\frac{2\gamma\Omega}{RkT}\right)\right] \\ & + Z_v\rho_N D_v\,(C_v - C_v^{eq}) \\ & + Z_v\rho_l D_v\left[C_v - C_v^{eq}\exp\left(-\frac{K}{2(\bar{m}_i)^{1/2}\,kT}\right)\right] \\ & + 4\pi R_p N_p D_v C_v + k_{iv}C_iC_v \end{aligned} \tag{19.136}$$

and

$$\begin{aligned} \nu\Sigma_s\Phi = {} & 4\pi RND_iC_i + Z_i\,(\rho_N + \rho_l)\,D_iC_i \\ & + 4\pi R_pN_pD_vC_v + k_{iv}C_iC_v \end{aligned} \tag{19.137}$$

Equations 19.136 and 19.137 can be solved for C_v and C_i (analytical solutions are reported in Ref. 23). For N, ρ_l, and $N_p = 0$, the point-defect balances given above reduce to those obtained earlier for treating fission-gas bubble growth in the fuel (Eqs. 13.186 and 13.187, in which $C_i^{eq} = 0$). The general shape of plots of C_v and C_i as functions of temperature are shown in Fig. 13.17. Such solutions are needed for fixing the supersaturations S_v and S_i in nucleation theory and for void growth.

19.5.11 The Void-Growth Law

The void-growth law is the time rate of change of the void radius R at any instant during irradiation. The void is assumed to be spherical, and its growth is controlled by diffusion of vacancies and interstitials from the bulk of the solid to the void surface. The growth law under these circumstances was derived in Sec. 13.9 for the case of a cavity that contained some gas (i.e., a bubble). The same growth law is valid for the gas-free cavity (the void) provided that the internal gas pressure is set equal to zero wherever it appears. The void-growth law is obtained from Eqs. 13.171 and 13.176, with p = 0 in the latter,

$$\begin{aligned} \dot{R} &= \frac{dR}{dt} \\ &= \frac{\Omega}{R}\left\{D_v\left[C_v - C_v^{eq}\exp\left(\frac{2\gamma\Omega}{RkT}\right)\right] - D_iC_i\right\} \end{aligned} \tag{19.138}$$

The concentration of interstitials at the void surface (Eq. 13.179) has been neglected because of the large energy of formation of this point defect.

Brailsford and Bullough[23] have inserted the solutions of Eqs. 19.136 and 19.137 into Eq. 19.138 and expressed the void-growth rate in the following form:

$$\dot{R} = \dot{R}_0\,F(\eta) + \dot{R}_e \tag{19.139}$$

where $\dot{R}_0$ is the void-growth rate in the absence of both homogeneous recombination ($k_{iv} = 0$) and thermal emission ($C_v^{eq} = 0$),

$$\dot{R}_0 = \frac{\nu\Sigma_s\Phi\rho_d(Z_i - Z_v)\Omega}{R(Z_v\rho_d + 4\pi RN)(Z_i\rho_d + 4\pi RN + 4\pi R_pN_p)} \quad (19.140)$$

where

$$\rho_d = \rho_N + \rho_l \quad (19.141)$$

is the total dislocation density in the solid. This growth contribution is independent of temperature and depends on the dislocation bias for interstitials $Z_i - Z_v$ and the morphology of the solid (i.e., the number and size of voids, precipitates, and the dislocation density). It is also directly proportional to the defect-production rate, or the fast-neutron flux.

The effect of homogeneous recombination on void growth is contained in the factor F in Eq. 19.139, which is*

$$F(\eta) = \frac{2}{\eta}[(1+\eta)^{1/2} - 1] \quad (19.142)$$

where η is the dimensionless parameter

$$\eta = 4k_{iv}\nu\Sigma_s\Phi\,[D_vD_i(Z_v\rho_d + 4\pi RN + 4\pi R_pN_p) \times (Z_i\rho_d + 4\pi RN + 4\pi R_pN_p)]^{-1} \quad (19.143a)$$

or, eliminating k_{iv} by use of Eq. 13.42 and setting $Z_i = Z_v$,

$$\eta = \frac{4z_{iv}\nu\Sigma_s\Phi\Omega}{D_va_o^2(Z_v\rho_d + 4\pi RN + 4\pi R_pN_p)^2} \quad (19.143b)$$

When homogeneous recombination is negligible ($k_{iv} \to 0$ or $\eta \to 0$), the factor F reduces to unity.

The effect of thermal emission from the various sinks is contained in the void-shrinkage term $\dot{R}_e$:

$$\dot{R}_e = -D_vC_v^{eq}\Omega\left\{4\pi R_pN_p\exp\left(\frac{2\gamma}{R}\frac{\Omega}{kT}\right) + Z_v\rho_N\left(\frac{2\gamma}{R}\frac{\Omega}{kT}\right) + Z_v\rho_l\left(\frac{2\gamma}{R}\frac{\Omega}{kT} + [K/2(\bar{m}_i)^{1/2}kT]\right)\right\} \times [R(Z_v\rho_d + 4\pi RN + 4\pi R_pN_p)]^{-1} \quad (19.144)$$

In the terms in the second and third lines of Eq. 19.144, differences in exponentials have been approximated by differences in the arguments. The value of $\dot{R}_e$ is independent of the defect-production rate and approaches zero at temperatures sufficiently low to render thermal emission negligible (i.e., $C_v^{eq} \to 0$).

19.5.12 The Factor $\dot{R}_0$

When no coherent precipitates are present, $\dot{R}_0$ can be written as

$$\dot{R}_0 = \frac{\nu\Sigma_s\Phi\Omega}{4\pi R^2N}\left(\frac{Z_i - Z_v}{Z_v}\right)\frac{x}{(1+x)^2} \quad (19.145)$$

where

$$x = \frac{4\pi RN}{Z_v\rho_d} \quad (19.146)$$

Equation 19.145 demonstrates that both a biased sink (with $Z_i - Z_v$ greater than zero) and a neutral sink (which for voids provides the term $4\pi RN$) are necessary for void growth. The balance between the strengths of the neutral and biased sinks, as exemplified by the dimensionless quantity x, is crucial to void growth. The void-growth rate is a maximum when $x = 1$. If x is less than unity (as it would be at the beginning of irradiation), decreasing x by increasing the dislocation density reduces the rate of void growth. This behavior explains the ability of heavily cold-worked metals to resist void swelling at low fluences. If, however, $x > 1$ because of the development of a sizable void population, the primary role of the dislocations is to provide a preferential sink for interstitials, thereby permitting the excess vacancies to flow to the voids. In this case, highly cold-worked material promotes rather than deters void growth.

When coherent precipitates are present in the alloy and voids are not strong sinks for vacancies, $\dot{R}_0$ becomes

$$\dot{R}_0 = \frac{\nu\Sigma_s\Phi\Omega}{R}\left(\frac{Z_i - Z_v}{Z_v}\right)\frac{1}{Z_i\rho_d + 4\pi R_pN_p} \quad (19.147)$$

In this case the dislocations and the precipitate particles combine to reduce void growth. This theoretical prediction is in accord with the very low irradiation swelling of precipitate-containing alloys, such as Inconel and the steel PE-16.

19.5.13 Temperature Dependence of Void Growth

The two highly temperature sensitive parameters in the void-growth law are the vacancy diffusion coefficient D_v and the equilibrium vacancy concentration C_v^{eq}. The temperature dependence of the parameter η is controlled by D_v and the product $D_vC_v^{eq}$ appears in $\dot{R}_e$. At low temperatures, D_v becomes small and Eq. 19.143b shows that η becomes large. In this limit the factor F becomes small. As the temperature is reduced, Eq. 19.144 indicates that $\dot{R}_e$ approaches zero. Since both $F(\eta)$ and $\dot{R}_e$ become small at low temperature, Eq. 19.139 shows that void growth ceases in this limit.

At the opposite extreme of high temperature, η becomes small and F approaches unity; $\dot{R}_e$ then becomes increasingly negative. Thus the theory predicts a temperature at which the void-growth rate is a maximum, which corresponds to the observed peak swelling temperature. Beyond this temperature, void growth should rapidly decrease and eventually become negative since the voids tend to evaporate rather than grow. Figure 19.18 shows how the growth rate changes with temperature for typical fast reactor conditions. The characteristic bell-shaped swelling-temperature plot (Fig. 19.3) is quite well reproduced by the theory. The temperature limits of observable swelling

*A quantity denoted by μ in Ref. 23 has been omitted in Eq. 19.142. This simplification has no significant effect on the numerical values of the void-growth rate.

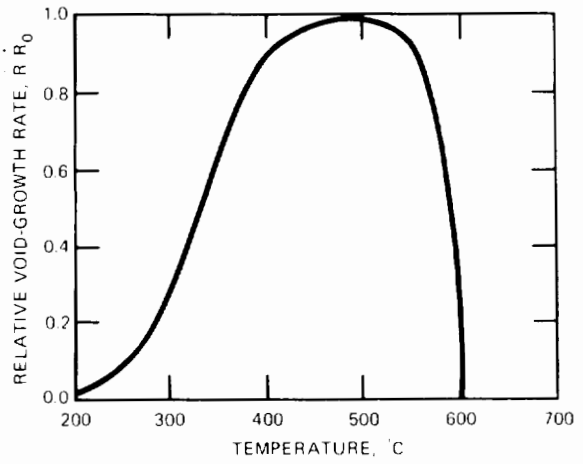

Fig. 19.18 Temperature dependence of the void-growth rate in stainless steel under fast-neutron irradiation. (After Ref. 23.)

and the peak swelling temperature are in accord with observations.

Brailsford and Bullough[23] have deduced an approximate analytical swelling law by simplification of the foregoing equations. However, in view of the change of the void density N and the dislocation density ρ_d during irradiation, the void-growth law should be incorporated into a more general analysis that includes the evolution of the microstructural features of the solid with irradiation time. Such a computation would require a loop-growth law in addition to a void-growth law. The loop size and concentration couple back into the void (and loop) growth laws via ρ_N, ρ_l, and the average loop size $\bar{m}$.

19.5.14 Stress-Enhanced Void Growth

The growth law developed above is valid only if the void contains no gas and if the metal is not under stress. However, in the temperature range for void growth, helium atoms produced by (n,α) reactions in the metal are sufficiently mobile to form gas-atom clusters in the lattice. As shown in Sec. 19.3, voids readily nucleate on these clusters; thus some gas must be contained in the voids as they enter their growth stage. In addition, the cladding of a fuel pin is always stressed, either by contact with swelling fuel or by internal pressure in the fuel pin arising from released fission gases. The state of stress in an internally loaded cylindrical tube is biaxial, but, to simplify matters, we consider here a metal subject to uniform hydrostatic tension. The theory of void growth needs modification to account for these two complications. We present the analysis of Brailsford and Bullough.[25]

Equation 19.139 shows that the void-growth rate consists of two components; $\dot{R}_e$ contains the thermal emission terms and hence is the only part affected by the state of stress or by internal gas pressure. Consequently, it follows that internal gas pressure and stress begin to influence the growth rate only when $\dot{R}_e$ becomes significant; i.e., for temperatures greater than the peak swelling temperature. Thus, we need only be concerned with $\dot{R}_e$, and, in particular, with how internal pressure and stress affect the equilibrium vacancy concentrations at the voids and the dislocations. Because stress- and gas-assisted growth are important only at high temperatures, we may neglect the presence of interstitial loops. These will have virtually disappeared by vacancy capture by ~600°C (see Fig. 19.7). The vacancy balances (with the deletion of the above-mentioned terms) are given by Eq. 19.136 if the vacancy concentration at the void surface is replaced by

$$C_v^{eq} \exp\left[\left(\frac{2\gamma}{R} - p\right)\left(\frac{\Omega}{kT}\right)\right]$$

The vacancy concentration at the void surface depends only on the normal stress at this point, which by a force balance is equal to $(2\gamma/R) - p$ (see Eq. 13.6). The stress in the medium does not affect the vacancy concentration at the void provided that the volume of a vacancy in the solid is equal to the atomic volume or that there is no lattice contraction around a vacancy. If this is not so (and, in general, it is not), the above expression for the vacancy concentration at the void surface must be modified.[26,27] We neglect this effect here but consider it in problem 19.8 at the end of this chapter.

The other term in the vacancy balance equation which needs to be altered is the equilibrium concentration of vacancies at the network dislocations, which depends on stress according to

$$C_v^{eq} \exp\left(\frac{\sigma\Omega}{kT}\right)$$

where σ is the hydrostatic tension in the solid.

If the modified vacancy balance and the unchanged interstitial balance given by Eq. 19.137 are substituted into the void-growth rate formula (Eq. 19.138 in which the vacancy concentration at the void surface altered to account for internal gas pressure as indicated above), $\dot{R}_0$ and $F(\eta)$ are found to be unchanged. However, $\dot{R}_e$, which was formerly given by Eq. 19.144, becomes (with N_p and $\rho_l = 0$)

$$\dot{R}_e = \frac{D_v C_v^{eq} \Omega^2 Z_v \rho_d \left(\sigma + p - \frac{2\gamma}{R}\right)}{RkT(Z_v\rho_d + 4\pi RN)} \qquad (19.148)$$

In the gas- and stress-free case, the parenthetical term in the numerator is always negative, and $\dot{R}_e$ represents a shrinkage. However, the sign of $\dot{R}_e$ can change when the void contains gas and the solid is in tension. Shrinkage due to thermal emission changes to stress-enhanced growth* when

$$\sigma + p = \frac{2\gamma}{R} \qquad (19.149)$$

The critical stress for unlimited void growth, which depends on the gas content of the cavity, can be obtained in the same manner as that employed in deriving the analogous condition for void growth of helium bubbles on grain boundaries (Sec. 18.10). Suppose that the void contains j helium atoms. The internal pressure is given by the perfect gas law (Eq. 18.96), and Eq. 19.149 becomes

*Stress-enhanced swelling is also called volume creep.

$$\sigma = \frac{2\gamma}{R} - \frac{3jkT}{4\pi R^3}$$

The critical void radius occurs when $d\sigma/dR = 0$ and the stress at this void size is the critical stress for unlimited void growth:

$$\sigma_{crit} = \left(\frac{128\pi\gamma^3}{81jkT}\right)^{1/2} \qquad (19.150)$$

which, if j is expressed in terms of the radius of the stress-free equilibrium bubble containing j helium atoms (by Eq. 18.94), reduces to the Hyam–Sumner relationship (Eq. 18.98).* The only difference between helium bubbles on a grain boundary and helium-containing voids in the grains of the solid is the growth law, which is given by Eq. 18.102 for grain-boundary helium bubbles and by Eq. 19.148 for helium-containing voids within the grain.

Whether unbounded stress-enhanced void growth will occur for a specified hydrostatic tension depends on the number of gas atoms in the void. The total quantity of helium gas produced in the metal was discussed in Sec. 18.10. The helium content of stainless steel increases linearly with time (Fig. 18.40). If there are M atoms of helium per unit volume of the metal and if all the gas is equally distributed among N equal-size voids, j would be fixed as M/N. However, the available helium is, in general, partitioned among the matrix, the voids, and the grain-boundary bubbles. Determination of the fraction of the gas which is in the voids requires calculations similar to those presented in Secs. 13.9 and 15.7 for obtaining the distribution of fission-gas atoms in the same three locations in the fuel. We saw in Sec. 19.3 that void nucleation requires only a few helium atoms per void embryo. Unless much more helium is collected by the voids during the growth period, j in Eq. 19.150 may be quite small, and the critical stress may always be much larger than the applied stress (when $\sigma < \sigma_{crit}$, the void shrinks rather than expands).

Brailsford and Bullough have integrated the void-growth law (Eq. 19.139) with $\dot{R}_c$ given by Eq. 19.148.† The computations were performed for applied uniaxial tension, which requires that σ in Eq. 19.148 be replaced by $\sigma/3$. Helium was generated at a rate appropriate to fast reactor conditions; so j increased linearly with time. Since nucleation theory was not incorporated into the calculation, the void and loop densities had to be arbitrarily specified. Typical results of these computations are shown in Fig. 19.19, in which the ordinate is the volume swelling for a population of uniform size voids. Stress-assisted growth becomes dramatic at high temperature because $D_v C_v^{eq}$ in Eq. 19.148 becomes large. The rather sudden onset of swelling in the high-stress 700 and 800°C curves is due to the delay time required for sufficient helium to have trickled into the voids to render σ_{crit} of Eq. 19.150 equal to the specified stress. The 600°C results are insensitive to stress because the first term in Eq. 19.139 is the primary contributor to void growth at this temperature.

Figure 19.20 shows similar theoretical results as a function of temperature. The double hump in the swelling curve has not been confirmed by reactor irradiations of steel, but this unexpected shape has been found in ion-bombarded metals at a higher dose than obtainable with fast neutrons.

Restriction of the stress enhancement of void growth to temperatures in excess of 600°C suggests that the assump-

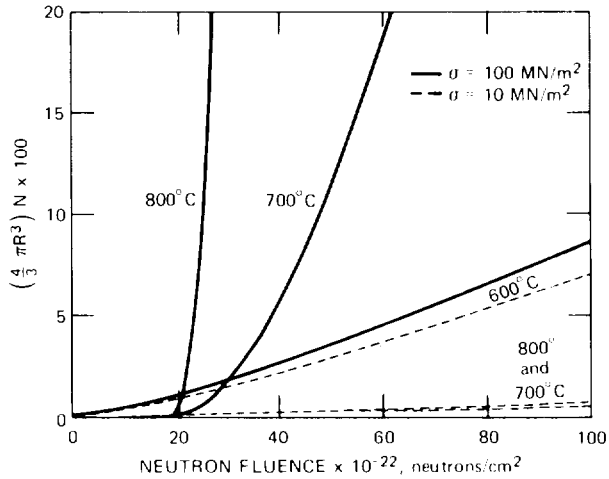

Fig. 19.19 Stress-enhanced swelling for various stress levels and temperatures as a function of fluence. (After Ref. 25.)

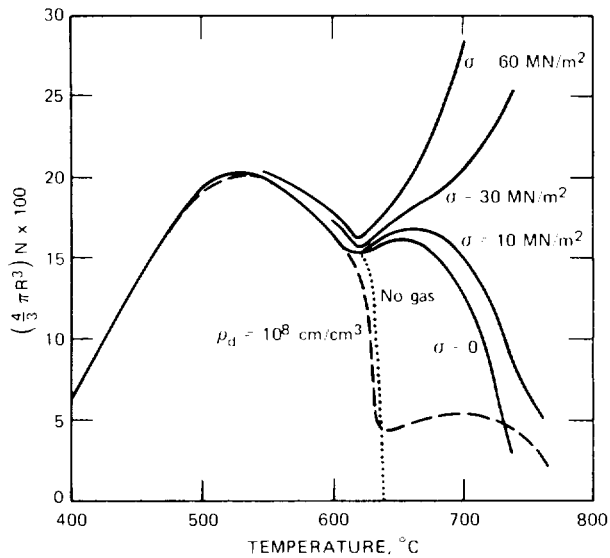

Fig. 19.20 Temperature dependence of stress-enhanced void growth in steel. The solid curves apply to a dislocation density of 10^9 cm^{-2} and a helium production rate of 10^{-6} ppma/sec. (From A. D. Brailsford and R. Bullough, British Report AERE-TP-542, 1973.)

*Equation 40 of Ref. 25 (when divided by 3 to convert from uniaxial to hydrostatic stress) appears to be in error by a factor of 2.

†Actually, the complete theory, with loops and grain boundaries included as sinks in $\dot{R}$, was employed, and loop growth laws were used to determine the change in the dislocation population. The simplified form given by Eq. 19.148 is accurate at high temperatures.

tion inherent in the analysis that all helium is in the voids may be unrealistic. If most of the gas agglomerates on grain boundaries, the growth law is that of Eq. 18.102, not Eq. 19.148.

19.5.15 Saturation of Void Growth

The theory just developed predicts that voids continue to grow indefinitely in an irradiated metal; no mechanism for saturation of growth is provided. Equation 19.145 shows that as the void size R increases the growth rate decreases but never ceases entirely. The only way that void growth can be completely halted is to remove the preferential bias of the dislocations for interstitials or, equivalently, to imbue the voids with the same preferential attraction for interstitials as the dislocations.

Harkness and Li[28] have proposed a mechanism of terminating void growth which is based on the first of these two possibilities. They seek to determine the conditions under which all the dislocations become interconnected with the voids in a stable manner. If the dislocations are securely pinned to voids, they (the dislocations) can no longer climb freely, and hence their ability to absorb more interstitials than vacancies is eliminated. Here we reanalyze their proposal by extension of the method used previously to determine the equilibrium concentration of point defects at an interstitial dislocation loop.

Consider a single void and the curved length of dislocation line between voids. The associated solid contains n_v vacancies and n_i interstitials at concentrations C_v and C_i, respectively. We calculate the void radius R and the dislocation-line length $\mathscr{l}$ for which the system is stationary in the specified point-defect environment. The void-dislocation segment configuration is depicted in Fig. 19.21(b), where the two halves of the void at the termination of the dislocation-line segment are shown in place of a single void. The remainder of the solid is assumed to be a repetition of the basic unit shown in Fig. 19.21(b), which means that the microstructure appears as sketched in Fig. 18.22(b). The case in which the vacancies and interstitials are in equilibrium (i.e., $C_iC_v = C_i^{eq}C_v^{eq}$) is treated first. The derivation is then extended to arbitrary point-defect concentrations. The general method of calculations of this type have been outlined by Straalsund[29] and by Wiedersich and Herschbach.[30]

The Gibbs free energy of the system shown in Fig. 19.21(b) is given by

$$G = G_0 + \epsilon(m_v,m_i) + n_v\mu_v + n_i\mu_i \qquad (19.151)$$

where μ_v and μ_i are the chemical potentials of the vacancies and interstitials (for the first portion of the analysis, $\mu_v = -\mu_i$, indicating equilibrium between the two types of point defects); and G_0 is the free energy of the system containing the length l of dislocation line, but no void, in a solid wherein the point-defect concentrations are C_v^{eq} and C_i^{eq}, respectively [Fig. 19.21(a)]. As with the interstitial loop, a void is not thermodynamically stable under these conditions. Dislocation lines, however, can exist in a solid containing equilibrium point-defect concentrations. When the point-defect concentrations are changed from C_v^{eq} and C_i^{eq}, μ_v and μ_i are no longer zero, and the void-dislocation

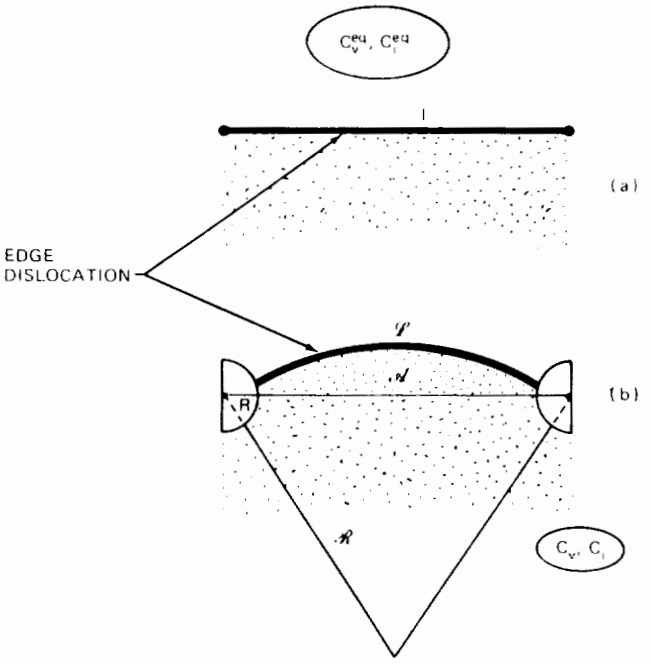

Fig. 19.21 Unit of a system of interconnected voids and dislocations. The shaded area below the dislocation-line segment denotes the extra half-sheet of atoms comprising the edge dislocation.

line segment shown in Fig. 19.21(b) is created from the n_v vacancies and n_i interstitials in the piece of solid under examination. The energy of the entity shown in Fig. 19.21(b) is denoted by $\epsilon(m_v,m_i)$, where m_v is the number of vacancies needed to form the void and m_i is the number of interstitials required for the dislocation line to climb from its original location in Fig. 19.21(a) to the equilibrium position in Fig. 19.21(b). If C_i and C_v are such that climb occurs in the opposite direction from that shown in Fig. 19.21(b), m_i is negative, which means that vacancies rather than interstitials have been absorbed by the pinned segment of dislocation line. The energy $\epsilon(m_v,m_i)$ is given by the sum of the energies of the void and the associated length of dislocation line:

$$\epsilon(m_v,m_i) = 4\pi R^2\gamma + (\mathscr{l}-l)\tau_d \qquad (19.152)$$

where γ is the surface tension of the solid and τ_d is the line tension of the dislocation. The change in the length of line in going from the configuration of Fig. 19.21(a) to that of Fig. 19.21(b) is $\mathscr{l} - l$. The first term on the right of Eq. 19.152 depends only on the number of vacancies in the void because m_v and R are related by

$$m_v = \frac{4\pi R^3}{3\Omega} \qquad (19.153)$$

Similarly, the second term on the right is a function of m_i, which is related to the area of the circular segment added to the half-sheet of atoms comprising the edge dislocation:

$$m_i = \frac{b\cdot\mathscr{A}}{\Omega} \qquad (19.154)$$

If the system shown in Fig. 19.21(b) is at equilibrium, the criterion of chemical equilibrium requires that the Gibbs free energy given by Eq. 19.151 be invariant when small perturbations δm_v, δm_i, δn_v, and δn_i are applied,

$$\delta G = \left(\frac{\partial \epsilon}{\partial m_v}\right)\delta m_v + \left(\frac{\partial \epsilon}{\partial m_i}\right)\delta m_i + \mu_v \delta n_v + \mu_i \delta n_i = 0$$

The perturbations in the numbers of point defects in each location are related by the balance:

$$\delta m_i - \delta m_v = \delta n_v - \delta n_i$$

The perturbation δm_v can be eliminated by combining the preceding two equations. The resulting equation contains δm_i, δn_v, and δn_i. Since each of these three perturbations is independent and arbitrary, the coefficients of all three must be individually equated to zero to attain the minimum Gibbs free energy of the system, which leads to three equations:

$$\left(\frac{\partial \epsilon}{\partial m_v}\right)_{m_i} + \left(\frac{\partial \epsilon}{\partial m_i}\right)_{m_v} = 0 \qquad (19.155a)$$

$$\left(\frac{\partial \epsilon}{\partial m_v}\right)_{m_i} - \mu_v = 0 \qquad (19.155b)$$

$$\left(\frac{\partial \epsilon}{\partial m_v}\right)_{m_i} + \mu_i = 0 \qquad (19.155c)$$

Because we have required equilibrium between the two types of point defects in the bulk solid (i.e., $\mu_i = -\mu_v$), Eqs. 19.155b and 19.155c are equivalent. Thus there are two independent relations, which serve to fix the equilibrium void radius R and the dislocation configuration (determined, for convenience, by the radius of curvature $\mathscr{R}$).

The equilibrium void size is obtained from Eq. 19.155b, which can be written

$$\left(\frac{\partial \epsilon}{\partial m_v}\right)_{m_i} = \left(\frac{\partial \epsilon}{\partial R}\right)_{\mathscr{P}} \frac{dR}{dm_v} = \left(\frac{2\gamma}{R}\right)\Omega$$

The first term in the product of this formula is, according to Eq. 19.152, equal to $8\pi R\gamma$, and Eq. 19.153 shows that the second term is $\Omega/4\pi R^2$. The chemical potential of the vacancies is $kT \ln(C_v/C_v^{eq})$; so Eq. 19.155b yields

$$C_v = C_v^{eq} \exp\left(\frac{2\gamma\ \Omega}{R\ kT}\right) \qquad (19.156a)$$

and, using the restraint $C_v C_i = C_v^{eq} C_i^{eq}$,

$$C_i = C_i^{eq} \exp\left(-\frac{2\gamma\ \Omega}{R\ kT}\right) \qquad (19.156b)$$

Equation 19.156a can be recognized as the equilibrium concentration of vacancies at the surface of an isolated void in the solid (i.e., Eq. 19.95).

Combining Eqs. 19.155a and 19.155b yields

$$\left(\frac{\partial \epsilon}{\partial m_i}\right)_{m_v} + \mu_v = 0$$

The derivative in this formula is obtained from Eqs. 19.152 and 19.154:

$$\left(\frac{\partial \epsilon}{\partial m_i}\right)_{m_v} = \tau_d \left(\frac{\partial \mathscr{P}}{\partial m_i}\right)_{m_v}$$

$$= \tau_d \left(\frac{d\mathscr{A}}{dm_i}\right)\left(\frac{\partial \mathscr{P}}{\partial \mathscr{A}}\right)_R$$

$$= \frac{\tau_d \Omega}{b}\left(\frac{\partial \mathscr{P}}{\partial \mathscr{A}}\right)_R$$

The partial derivative in the last line of this set of equalities (which is taken at constant R because m_v is held constant in the derivative on the left) is determined solely by the geometry of the curved dislocation in Fig. 19.21(b). In problem 19.16 at the end of this chapter, $(\partial \mathscr{P}/\partial \mathscr{A})_R$ is found to be of the form

$$\left(\frac{\partial \mathscr{P}}{\partial \mathscr{A}}\right)_R = \frac{1}{\mathscr{R} f(R, \mathscr{R}, l)} \qquad (19.157)$$

where the function $f(R, \mathscr{R}, l)$ approaches unity as the void radius approaches zero. Combining the preceding three equations with the vacancy chemical potential yields

$$C_v = C_v^{eq} \exp\left(-\frac{\tau_d}{b\mathscr{R}f}\frac{\Omega}{kT}\right) \qquad (19.158a)$$

and, with the restriction $C_v C_i = C_v^{eq} C_i^{eq}$,

$$C_i = C_i^{eq} \exp\left(\frac{\tau_d}{b\mathscr{R}f}\frac{\Omega}{kT}\right) \qquad (19.158b)$$

If either C_v or C_i is specified, Eqs. 19.156 and 19.158 determine the void size R and the dislocation line radius of curvature $\mathscr{R}$ for a specified void spacing l, which is related to the size and density of voids in the solid by Eq. 18.25:

$$l = \frac{1}{(2RN)^{1/2}} \qquad (19.159)$$

We now examine the case in which the vacancies and the interstitials are not in equilibrium (i.e., $C_i C_v \neq C_i^{eq} C_v^{eq}$). This situation cannot be treated by equilibrium methods;[29,30] so, instead of a thermodynamic analysis, we can only require that the system be in a stationary state. This means that the voids are not growing and the dislocations are not climbing and that the stationary configuration is affected by kinetic factors as well as equilibrium factors.

The existence of a stationary state requires that the net flux of point defects to the void and to the dislocation segment each be equal to zero. Following the argument applied to interstitial loops in the nonequilibrium solid, Eqs. 19.156a and 19.156b give the concentration of point defects at the surface of the void, and Eqs.19.158a and 19.158b apply to the surface of the dislocation line segment between the voids. The concentrations C_i and C_v pertain to the bulk solid, far from the void and dislocation-line surfaces.

The fluxes of point defects to a unit area of void are

$$J_v^{void} = 4\pi R D_v (C_v - C_v^{void})$$

$$J_i^{void} = 4\pi R D_i (C_i - C_i^{void})$$

where C_v^{void} and C_i^{void} are now given by Eqs. 19.156a and 19.156b, respectively. Using these void surface concentrations and the zero net flux condition,

$$J_v^{void} = J_i^{void}$$

yields

$$D_vC_v - D_iC_i = D_vC_v^{eq} \exp\left(\frac{2\gamma\ \Omega}{R\ kT}\right) - D_iC_i^{eq} \exp\left(-\frac{2\gamma\ \Omega}{R\ kT}\right) \quad (19.160)$$

Similarly, the fluxes of point defects to a unit length of dislocation line are

$$J_v^d = Z_vD_v\,(C_v - C_v^d)$$

$$J_i^d = Z_iD_i\,(C_i - C_i^d)$$

where C_v^d and C_i^d are given by Eqs. 19.158a and 19.158b, respectively. Using these concentrations at the surface of the dislocation line and the zero net flux condition,

$$J_v^d = J_i^d$$

yields

$$Z_vD_vC_v - Z_iD_iC_i = Z_vD_vC_v^{eq} \exp\left(-\frac{\tau_d}{b\mathscr{R}f}\frac{\Omega}{kT}\right) - Z_iD_iC_i^{eq} \exp\left(\frac{\tau_d}{b\mathscr{R}f}\frac{\Omega}{kT}\right) \quad (19.161)$$

If C_i and C_v are specified, R and $\mathscr{R}$ could be obtained directly from Eqs. 19.160 and 19.161.

The point-defect balances are used to determine the point-defect concentrations in the solid. At the stationary state that produces termination of void growth, each term in the vacancy balance of Eq. 19.134 is equal to the corresponding term in the interstitial balance of Eq. 19.135. In the saturated void-growth state, both network dislocations and loop dislocations are assumed to be interconnected to the voids, as shown in Fig. 19.21(b), so no distinction is made between them. The point-defect balances become

$$\nu\Sigma_s\Phi = 4\pi RND_v\left[C_v - C_v^{eq} \exp\left(\frac{2\gamma\ \Omega}{R\ kT}\right)\right] + Z_v\rho_dD_v\left[C_v - C_v^{eq} \exp\left(-\frac{\tau_d}{b\mathscr{R}f}\frac{\Omega}{kT}\right)\right] + 4\pi R_pN_pD_vC_v + k_{iv}C_iC_v \quad (19.162)$$

$$\nu\Sigma_s\Phi = 4\pi RND_i\left[C_i - C_i^{eq} \exp\left(-\frac{2\gamma\ \Omega}{R\ kT}\right)\right] + Z_i\rho_dD_i\left[C_i - C_i^{eq} \exp\left(\frac{\tau_d}{b\mathscr{R}f}\frac{\Omega}{kT}\right)\right] + 4\pi R_pN_pD_vC_v + k_{iv}C_iC_v \quad (19.163)$$

These equations differ from those which apply during void growth (Eqs. 19.136 and 19.137) in that the thermal emission terms from the dislocation have been altered to accommodate the picture of interconnected voids and dislocations in which the latter have ceased climbing. During growth, network dislocations are free to climb and dislocation loops are distinct from network dislocations. However, the two point-defect balances are not independent relations when saturation of void growth and dislocation climb occurs. Equation 19.163, for example, can be obtained by combining Eqs. 19.160 to 19.162. These three equations contain four unknowns, C_v, C_i, R, and $\mathscr{R}$. They can be solved for $\mathscr{R}$ as a function of R, N, and ρ_d. Prior to saturation, these three quantities increase by the void and loop growth and nucleation processes described earlier. When R, N, and ρ_d attain values such that Eqs. 19.160 to 19.162 yield $\mathscr{R} = 1/2$, a stable interconnected network of voids and dislocations becomes possible, and void growth and dislocation climb cease provided that all voids and dislocations are linked together. If any dislocations are free to climb, however, growth does not terminate.

Bullough and coworkers[24,31] have proposed mechanisms for termination of void growth which are quite different from the saturation model just described. They calculate the force exerted on a circular dislocation loop by a nearby void. This force is determined by noting that the elastic stress field emanating from an isolated dislocation (e.g., Eq. 8.7 for a screw dislocation) cannot apply at the surface of the void, which must be free of all tractions. Willis and Bullough[31] add to the stress field of the dislocation an image or induced stress field whose magnitude and position dependence are determined by the requirement that the net stresses at the void surface vanish (the surface-tension force, $2\gamma/R$, appears to have been neglected). Once the field that performs the desired function at the void surface is found, the induced stress field away from the surface can be calculated. In particular, the value of the induced stress at the location of the dislocation loop enables the glide force and the climb force on the loop to be computed (by multiplication of the appropriate stress component by the Burgers vector of the loop). These forces are shown in Fig. 19.22. If the loop is unfaulted and of the interstitial type, the glide force is attractive. That is, if the critical glide stress (analogous to the critical resolved shear stress) is exceeded, the loop will glide directly into the void and be annihilated. When an interstitial dislocation loop is captured by a void, the latter shrinks by an amount equivalent to the number of interstitials contained in the loop. In addition to a glide force, the void–loop interaction induces a climb force on the loop which causes it to collapse. For this force to cause loop shrinkage, though, it would need to be greater than the climb force causing loop growth arising from interstitial supersaturation of the surrounding solid (Eq. 19.153). If the loop initially had a radius greater than that of the void and could not shrink by the induced climb force, it would be drawn toward the void and be trapped as a sort of Saturn ring around the periphery of the void.

In any case, the glide force is always effective in eliminating dislocation loops with radii smaller than that of

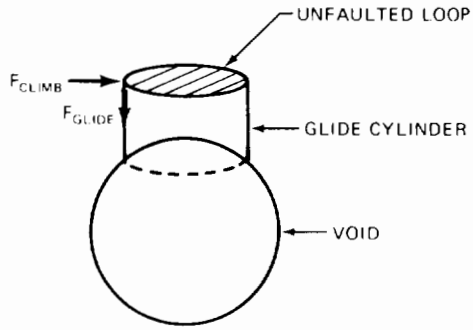

Fig. 19.22 Forces on a dislocation loop near a void. (After Ref. 31.)

the void provided that the loop lies within a capture volume around the void. The capture volume extends from the void surface to the radial position where the attractive stress field due to the void–loop interaction (i.e., the image field, which decreases rapidly with distance from the center of the void) is just equal to the critical glide stress. Loops farther out cannot be started off by the attractive glide force. For large voids (i.e., $R > 500$ Å), Willis and Bullough[31] calculate that the thickness of the spherical-shell capture volume is ~200 Å. Loss of dislocations from this entire volume around the voids results in cessation of void growth (because of the absence of the dislocations and their biasing effect) when the voids are sufficiently numerous that their capture volumes overlap.

According to the model just outlined, void-growth saturation should be accompanied by a drastic reduction in dislocation density. The expected reduction in dislocation density is observed in pure metals, such as nickel, after long irradiation, but it does not occur in stainless steel because of the greater difficulty in moving dislocations in such an impure alloy. However, even when the voids do not succeed in swallowing the dislocations, the induced stress field created by the necessity of maintaining the void surface stress-free persists. Voids then appear to contain image dislocations that preferentially absorb interstitials over vacancies just as real dislocations do. By this mechanism the neutrality of the void as a point-defect source is destroyed, and the void acquires a bias of its own for interstitials. The rates of point-defect absorption by voids which harbor image dislocations are given by multiplying Eqs. 19.95 and 19.96 by W_v and W_i, which are bias factors akin to Z_v and Z_i for dislocations and Y_v and Y_i for coherent precipitates. Using the modified void sink strengths in the point-defect balances and in the void growth law leads to replacement of $Z_i - Z_v$ in Eq. 19.145 by $Z_i - W_i Z_v / W_v$. When this difference becomes zero, void growth ceases completely.

19.6 THE VOID CONTINUITY EQUATION AND VOID SWELLING

Section 19.3 described methods of calculating the rates at which small voids and dislocation loops reach the critical size for continued growth. In Sec. 19.4, overall conservation equations (the point-defect balances) were developed for vacancies and interstitials to permit calculation of the instantaneous concentrations of point defects in the bulk of the solid. These balances require knowledge of the numbers and sizes of voids and dislocation loops in the material at the moment that the point-defect balances are applied. This information is obtained from void and loop conservation equations, which are derived in this section.

19.6.1 The Delta Function Distribution

Most theories of void growth place a great deal of emphasis on determination of the void-growth law, $\dot{R}$, but relatively little is said about what is to be done with this formula once it is obtained. Confrontation of the conservation equations governing the entire population of voids and loops in the solid is avoided by assuming simplified size distributions for these two types of defect clusters. Specifically, all voids are assumed to be of the same size at any given time, or the distribution is a delta function centered on the value of R(t) obtained by integration of the growth law. Similarly, the loop size distribution is assumed to be a delta function. This approach is valid provided that (1) nucleation and growth are distinct, sequential processes and (2) all void (or loop) nuclei are the same size.

If all voids and loops are nucleated at the same time and with the same size and processes that can change the size of a cluster in large chunks (i.e., coalescence or macroscopic resolution) are negligible, the void and loop distributions will remain delta functions throughout irradiation. That is, with time, all loops and voids simply grow uniformly but their number density remains constant. The void size at any time is determined by simultaneously integrating the void-growth law of Eq. 19.139 and the analogous growth laws for loops. Because of the complex dependence of $\dot{R}$ on R, numerical integration is generally required.

The zero in time (or fluence) for growth is the end of the nucleation stage, which for stainless steel is taken to be the incubation fluence of 10^{22} neutrons/cm^2 required before any voids are observed. It is assumed that the nucleation process provides N voids/cm^3 of starting size R_c (the radius of the critical nuclei) and N_l loops/cm^3 of initial size R_{lc}. By integration of the growth laws, R(t) and $R_l(t)$ are determined, and the swelling at time t (or fluence ϕt) is calculated from Eq. 19.10. This approach is followed by Brailsford and Bullough.[25]

19.6.2 Eulerian Void Continuity Equation

When the nucleation and growth processes overlap in time, the void and loop conservation equations cannot be circumvented. In this instance, void and loop size distributions evolve during irradiation. The voids and loops present at a particular time arise from nuclei produced from the beginning of irradiation up to the time in question, and hence a distribution of sizes must be present. The continuity equation for voids was derived by Sears.[32] It is similar to the continuity equation for fission-gas bubbles in the fuel (Chap. 13).

The void distribution function N(R,t) dR is the number of voids per unit volume with radii between R and R + dR at time t. It is convenient to begin with a slightly different distribution function, N(m,t), which is the number of voids

per unit volume containing m vacancies at time t. Inasmuch as R and m are related by

$$m = \frac{4\pi R^3}{3\Omega} \tag{19.164}$$

the two distribution functions satisfy

$$N(R,t) = \left(\frac{4\pi R^2}{\Omega}\right) N(m,t) \tag{19.165}$$

Let us define the current of voids in size space, I_m, as the number of voids passing from size m to size m + 1 per unit volume per second. Here I_m is similar to the nucleation rate considered in Sec. 19.3 except that it is defined for void sizes well beyond the critical void cluster size to which nucleation theory is restricted. The rate per unit volume at which voids enter the size m class is I_{m-1}. The rate at which voids leave this size class is I_m. Therefore, the void conservation statement is

$$\frac{\partial N}{\partial t} = I_{m-1} - I_m = -\frac{\partial I}{\partial m} \tag{19.166}$$

Because I_m varies slowly with m, the difference $I_{m-1} - I_m$ can be approximated by the derivative indicated on the extreme right side of the above equation. Equation 19.166 applies only if the nucleation process does not produce voids of size m (i.e., if $m > m_c$). The current I_m is given by Eq. 19.40, but for simplicity the thermal emission term is neglected in the present analysis (it can be easily reinstated). Thus

$$I_m = \beta_v(m)\, N(m,t) - \beta_i(m+1)\, N(m+1,t) \sim (\beta_v - \beta_i)\, N(m,t) \tag{19.167}$$

where the difference between $\beta_i(m+1)\, N(m+1,t)$ and $\beta_i(m)\, N(m,t)$ has been neglected. The arrival rate β_v is given by Eq.. 19.37 in which the denominator is very near unity because the voids are large. The formula for β_i is the same as that for β_v if the subscripts are appropriately altered and I_m can be expressed in terms of the growth law by noting that Eq. 19.138 (without the thermal emission term) can be written as

$$\dot{R} = (\beta_v - \beta_i)\frac{\Omega}{4\pi R^2} \tag{19.168}$$

If Eq. 19.167 is inserted into Eq. 19.166, the size variable is changed from m to R by Eq. 19.164, the distribution function is changed from N(m,t) to N(R,t) by Eq. 19.165, and Eq. 19.168 is used, the void continuity equation is found to be

$$\frac{\partial N}{\partial t} = -\frac{\partial}{\partial R}(\dot{R}N) \tag{19.169}$$

which is valid for $t > 0$ and $R > R_c$, the radius of the critical void nucleus.

In addition to the growth law $\dot{R}$, Eq. 19.169 requires an initial condition and a boundary condition (only one of each, since the equation is first order in each variable). The initial condition is

$$N(R,0) = 0 \quad \text{(for all R)} \tag{19.170}$$

which states that the metal contains no voids at the start of irradiation.

The boundary condition is related to the nucleation process, which proceeds simultaneously with growth. It is usually assumed that all void nuclei enter the solid as small clusters containing m_c atoms at a rate I_{nucl} cm^{-3} sec^{-1}. The critical void size and the nucleation rate are prescribed by nucleation theory for the prevailing point-defect supersaturations (Sec. 19.3). The balance equation for voids of size m_c is

$$\frac{\partial N(m_c,t)}{\partial t} = I_{nucl} - I_{m_c} \tag{19.171}$$

where I_{m_c} is the current of voids passing from size m_c to the next largest size. It is generally sufficient to apply a quasi-stationary approximation to Eq. 19.171 and equate I_{nucl} to I_{m_c}. With the same manipulations used to obtain Eq. 19.169, the steady-state form of Eq. 19.171 provides the boundary condition

$$N(R_c,t) = \frac{I_{nucl}(t)}{\dot{R}_c} \quad \text{(for all t)} \tag{19.172}$$

where $\dot{R}_c$ is the growth rate of the critical size void nucleus.

Equations similar to Eqs. 19.169 and 19.172 are needed for dislocation loops as well as for voids. For loops, unfaulting of sessile loops to form glissile loops would have to be added as a loss mechanism, and an additional conservation equation would be needed to describe the time rate of change of the network dislocations as well.

Determination of the void and loop distribution functions requires simultaneous solution of the conservation equations for these defect clusters together with their growth laws. Note that calculation of the evolution of the void and loop populations during irradiation is no longer simply a matter of integrating the growth laws. Rather, the growth laws must be integrated in the form that they appear in the void and loop conservation equations, where $\dot{R}$ and $\dot{R}_l$ are multiplied by N and N_l in a derivative. At any time t, the swelling is given by Eq. 19.9.

This unified approach to void swelling has been applied in the computer program developed by Li et al.,[21] a flow chart of which is shown in Fig. 19.23. They employed the conservation equation (Eq. 19.169) and the analogous partial differential equation for loops in terms of the m variable (for voids) rather than the R variable as was done here. A multigrouping scheme was used to reduce the size of the m increments. A similar method was used by these authors in connection with bubble growth by coalescence (Eq. 13.201 is analogous to Eq. 19.169).

We do not present any results of either the delta function Brailsford–Bullough method of calculating void swelling or the Li–Harkness unified approach. The former is very good on the growth law but does not account for continued nucleation of new voids and loops during irradiation. The latter treats the void distribution function more realistically but incorporates inaccurate nucleation theory and does not contain the detail in the growth laws that the Brailsford–Bullough method provides. Despite these shortcomings of each method, there are enough unknown physical quantities in each model to provide a sufficient number of adjustable parameters to fit the

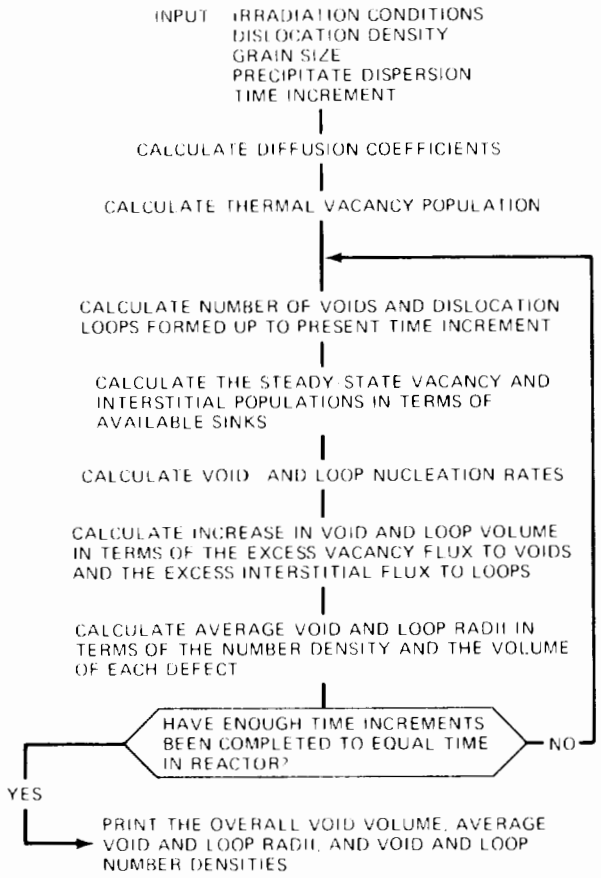

Fig. 19.23 Flow chart of a computer program for calculating void swelling. (After Ref. 21.)

experimentally observed void-swelling patterns discussed in Sec. 19.2. Neither model needs outlandish values of the adjustable parameters to qualitatively reproduce a wide variety of experimental results, which implies that the basic concepts of the models are sound. This sort of semiagreement between theory and experiment means that the model calculations are best used to extrapolate existing data rather than to determine absolute swelling from first principles. The theory is an aid to experiment but certainly cannot supplant the continued acquisition of data on void swelling by fast-neutron irradiation.

19.6.3 Lagrangian Void Continuity Equation

The method of accounting for the change in size and density of loops and voids during irradiation which was described above is Eulerian in nature because it follows flows of defects into and out of a fixed interval of cluster size. For some special cases a Lagrangian approach may be more useful. The void conservation equation can be succinctly derived by noting that all voids in the size range R to R + dR at time t arise from nuclei created (at size R_c) in the time interval τ to $\tau + d\tau$, or

$$N(R,t)\, dR = I_{nucl}(\tau)\, d\tau$$

which can be rearranged to give

$$N(R,t) = I_{nucl}[\tau(R,t)] \left(\frac{\partial \tau}{\partial R}\right)_t \qquad (19.173)$$

The problem is to determine the relation between τ and the variables t and R in order that the argument of I_{nucl} and the Jacobian $(\partial\tau/\partial R)_t$ be expressed in terms of these quantities. This identification is accomplished by regarding the function $R(t,\tau)$ as the radius at time t of a void nucleated at time τ, which can be obtained by writing the growth law as

$$\frac{dR}{dt} = \dot{R} \qquad (19.174)$$

Equation 19.174 can be integrated provided that $\dot{R}$ is known explicitly as a function of R and t. That this is usually not the case is the reason that the Lagrangian approach is restricted to special situations. Sears[32] considers the artificial case in which C_v and C_i are independent of R (which, in general, is not true because the point-defect balances depend on the void average size). In this case Eqs. 19.174 and 19.138 can be combined and integrated to give

$$R^2(t,\tau) = R_c^2 + 2\Omega \int_\tau^t (D_v C_v - D_i C_i)dt' \qquad (19.175)$$

If the integral on the right can be performed (i.e., if the time variations of C_v and C_i are known a priori), Eq. 19.175 can be solved for τ as a function of R and t, and the right-hand side of Eq. 19.173 can be expressed entirely in terms of the last two variables.

A more realistic case in which a Lagrangian defect conservation equation is employed in the analysis of thermal annealing of depleted zones is discussed in Sec. 18.5.

19.7 IRRADIATION CREEP

Irradiation creep refers either to augmentation of thermal creep by irradiation or to development of creep under conditions in which thermal creep is absent. The former is termed *irradiation-enhanced creep*, and the latter is known as *irradiation-induced creep*. A sizeable number of thermal creep mechanisms have been identified (see Sec. 16.6), and an even greater number of irradiation creep theories have been proposed.[33] To be classed as irradiation creep, the applied stress must cause nonuniform deformation of the solid (not just swelling), and the deformation rate must change when the fast-neutron flux is altered.

Irradiation creep theories applicable to austenitic stainless steels can be divided into two broad categories, the distinction resting on whether or not irradiation-produced dislocation loops and voids are involved in the creep process. Inasmuch as the nucleation of these clusters is strongly temperature dependent, the two regimes are equivalent to low and high temperatures. The boundary occurs roughly at the minimum temperature for void formation (~350°C in stainless steel).

High-temperature irradiation creep is usually ascribed to (1) stress orientation of nucleating dislocation loops or (2) accelerated climb of dislocations followed by glide.

Two types of low-temperature irradiation creep have been identified. The first is a transient creep due to climb of pinned segments of the dislocation network in the solid, and the second is a steady-state form of creep arising from collapse of vacancy loops. Figure 19.24 demonstrates the simultaneous operation of transient and steady creep at low temperatures. After a long time of irradiation at a high stress, the load on the in-pile test specimen is reduced. The vertical line on the left of the graph represents immediate elastic strain recovery, following which an incubation period of ~2000 hr is required before establishment of steady-state irradiation creep characteristic of the lower stress level. The strain offset between the end of the elastic recovery and the backward extrapolation of the new steady-state creep line represents the amplitude of the transient component of the low-temperature irradiation creep. The data in Fig. 19.24 can be represented by the formula:

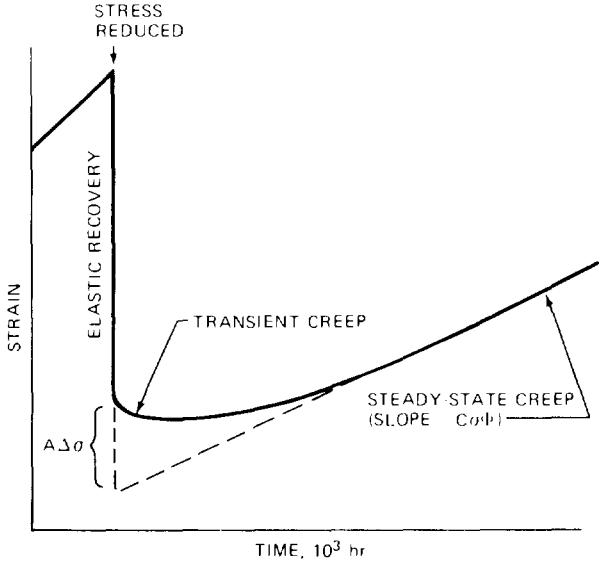

Fig. 19.24 Strain recovery in type 304 stainless steel irradiated at 100°C following a stress reduction in pile. (After E. R. Gilbert and L. D. Blackburn, in *Second International Conference on the Strength of Metals and Alloys*, p. 773, American Society for Metals, 1970.)

$$\epsilon = A\sigma\left[1 - \exp\left(-\frac{\Phi t}{B}\right)\right] + C\sigma\Phi t \qquad (19.176)$$

The first term on the right represents the recoverable transient strain. The steady-state creep rate is contained in the second term. Here, we explain the mechanisms by which these two forms of low-temperature irradiation creep occur and provide estimates of the constants A, B, and C in Eq. 19.176.

19.7.1 Transient Creep

Models of transient irradiation creep have been advanced by Hesketh[34] and by Lewthwaite and Proctor.[35] A slightly modified form of Hesketh's analysis will be reviewed here.

Consider a metal in which the dislocation density is ρ_d. The dislocation network is modeled as a cubical grid of dislocation segments, with the distance between junctions where the segments of dislocation line are pinned (Sec. 13.12) given by

$$l = \left(\frac{3}{\rho_d}\right)^{1/2} \qquad (19.177)$$

Since the theory is designed for temperatures well below the temperature of void formation, we will assume that the vacancies produced by the collision cascades are immobile. The vacancy and interstitial diffusion coefficients in stainless steel are approximately given by $D_v \sim \exp(-\epsilon_v^*/kT)$ and $D_i \sim \exp(-\epsilon_i^*/kT)$, where the diffusivities are in square centimeters per second, $\epsilon_v^* \sim 125$ kJ/mole, and $\epsilon_i^* \sim 13$ kJ/mole. At 100°C, $D_v \sim 10^{-18}$ cm²/sec and $D_i \sim 10^{-2}$ cm²/sec. The mean lifetime of a point defect can be estimated from Eq. 7.24 if the root-mean-square displacement of an atom at time t is identified with the size of the dislocation network. Taking r^2 equal to $l^2 \sim 10^{-10}$ cm² (for $\rho_d = 10^{10}$ cm^{-2}) and the above values of the point-defect diffusivities, we find the average time for a vacancy to reach a dislocation is $\sim 10^7$ sec, whereas an interstitial is absorbed in $\sim 10^{-9}$ sec. Thus, it is a fair approximation to consider the vacancies as totally immobile and the interstitials as mobile enough to maintain quasi-steady-state concentrations of this defect at all times. The basic results of the analysis do not depend on this restriction, but the analysis is simpler than the case in which both species are mobile.

Consider a specimen that has been irradiated in a stress-free state for a time long enough to establish a steady-state microstructure (the irradiation-produced interstitials cause the pinned segments of the dislocation network to climb until the line tension of the curved dislocation balances the chemical stress due to the interstitial supersaturation). During the initial irradiation soaking, no creep occurs since no stress is applied. Figure 19.25 shows a representative cube of the dislocation network of the solid during irradiation. Each of the sides of the cube is assumed to consist of segments of edge dislocations of length l. The Burgers vectors of the segments are randomly oriented. Bowing of the dislocations under irradiation is depicted as the circular segments terminating at the pinning points (for clarity, only one-half of the bowed segments are shown in the drawing). The segments take on this configuration because of absorption of interstitial atoms from the irradiated solid; so the shaded circular segments represent extensions of the half-sheets of atoms of which the edge dislocations consist. The accumulation of excess interstitial atoms by the dislocation segments cause each of them to acquire a common radius of curvature $\mathcal{R}$. The small irregular shapes within the cube in Fig. 19.25 are intended to represent the depleted zones which are formed in the collision cascade and which are stable against thermal annealing at low temperatures. The depleted zones are vacancy agglomerates.

Because irradiation creates equal numbers of vacancies and interstitials, a conservation condition relates the extent

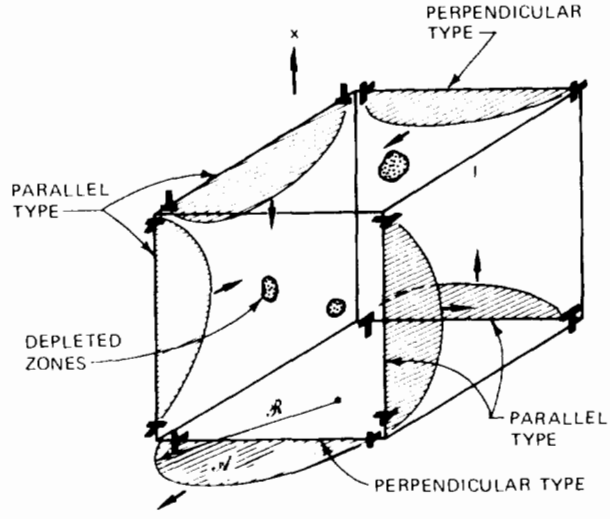

Fig. 19.25 Bowing of the segments of a dislocation network in an irradiation field. No stress is applied.

of climb of the dislocation segments, the number and size of the depleted zones, and the point-defect concentrations maintained by irradiation in the solid. The sum of the number of interstitials associated with the bowed dislocation lines and the bulk interstitial concentration C_i must be equal to the sum of the number of vacancies contained in the depleted zones and the bulk vacancy concentration C_v. This condition is independent of the point-defect balances, which equate the rates of production and destruction of each type of point defect.

The number of interstitial atoms associated with the bowed dislocation segments is obtained as follows. The cube shown in Fig. 19.25 contains 12 segments, but each of these is shared among four neighboring cubes; thus there are three segments associated with a volume l^3 of solid. With Eq. 19.177, the number of segments per unit volume is ρ_d/l. If the areas of the shaded circular segments in Fig. 19.25 are called $\mathscr{A}$, the number of interstitial atoms contained in each is $b\mathscr{A}/\Omega$. The area $\mathscr{A}$ is a function of the radius of curvature $\mathscr{R}$ and the cube slide l. The number of interstitials per unit volume contained in the bowed segments is $b\mathscr{A}\rho_d/l\Omega$.

At steady state, there will be a distribution N(R) of depleted zones, in which R, the zone radius, ranges from the maximum size created in the collision cascade, R_0, to zero size (see Sec. 18.5). A zone of radius R contains $4\pi R^3/3\Omega$ vacancies. Thus, the balance on the total number of point defects can be written*

$$C_i + \frac{b\rho_d\mathscr{A}}{l\Omega} = C_v + \frac{4\pi}{3\Omega}\int_0^{R_0} R^3 N(R)\, dR \quad (19.178)$$

The point-defect balances are

$$\nu_v \Sigma_s \Phi = k_{iv} C_i C_v \quad (19.179)$$

$$\nu_i \Sigma_s \Phi = Z_i \rho_d D_i (C_i - C_i^d) + k_{iv} C_i C_v + 4\pi D_i C_i \int_0^{R_0} R\, N(R)\, dR \quad (19.180)$$

Because of the assumption that the vacancies are immobile, they do not diffuse to dislocations or to depleted zones. Vacancies are removed from the solid only by recombination with migrating interstitials. The interstitial balance (Eq. 19.180) is the same as that employed in the analysis of depleted-zone annealing (Sec. 18.5) except for the concentration of interstitials at the dislocation surface. In the annealing study the dislocations were assumed free to climb, and C_i^d was equal to $C_i^{eq} \simeq 0$. When the dislocations are pinned and climb is stopped by line tension, the interstitial concentration at the surface of the dislocation rises from C_i^{eq} for a straight dislocation free to climb to a value given by Eq. 19.158b when the line assumes a finite radius of curvature. When no voids are attached to the ends of the pinned segment, the factor f in Eq. 19.158b is unity, and C_i^d for the present analysis is given by

$$C_i^d = C_i^{eq} \exp\left[\frac{\tau_d}{b\mathscr{R}}\frac{\Omega}{kT}\right] \quad (19.181)$$

Recalling the analysis of depleted-zone annealing in Sec. 18.5, the number of interstitials and free vacancies (i.e., vacancies not contained in nascent depleted zones) are related by

$$\nu_i = \nu_v + \frac{4\pi R_0^3}{3\Omega} \quad (19.182)$$

The distribution of depleted zones, N(R), has been derived in the depleted-zone annealing analysis of Sec. 18.5. In the present application the vacancies are assumed to be immobile; thus Eq. 18.48 becomes

$$N(R) = \frac{\Sigma_s \Phi R}{D_i C_i \Omega} \quad (19.183)$$

If Eq. 19.179 is subtracted from Eq. 19.180, the difference $\nu_i - \nu_v$ is taken from Eq. 19.182, and the distribution of Eq. 19.183 is used in the integral of Eq. 19.180, we find that the point-defect balances require that $C_i = C_i^d$, or, with Eq. 19.181,

$$\frac{\tau_d}{b\mathscr{R}} = \frac{kT}{\Omega} \ln\left(\frac{C_i}{C_i^{eq}}\right) \quad (19.184)$$

The left-hand side of this equation is the applied stress needed to bow a dislocation line to a radius of curvature $\mathscr{R}$. The right-hand side is the effective, or chemical, stress on the dislocation line due to the interstitial supersaturation.

Equation 19.178 provides an additional relationship between C_i and $\mathscr{R}$. The integral can be removed by use of Eq. 19.183, and C_v can be expressed in terms of C_i by Eq. 19.179, yielding

$$C_i + \frac{b\rho_d\mathscr{A}}{l\Omega} = \frac{\nu_v \Sigma_s \Phi}{k_{iv} C_i} + \frac{4\pi}{15}\frac{\Sigma_s \Phi R_0^5}{\Omega^2 D_i C_i} \quad (19.185)$$

*A *conservation* statement analogous to Eq. 19.178 cannot be made during void growth because, in this instance, the dislocations are considered free to climb. Point defects can thus leave or enter a particular unit volume of solid by the motion of climbing dislocations. In the present situation, no point defects cross the surface of any unit volume in the solid, and correctly accounting for the fate of the nonrecombined point defects in this closed system leads to Eq. 19.178.

The radius $\mathscr{R}$ is contained in Eq. 19.185 in the area $\mathscr{A}$ (see problem 19.16 at the end of this chapter). Simultaneous solution of Eqs. 19.184 and 19.185 yields C_i and $\mathscr{R}$.

If the value of $\mathscr{R}$ determined by this method is less than l/2, the configuration shown in Fig. 19.25 cannot be maintained. In Eq. 19.184

$$\frac{\tau_d}{b\mathscr{R}}\frac{\Omega}{kT} \sim 10^{-4} \text{ cm}$$

for most metals at low temperatures (~100°C). For a metal with a dislocation density of 10^{10} cm^{-2}, the minimum value of $\mathscr{R}$ (equal to l/2) is $\sim 10^{-5}$ cm. Therefore, Eq. 19.185 limits the allowable interstitial supersaturation for the maintenance of a stable configuration of bowed dislocation segments of $C_i/C_i^{eq} \leq 10^4$. If the dislocation density is 10^{12} cm^{-2}, however, the maximum permissible supersaturation of interstitials is 10^{40}.

To approximately calculate C_i from Eq. 19.185, assume that the dislocation segments have bowed to nearly semicircular configurations ($\mathscr{R} \sim l/2$), so

$$\mathscr{A} \sim \frac{1}{2}\pi\mathscr{R}^2 = \frac{\pi l^2}{8}$$

Eliminating l in favor of ρ_d by using Eq. 19.177, Eq. 19.185 becomes

$$\Omega C_i + \left[\frac{\pi 3^{1/2}}{8} b(\rho_d)^{1/2}\right] = \frac{b^2\Omega\Sigma_s\Phi}{D_i} \times \left(\frac{\nu_v}{z_{iv}} + \frac{4\pi}{15}\frac{R_0^5}{\Omega b^2}\right)\frac{1}{\Omega C_i} \qquad (19.186)$$

where the vacancy–interstitial recombination coefficient, k_{iv}, has been expressed by Eq. 13.42 with $a_0 \sim b$. Using representative values of the constants in Eq. 19.186, we find that the second term on the left-hand side is very much larger than the coefficient of $1/\Omega C_i$ on the right-hand side. Therefore, the solution of the quadratic equation is

$$C_i = \frac{8}{\pi 3^{1/2}}\frac{b}{(\rho_d)^{1/2}D_i}\left(\frac{\nu_v}{z_{iv}} + \frac{4\pi}{15}\frac{R_0^5}{\Omega b^2}\right)\Sigma_s\Phi \qquad (19.187)$$

and $\mathscr{R}$ is determined by substitution of Eq. 19.187 into Eq. 19.184.

For a flux of 10^{13} neutrons cm^{-2} sec^{-1}, $R_0 \sim 8$ Å, and a dislocation density of 10^{12} cm^{-2}, Eq. 19.187 gives $C_i \sim 10^3$ cm^{-3}. The thermal equilibrium vacancy concentration at 100°C is about 10^{-36} cm^{-3}, so the vacancy supersaturation is $\sim 10^{39}$. This supersaturation is just a bit smaller than the value which, by Eq. 19.184, causes the dislocation segments to climb beyond the semicircular configuration ($\mathscr{R} = l/2$). Thus, the preceding analysis is limited to metals of high dislocation density and low fluxes. As the temperature is increased (which increases C_i^{eq}), these restrictions are less stringent than they are at ~100°C. Hesketh[34] discusses the consequences of interstitial supersaturations that are large enough to cause the dislocations to be pulled free of their pinning points by the chemical stress.

During the irradiation period preceding application of the stress to the specimen, all the dislocations climb by the same amount by absorption of excess interstitials. When uniaxial tension in the vertical direction in Fig. 19.25 is applied, the edge dislocations whose extra half-layer of atoms is perpendicular to the direction of the applied stress (i.e., those with Burgers vectors parallel to the stress direction) are induced to climb because the stress reduces the concentration of interstitials at the dislocation core. These dislocations are identified as "perpendicular type" in Fig. 19.25. They constitute one-third of all the dislocation segments in the solid. The remaining two-thirds of the dislocation segments have their Burgers vectors at 90° to the stress axis, or the extra half-sheet of atoms is parallel to the stress direction. These segments, labeled "parallel type" in Fig. 19.25, are not directly affected by application of the stress.

At the final steady-state configuration achieved following application of the stress, the radius of curvature of the perpendicular-type dislocations changes from $\mathscr{R}$ to $\mathscr{R}_\perp$, and that of the parallel-type segments changes from $\mathscr{R}$ to $\mathscr{R}_\parallel$. The interstitial concentrations at the cores of these two dislocation types are altered from the stress-free value given by Eq. 19.181 to

$$(C_i^d)_\perp = C_i^{eq}\exp\left(\frac{\tau_d}{b\mathscr{R}_\perp}\frac{\Omega}{kT}\right)\exp\left(-\frac{\sigma\Omega}{kT}\right) \qquad (19.188)$$

and

$$(C_i^d)_\parallel = C_i^{eq}\exp\left(\frac{\tau_d}{b\mathscr{R}_\parallel}\frac{\Omega}{kT}\right) \qquad (19.189)$$

The point-defect balances become

$$\nu_v\Sigma_s\Phi = k_{iv}C_i'C_v' \qquad (19.190a)$$

and

$$\nu_i\Sigma_s\Phi = \frac{1}{3}Z_i\rho_d D_i[C_i' - (C_i^d)_\perp] + \frac{2}{3}Z_i\rho_d D_i[C_i' - (C_i^d)_\parallel] + k_{iv}C_i'C_v' + 4\pi D_i C_i'\int_0^{R_0} R\,N(R)\,dR \qquad (19.190b)$$

where C_i' and C_v' are the concentrations of point defects in the bulk solid after the system has come to equilibrium with the applied stress. The depleted-zone distribution is given by Eq. 19.183 with C_i replaced by C_i'. Following the procedure used in the stress-free condition, satisfaction of the point-defect balances requires that the bracketed terms in Eq. 19.190b both vanish, or Eq. 19.184 is replaced by two conditions:

$$\frac{\tau_d}{b\mathscr{R}_\perp} - \sigma = \frac{kT}{\Omega}\ln\left(\frac{C_i'}{C_i^{eq}}\right) \qquad (19.191)$$

$$\frac{\tau_d}{b\mathscr{R}_\parallel} = \frac{kT}{\Omega}\ln\left(\frac{C_i'}{C_i^{eq}}\right) \qquad (19.192)$$

The overall balance of point defects, which was expressed by Eq. 19.185 in the absence of stress, now becomes

$$C_i' + \frac{b\rho_d}{l\Omega}\left(\frac{1}{3}\mathscr{A}_\perp + \frac{2}{3}\mathscr{A}_\parallel\right) = \frac{\nu_v\Sigma_s\Phi}{k_{iv}C_i'} + \frac{4\pi}{15}\frac{\Sigma_s\Phi R_0^5}{\Omega^2 D_i C_i'} \qquad (19.193)$$

where $\mathscr{A}_\perp$ and $\mathscr{A}_\parallel$ are climb areas corresponding to the radii of curvature $\mathscr{R}_\perp$ and $\mathscr{R}_\parallel$, respectively. The final

configuration of the dislocations in the stressed solid can be determined by solving Eqs. 19.191 to 19.193 for C_i', $\mathscr{R}_\perp$, and $\mathscr{R}_\parallel$. Inasmuch as the changes in the interstitial concentration and the radii of curvature of the two types of dislocations due to application of the stress are small compared to the values of these quantities established by prior irradiation, the new values can be expressed by

$$\mathscr{N}_\perp = \mathscr{N} + \left[\frac{d\mathscr{N}}{d(1/\mathscr{R})}\right]\left(\frac{1}{\mathscr{R}_\perp} - \frac{1}{\mathscr{R}}\right) \qquad (19.194)$$

$$\mathscr{N}_\parallel = \mathscr{N} + \left[\frac{d\mathscr{N}}{d(1/\mathscr{R})}\right]\left(\frac{1}{\mathscr{R}_\parallel} - \frac{1}{\mathscr{R}}\right) \qquad (19.195)$$

$$C_i' = C_i + \delta C_i \qquad (19.196)$$

Solution of Eqs. 19.191 to 19.193 using the above forms with $\delta C_i/C_i \sim 1$ is treated in problem 19.17 at the end of this chapter. To keep algebraic manipulations to a minimum, we make the even cruder approximation $\delta C_i \sim 0$, or $C_i' \sim C_i$, which permits the right side of Eq. 19.191 to be replaced by the left side of Eq. 19.184, or

$$\frac{\tau_d}{b}\left(\frac{1}{\mathscr{R}_\perp} - \frac{1}{\mathscr{R}}\right) = \sigma \qquad (19.197)$$

Since the applied stress is positive (tension), Eq. 19.197 shows that $\mathscr{R}_\perp < \mathscr{R}$, or the perpendicular-type dislocations advance slightly upon application of the stress. This means that atoms are added to the bowed dislocation segments which lie at right angles to the stress axis. This transfer of matter results in deformation, or strain, in the direction of the applied stress, the magnitude of which may be determined as follows.

Figure 19.26 shows a block of the irradiated metal with initial dimensions X, Y, and Z. One internal plane containing a perpendicular-type dislocation segment and two planes with parallel-type segments are shown in the sketch. The shaded crescent shapes represent the area changes due to application of the stress. For the perpendicular-type dislocations, the change in area is $\mathscr{N}_\perp - \mathscr{N}$. The solid shown in the figure contains $(\rho_d/l)XYZ$ dislocation segments of length l, one-third of which are of the perpendicular type. When these expand by $\mathscr{N}_\perp - \mathscr{N}$, a total of

$$\frac{1}{3}\frac{\rho_d}{l}(XYZ)\frac{b}{\Omega}(\mathscr{N}_\perp - \mathscr{N})$$

atoms are moved to planes perpendicular to the stress axis. Or the volume displaced in Ω times the above expression, which is related to the deformation in the stress direction, δX, by

$$\delta X\,(YZ) = \text{atoms moved} \times \Omega$$

Combining the above two expressions yields the terminal creep strain:

$$\epsilon = \frac{\delta X}{X} = \frac{\rho_d b(\mathscr{N}_\perp - \mathscr{N})}{3l} \qquad (19.198)$$

The area change $\mathscr{N}_\perp - \mathscr{N}$ can be obtained from Eq. 19.194, in which the difference in the reciprocal radii of curvature is expressed by Eq. 19.197, and we have

$$\epsilon = \frac{\rho_d b^2 \sigma}{3l\tau_d}\left[\frac{d\mathscr{N}}{d(1/\mathscr{R})}\right]$$

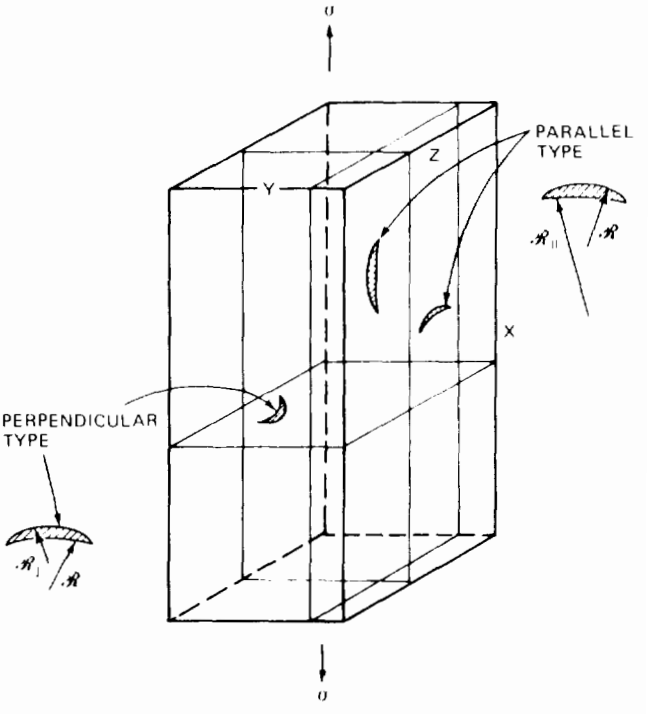

Fig. 19.26 Transient irradiation creep due to bowing of pinned dislocation segments.

In problem 19.16 at the end of this chapter, the bracketed term in the above formula is shown to be expressible in the form

$$\frac{d\mathscr{N}}{d(1/\mathscr{R})} = \frac{l^3}{12}F\left(\frac{1}{\mathscr{R}}\right) \qquad (19.199)$$

where F approaches unity as $1/\mathscr{R} \to 0$ but becomes large as the semicircular configuration ($\mathscr{R} = l/2$) is approached. The dislocation-line tension is approximately equal to Gb^2, where G is the shear modulus; so the terminal creep becomes

$$\epsilon = \frac{\rho_d l^2 F(1/\mathscr{R})}{36G}$$

Noting that according to Eq. 19.177, $\rho_d l^2 = 3$ and replacing the shear modulus G by Young's modulus $E = 2(1+\nu)G \sim 3G$, we have

$$\epsilon = \frac{F(1/\mathscr{R})}{4}\left(\frac{\sigma}{E}\right) = \frac{F(1/\mathscr{R})}{4}\epsilon_{\text{elastic}} \qquad (19.200)$$

If $F(1/\mathscr{R}) \sim 1$, Eq. 19.200 predicts that the amplitude of the transient strain should be one-fourth the elastic strain. This prediction is consistent with the experimental results shown in Fig. 19.24, in which the elastic recovery following stress reduction is several times larger than the magnitude of the transient strain recovery which follows. Lewthwaite and Proctor[35] report transient strains as large as three times the initial elastic deflection, which may be due to values of $F(1/\mathscr{R})$ larger than unity, owing to bowing of the dislocation to a nearly semicircular shape.

Comparison of Eqs. 19.176 and 19.200 indicates that the theoretical value of the constant A is

$$A = \frac{F(1/\mathscr{R})}{4E} \tag{19.201}$$

The terminal creep strain attained when an irradiated specimen is stressed at low temperatures depends on the flux to which the specimen is exposed. The coefficient A given by Eq. 19.201 is proportional to the geometric factor $F(1/\mathscr{R})$ given by Eq. 19.199, which increases as $\mathscr{R}$ decreases. According to Eq. 19.184, $\mathscr{R}$ becomes smaller as the interstitial concentration C_i becomes larger, and, by Eq. 19.187, C_i is directly proportional to the flux Φ. This effect may be responsible for the larger values of the coefficient A observed by Lewthwaite and Proctor,[35] who irradiated their specimens in a fast reactor with a fast-neutron flux of $\sim 2 \times 10^{14}$ neutrons cm^{-2} sec^{-1}, compared to the A values reported by Hesketh,[34] which were based on irradiations in a thermal reactor wherein the fission flux was $\sim 4 \times 10^{13}$ neutrons cm^{-2} sec^{-1}.

However, the major irradiation dependence of the transient creep mechanism we are considering here lies in the exponential term in Eq. 19.176. This equation shows that in the absence of irradiation the expected terminal creep strain would take infinitely long to be attained. Rather than attempt to compute B directly from the theory, we follow the technique used by Hesketh[34] and by Lewthwaite and Proctor[35] of computing the strain rate at the moment that the stress is applied. This initial strain rate, denoted by $\dot{\epsilon}_0$, is related to the constant B by

$$B = \frac{A\sigma\Phi}{\dot{\epsilon}_0} \tag{19.202}$$

The exact time variation of the strain is more complex than the simple exponential form given in Eq. 19.176, but the estimate based on Eq. 19.202 at least gives the correct initial strain rate.

From Eq. 19.198 the initial strain rate is

$$\dot{\epsilon}_0 = \frac{\rho_d b}{3l}\left(\frac{d\mathscr{R}_l}{dt}\right)_{t=0}$$

where zero time is when the stress is applied to the specimen. If m_i is the number of atoms contained in the curved dislocation segment,

$$\frac{d\mathscr{R}_l}{dt} = \frac{\Omega}{b}\frac{dm_i}{dt}$$

where dm_i/dt is the rate of flow of interstitials to the dislocation segment,

$$\frac{dm_i}{dt} = J_i^d l$$

where l is approximately the length of dislocation line between pinning points and J_i^d is the flux of interstitials per unit length of perpendicular-type dislocation line. Prior to application of the stress, the flux of interstitials to the dislocation lines is zero because the system is at equilibrium. However, application of the stress reduces the interstitial concentration at the core of the perpendicular-type lines, thus inducing an interstitial flux of

$$J_i^d = Z_i D_i [C_i - (C_i^d)_{\perp 0}]$$

where $(C_i^d)_{\perp 0}$ is the interstitial concentration at the core of the perpendicular-type dislocations at the moment that the stress is applied. Assembling the preceding four equations yields

$$\dot{\epsilon}_0 = \frac{1}{3}\rho_d \Omega Z_i D_i [C_i - (C_i^d)_{\perp 0}] \tag{19.203}$$

Just before the stress is applied, the concentration of interstitials at all dislocations in the solid is given by Eq. 19.181. After the specimen has been held at constant stress long enough for the new equilibrium configuration of the line segments to be attained, the interstitial concentration at the perpendicular-type dislocations is given by Eq. 19.188. However, at $t = 0$, the radius of curvature is still equal to the unstressed value $\mathscr{R}$, but the interstitial concentration at the dislocation core is instantaneously reduced by the second exponential term in Eq. 19.188. Therefore

$$(C_i^d)_{\perp 0} = C_i^{eq} \exp\left(\frac{\tau_d}{b\mathscr{R}}\frac{\Omega}{kT}\right)\exp\left(-\frac{\sigma\Omega}{kT}\right) \tag{19.204}$$

If we expand the second exponential term in a Taylor series, the driving force in Eq. 19.203 becomes

$$C_i - (C_i^d)_{\perp 0} = C_i - C_i^{eq}\exp\left(\frac{\tau_d}{b\mathscr{R}}\frac{\Omega}{kT}\right) + C_i^{eq}\exp\left(\frac{\tau_d}{b\mathscr{R}}\frac{\Omega}{kT}\right)\left(\frac{\sigma\Omega}{kT}\right)$$

Now, according to Eq. 19.184, the first two terms on the right-hand side of this equation are equal to each other, and the coefficient of $\sigma\Omega/kT$ in the last term is equal to C_i. Therefore, Eq. 19.203 becomes

$$\dot{\epsilon}_0 = \frac{1}{3}\rho_d \Omega Z_i D_i C_i \frac{\sigma\Omega}{kT}$$

Since C_i is not significantly changed at the instant of application of the stress, C_i in the above formula is given by Eq. 19.187, and the initial strain rate is

$$\dot{\epsilon}_0 = \frac{8}{3^{3/2}\pi}\frac{Z_i\Omega^2\sigma b(\rho_d)^{1/2}}{kT}\left(\frac{\nu_v}{z_{iv}} + \frac{4\pi}{15}\frac{R_0^5}{\Omega b^2}\right)\Sigma_s\Phi \tag{19.205}$$

Substituting Eqs. 19.205 and 19.201 [the latter with $F(1/\mathscr{R}) \simeq 1$] into Eq. 19.202 yields the coefficient B,

$$B = \frac{3^{3/2}\pi}{32}\frac{kT}{\Sigma_s E Z_i \Omega^2 b(\rho_d)^{1/2}\left(\frac{\nu_v}{z_{iv}} + \frac{4\pi}{15}\frac{R_0^5}{\Omega b^2}\right)} \tag{19.206}$$

Evaluating Eq. 19.206 for $\rho_d = 10^{12}$ cm^{-2} yields $B \simeq 10^{20}$ cm^{-2}, which is of the order of magnitude of the value of this parameter observed by Lewthwaite and Proctor.[35] Equation 19.205 indicates that the higher the dislocation density, the more rapidly is the terminal creep strain achieved. This prediction is also in accord with measurements of transient creep in cold-worked and annealed stainless steel.[35]

19.7.2 Steady-State Irradiation Creep by Vacancy Disk Collapse

Although dislocation loops formed by condensation of excess vacancies are not observed in the microstructure of metals irradiated above the low-temperature limit for void formation, vacancy loops are formed and persist during low-temperature irradiations. Vacancy loops are produced by collapse of platelets or disks of vacancies [Fig. 18.4(a)]. The latter are formed from the vacancies and small vacancy clusters in the depleted zone of a displacement spike. The mechanism by which the configuration shown in Fig. 17.27 transforms into a disk of vacancies is not known, but such platelets must be the intermediate step between the formless collection of vacancies in a displacement spike core and the regular configuration of a vacancy loop condensed on a close-packed plane. At the low temperatures where vacancy loops are observed, homogeneous nucleation of these defect clusters from the free vacancies in the matrix is virtually impossible because of the low value of the vacancy diffusion coefficient. Therefore, the vacancy platelets or vacancy loops must have originated from the complement of vacancies in the depleted zone created by the primary knock-on atom. Hesketh[36] has proposed a theory of irradiation creep based on the effect of stress on the propensity of vacancy disks to collapse into vacancy loops. This theory is reviewed here.

The process by which the depleted zone is transformed first into a vacancy platelet and then into a vacancy loop is depicted in Fig. 19.27. If the depleted zone contains m vacancies (either isolated or in small clusters), the radius of the vacancy platelet, R, formed from these vacancies is

$$m = \frac{\pi R^2}{a_0^2} \tag{19.207}$$

The disk is assumed to be 1 atom layer thick (i.e., a thickness equal approximately to a lattice constant a_0). Figure 19.27(b) shows the platelet as a circular disk. However, computer simulation of the stability of shapes of this sort in metals shows that the disk will partially collapse near the center, in somewhat the same fashion that neighboring atoms relax into a single vacant lattice site. The relaxed or minimum-energy configuration is shown in Fig. 19.27(c). The computer studies also show that the distance separating the opposite faces of the platelet at the center, s, is given by

$$s = a_0\left(1 - \frac{R}{R_c}\right) \tag{19.208}$$

where R_c is the critical platelet radius beyond which total collapse into the loop of Fig. 19.27(d) is assured. The critical radius is related to the number of vacancies in the critical size disk by

$$m_c = \frac{\pi R_c^2}{a_0^2} \tag{19.209}$$

When $R = R_c$ (or $m = m_c$), the two faces of the disk just touch at the center, and this is the necessary condition for collapse of the entire platelet into a loop. Hesketh assumes that in small disks ($m < m_c$) the platelets retain the configuration shown in Fig. 19.27(b) and that in disks larger than the critical size the platelets collapse to the loop configuration shown in Fig. 19.27(d).

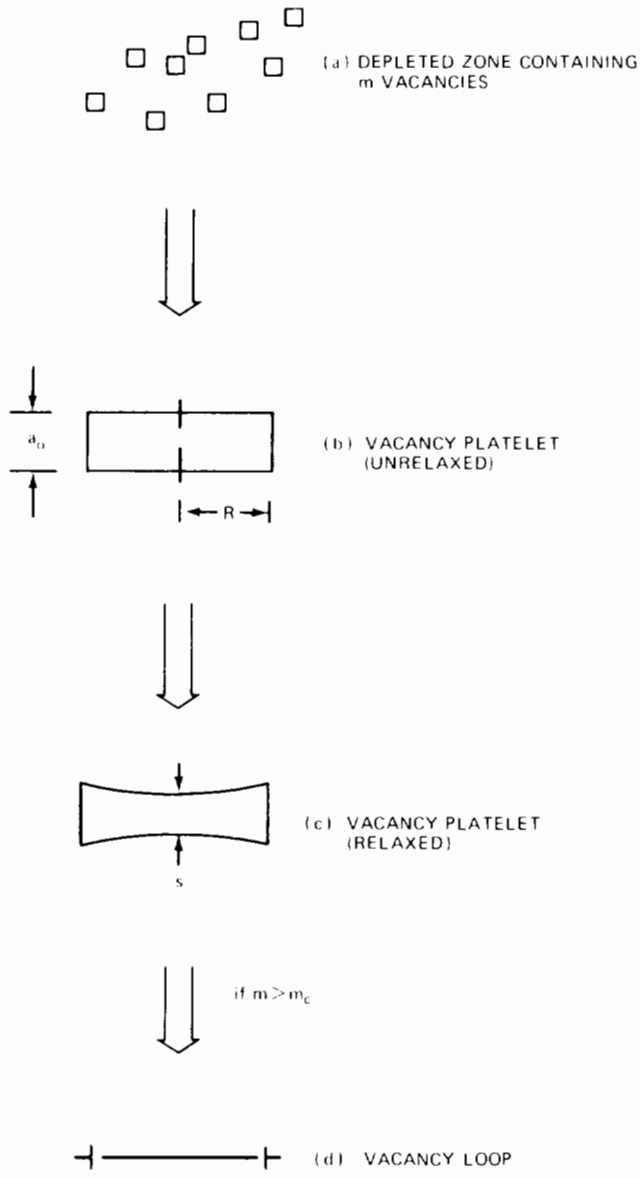

Fig. 19.27 Formation of vacancy disks and loops in an irradiated solid at low temperature.

We next determine how an applied stress perpendicular to the faces of the disk affects the critical size for collapse. Figure 19.28(a) shows that a compressive stress tends to reduce the central separation of the two faces. Conversely, tension would tend to bulge the two faces outward. The change in separation, s, due to the stress, σ, can be estimated by adapting the solution to a similar problem which has been treated by classical elasticity theory; this results in

$$s(\sigma) \sim s(0) - \frac{4}{E} R\sigma \tag{19.210}$$

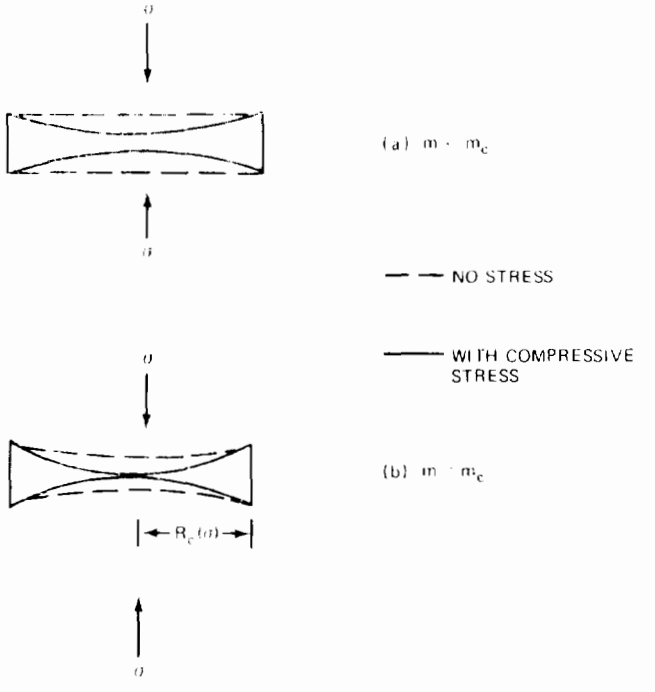

Fig. 19.28 Effect of stress on the shape of vacancy platelets.

where $s(\sigma)$ is the separation of the faces at stress σ and E is Young's modulus.* The stress effect suggested by Eq. 19.210 is plausible. Stress is more effective for large disks than for small ones and for weak solids (low E) than for strong ones.

Figure 19.28(b) shows the disk that contains just the right number of vacancies to render $s(\sigma) = 0$ (i.e., collapse occurs at this stress). The radius of such a disk, $R_c(\sigma)$, is less than the critical radius for collapse of a disk in a stress-free solid. The dashed lines show the configuration of a disk of the same radius when $\sigma = 0$. The interplanar separation s(0) can be obtained from Eq. 19.208 by setting $R = R_c(\sigma)$ and $R_c = R_c(0)$:

$$s(0) = a_o \frac{\Delta R_c}{R_c}$$

where $\Delta R_c = R_c(0) - R_c(\sigma)$ and $R_c(0)$ in the denominator has been denoted simply by R_c, since ΔR_c is small compared to either $R_c(\sigma)$ or $R_c(0)$.

Another expression for s(0) can be obtained by setting $s(\sigma) = 0$ at $R = R_c$ in Eq. 19.210, which gives

$$s(0) = \frac{4}{E} R_c \sigma$$

Equating the right-hand sides of the above two equations permits R_c to be written as

$$\Delta R_c = \frac{4}{E} \frac{R_c^2}{a_o} \sigma \qquad (19.211)$$

The stress effect can be expressed in terms of the change in the number of vacancies in the critical-size disk by use of Eq. 19.209:

$$\Delta m_c = \left(\frac{dm_c}{dR_c}\right) \Delta R_c = \frac{2\pi R_c}{a_o^2} \Delta R_c \qquad (19.212)$$

Substituting Eq. 19.211 into Eq. 19.212 and eliminating the ratio $(R_c/a_o)^3$ by using Eq. 19.209 yields

$$\Delta m_c = \frac{8}{\pi^{1/2}} \frac{m_c^{3/2}}{E} \sigma \qquad (19.213)$$

This formula gives the reduction in the critical size for disk collapse as a function of the applied compression. We next need the number of vacancy platelets formed in the solid which are affected by this alteration. Figure 19.29 shows a typical distribution of cluster sizes due to a single fast-neutron collision with a lattice atom. This distribution represents low-temperature irradiation, so the cluster distribution is not perturbed by vacancy or interstitial absorption from the matrix. Rather, Fig. 19.29 is supposed to represent the cluster distribution shown as the dashed histogram in Fig. 17.29(b). Hesketh takes the distribution to be of the form

$$N(m) = \frac{K}{m^2}$$

where K is a constant and N(m) is the number of depleted zones (or disks) formed from a single primary knock-on atom (PKA) which contain between m and m + dm vacancies.* The distribution applies to depleted zones for

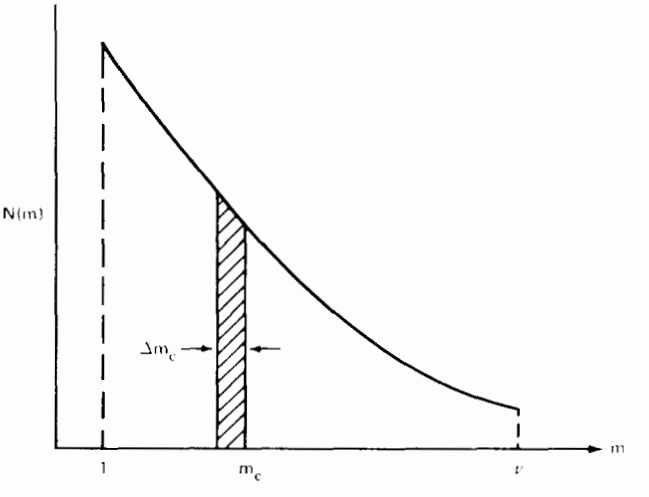

Fig. 19.29 Nascent cluster size distribution in an irradiated metal.

*A factor $1 - \nu^2$, where ν is Poisson's ratio, has been omitted from the second term on the right of Eq. 19.210 for simplicity. This factor is retained in Hesketh's analysis but is of no consequence numerically.

*The cluster distribution shown in Fig. 19.29 is very different from that used in the analysis of depleted-zone annealing in Sec. 18.5. Here, the distribution consisted of two delta functions, one at m = 1 and the other at the m value corresponding to a zone radius of R_0.

which $1 \leq m \leq \nu$, where ν is the total number of Frenkel pairs created by a PKA (as calculated by isolated cascade theory, Sec. 17.7). For a typical fast-neutron spectrum, $\nu \sim 500$ if annealing of the cascade is neglected. The constant K in the above distribution is determined by the requirement that the total number of vacancies contained in all clusters be equal to ν, or

$$\nu = \int_1^{\nu} m\, N(m)\, dm$$

The preceding two equations yield $K = \nu/\ln \nu$, and the distribution is

$$N(m) = \left(\frac{\nu}{\ln \nu}\right)\frac{1}{m^2} \qquad (19.214)$$

In an irradiated solid, vacancy platelets are formed with random orientations. Application of uniaxial stress does not change the randomness of the formation pattern. However, the vacancy disks that are perpendicular to the stress axis exhibit a different critical collapse size from the remaining platelets. Figure 19.30 shows a block of solid of dimensions x, y, and z (perpendicular to the drawing) subject to compressive stress along the x-axis. Of the vacancy platelets formed by irradiation, one-third are of the perpendicular type, which are affected by the stress, and the remainder are not influenced by the stress.

The number of platelets created in the parallel orientation which collapse to vacancy loops is represented by the area under the distribution to the right of m_c in Fig. 19.29. Among the perpendicular-type platelets, all those to the right of the abscissa $m_c - \Delta m_c$ are collapsed. The shaded area in Fig. 19.29, which is equal to $N(m_c)\,\Delta m_c$, represents the extra number of disks that are collapsed solely because the stress affects the perpendicular-type platelets but not the parallel-type disks. Because of the survival of a greater proportion of the parallel-type vacancy disks, the block of solid deforms more rapidly in the directions transverse to the stress axis than along it. The number of vacancies contained in the differential area in Fig. 19.29 is $m_c\, N(m_c)\, \Delta m_c$. The difference between the volume of empty space added per unit time to each of the two parallel-type disks (oriented perpendicular to the y and z axes) and that in the x-direction is

$$\frac{1}{3}\Sigma_s\, \Phi(XYZ)\, \Omega m_c\, N(m_c)\, \Delta m_c = (XZ)\frac{dY}{dt} - (YZ)\frac{dX}{dt} = (XY)\frac{dZ}{dt} - (YZ)\frac{dX}{dt}$$

Or, in terms of the strain rates in the principal directions,

$$\dot{\epsilon}_y - \dot{\epsilon}_x = \dot{\epsilon}_z - \dot{\epsilon}_x = \frac{1}{3}\Sigma_s\, \Phi\Omega m_c\, N(m_c)\, \Delta m_c \qquad (19.215)$$

where

$$\dot{\epsilon}_x = \frac{1}{X}\frac{dX}{dt}$$

$$\dot{\epsilon}_y = \frac{1}{Y}\frac{dY}{dt}$$

$$\dot{\epsilon}_z = \frac{1}{Z}\frac{dZ}{dt}$$

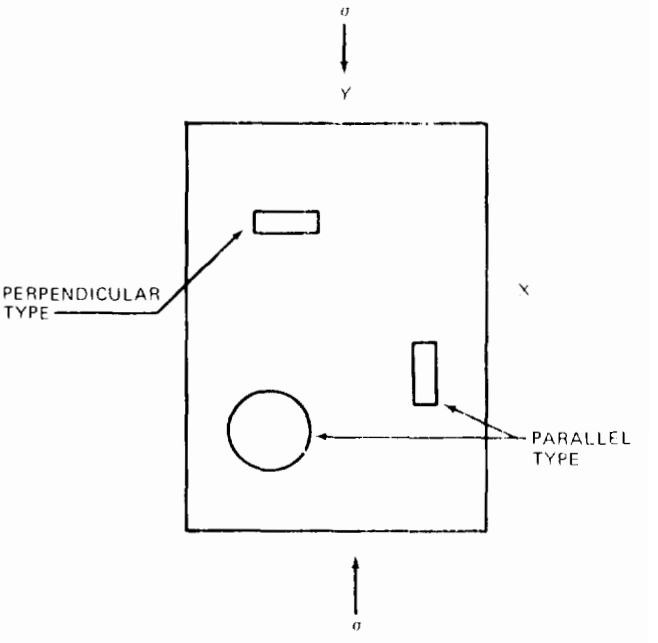

Fig. 19.30 Vacancy platelets in an irradiated solid.

Because uncollapsed platelets are present in disks of all orientations in the solid, continual buildup of disk volume occurs, and the solid undergoes volumetric swelling as well as creep (the latter is due to relative deformation in the three principal directions). The volume swelling rate is given by

$$\left(\frac{\dot{\Delta V}}{V}\right) = 3\dot{\epsilon}_v = 3\dot{\epsilon}_z \qquad (19.216)$$

The creep strain along the x-axis is the difference between the total strain rate in this direction and the component of volumetric swelling, or

$$(\dot{\epsilon}_x)_{creep} = \left|\dot{\epsilon}_x - \frac{1}{3}\left(\frac{\dot{\Delta V}}{V}\right)\right| = \frac{1}{3}\Sigma_s\, \Phi\Omega m_c\, N(m_c)\, \Delta m_c$$

Using Eq. 19.214 for $N(m_c)$ and Eq. 19.213 for Δm_c, we find the irradiation creep induced by the compressive stress to be

$$(\dot{\epsilon}_x)_{creep} = \left[\frac{8}{3\pi^{1/2}}\,\frac{1}{E}\left(\frac{\nu}{\ln \nu}\right)(m_c)^{1/2}\,\Omega\Sigma_s\right]\sigma\Phi = C\sigma\Phi \qquad (19.217)$$

Comparison of Eq. 19.217 with the second term on the right side of Eq. 19.176 shows that the coefficient C can be identified with the bracketed term in the above formula. Determining a numerical value from the parameters

$E = 2.1 \times 10^8$ kN/m^2
$\Omega = 12$ Å^3
$\Sigma_s = 0.2$ cm^{-1}
$\nu = 500$
$m_c = 200$

we find C to be 20×10^{-30} cm^2 kN^{-1} m^{-2}. Experimental values of this coefficient obtained from in-pile creep tests

on steel are shown in Fig. 19.31. There is quite good agreement between the magnitude of the theoretical and observed creep-rate coefficients. However, the theory does not predict the pronounced decrease in C with temperature (this behavior is also contrary to thermal creep, which should increase rapidly with temperature). The absence of a temperature effect in the theory just presented arises from the implicit assumption that all the uncollapsed vacancy platelets formed in the collision cascade are stable indefinitely in the irradiated solid. That is, their number simply increases linearly with time (or fluence). Had the theory included destruction of the vacancy platelets by vacancy emission to the bulk of the solid or by absorption of the radiation-produced interstitials (which are mobile at the temperatures for which C has been measured), the number of surviving disks would have decreased drastically with increasing temperature. Thus, although the rapid drop of C with temperature is not explicitly included in Hesketh's analysis, this observation is at least consistent with his model.

The continuous (and linear) increase in the number of uncollapsed loops with time is responsible for the fact that the theoretical creep rate is constant (i.e., creep is steady state). However, as shown in problem 19.18 at the end of this chapter, lack of a mechanism for removal of vacancy platelets smaller than the critical size for collapse leads to predicted swellings which are far larger than have been observed in low-temperature irradiations (although low-temperature swelling due to accumulation of depleted zones and their progeny, vacancy disks, has been observed; see Fig. 16 of Ref. 33).

Contrary to the transient creep mechanism discussed earlier in this section, steady-state creep by stress-assisted vacancy disk collapse is irreversible. When the stress is removed, the extra $N(m_c)\,\Delta m_c$ disks that were collapsed because of the stress do not spontaneously pop back into

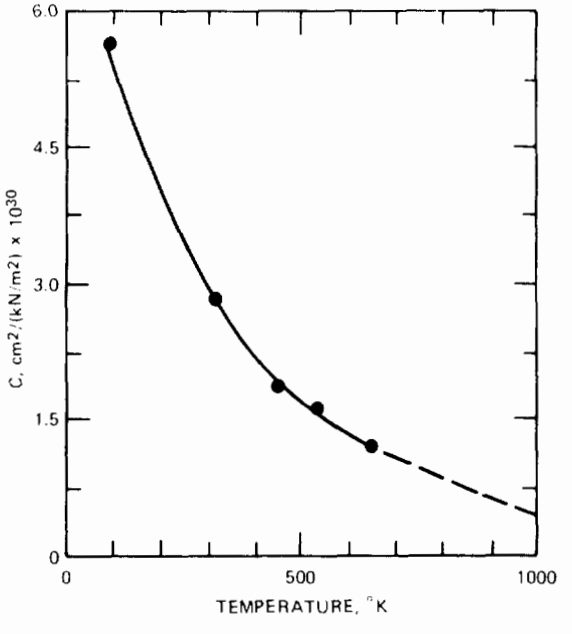

Fig. 19.31 Temperature dependence of the irradiation creep coefficient C (Ref. 33).

platelets. Thus, the creep strain persists. However, a difficulty arises if the theory is applied to creep induced by tension rather than compression. In the former case, $N(m_c)\,\Delta m_c$ represents extra platelets perpendicular to the stress which have not collapsed because stress aids in their survival by causing the disk faces to bulge outward. When this stress is removed, one would expect that platelets larger than the stress-free critical size would no longer be stable and that collapse would occur, thereby removing the creep deformation established during the time that the tensile stress was applied.

19.7.3 Steady-State Creep Due to Stress-Oriented Nucleation of Interstitial Loops

At temperatures roughly bracketed by the onset of observable void formation and peak swelling (about 350 to 500°C in stainless steel), irradiation creep can be produced by preferential nucleation of interstitial loops on suitably oriented planes by the prevailing stress state. This mechanism was first proposed by Hesketh[37] and has subsequently been applied to stainless steel by Lewthwaite,[38] Wolfer et al.,[39] and Brailsford and Bullough.[40]

During irradiation interstitials nucleate into loops on a particular set of planes in the solid (e.g., the {111} planes in the fcc lattice). Loop nuclei formed on planes favorably oriented with respect to the applied stress have a greater chance of surviving than those created on planes where the nucleation process is unaffected by the stress. Although there are many sets of equivalent {111} planes in the fcc lattice, for simplicity we consider only the planes perpendicular to the applied stress (called perpendicular type) and those lying along the stress axis (parallel type). There are twice as many of the latter as of the former. The situation can be visualized by regarding the objects in the block shown in Fig. 19.30 as interstitial dislocation loops and considering the case of an applied tension rather than compression (although this is not an important choice).

Because stress favors the nucleation of perpendicular-type loops, there will be a slightly higher concentration of these clusters than of either of the two parallel-type loops on the planes lying along the stress direction. In addition to preferential loop nucleation on planes perpendicular to the tensile axis, the growth of the perpendicular-type loops is somewhat more rapid than that of the parallel-type loops. However, this effect has been shown to be of secondary importance[40] and will be neglected here.

Preferential nucleation of the perpendicular-type loops occurs because this orientation allows the applied stress to do work on the circular dislocation line as it grows. The energy of formation is lowered by the amount of external work communicated to the system in this manner. Consider generation of a loop from zero size to the critical nucleation radius R_{1c}. The stress has no bearing on the formation process for parallel-type loops, and the energy of the critical-size loop (assuming that the loop can be regarded as a macroscopic dislocation line with a line tension τ_d) is

$$E_{\parallel} = 2\pi R_{1c}\tau_d \qquad (19.218)$$

However, a tensile stress σ exerts a force σb per unit length in the outward radial direction of growing perpendicular-type loops [see Fig. 8.10(b)]. As the loop expands from radius R_l to $R_l + dR_l$, the change in energy is

$$dE_l = 2\pi\tau_d\, dR_l - 2\pi R_l \sigma b\, dR_l$$

or, upon integrating from $R_l = 0$ to $R_l = R_{lc}$,

$$E_\perp = 2\pi R_{lc}\tau_d - \pi R_{lc}^2 \sigma b \qquad (19.219)$$

Assuming that the probability of nucleating a loop in a particular orientation is proportional to a Boltzmann factor involving the energy of formation, the relative nucleation rates of the perpendicular- and parallel-type loops are related by*

$$\frac{P_\perp}{P_\parallel} = \frac{\exp(-E_\perp/kT)}{\exp(-E_\parallel/kT)} = \exp\left(\frac{\pi R_{lc}^2 \sigma b}{kT}\right) \qquad (19.220)$$

The probabilities of nucleating loops on either of the two types of orthogonal planes must sum to unity:

$$P_\perp + 2P_\parallel = 1 \qquad (19.221)$$

The area per atom on the (111) plane of the fcc structure is $3^{1/2}\, a_o^2/4$ and the Burgers vector of the $a_o/3\langle 111\rangle$ faulted dislocation loop is $b = a_o/3^{1/2}$. Therefore, the number of interstitials in a dislocation loop of radius R_l is

$$m_i = \frac{4\pi R_l^2}{3^{1/2} a_o^2} = \frac{\pi R_l^2\, a_o}{3^{1/2}\Omega} = \frac{\pi R_l^2\, b}{\Omega} \qquad (19.222)$$

Where the relation between atomic volume and lattice constant for the fcc structure, $\Omega = a_o^3/4$, has been employed. Using Eq. 19.222 (with a subscript c attached to m_i and R_l to denote the critical-size loop) in Eq. 19.220 and combining the latter with Eq. 19.221 yields

$$P_\perp = \frac{\exp(m_{ic}\sigma\Omega/kT)}{2 + \exp(m_{ic}\sigma\Omega/kT)} \sim \frac{1}{3}\left(1 + \frac{2}{3}\frac{m_{ic}\sigma\Omega}{kT}\right) \qquad (19.223)$$

where Taylor series expansions have been applied to the exponential terms. If the total density of interstitial loops is N_l (given, for example, by Eq. 19.18), the number density of perpendicular-type loops is $P_\perp N_l$, which is greater than the density of loops on either of the two sets of planes parallel to the stress axis. At some time during irradiation, the radii of all the loops will have grown from R_{lc} to R_l, but, because the effect of stress on growth subsequent to nucleation has been neglected, $R_{l\perp} = R_{l\parallel} = R_l$. The loop radius can be obtained from Eq. 19.16.

The number of interstitial atoms per unit volume contained in the perpendicular type loops is $m_i N_l P_\perp$, where m_i is related to the loop radius by Eq. 19.222. If loop nucleation had occurred in the absence of stress, the number of interstitials per unit volume in loops of all orientations would have been $m_i N_l/3$ (i.e., $P_\perp = 1/3$). Therefore, the additional number of interstitials present in the perpendicular-type loops as a result of the slightly greater number of these clusters is

Extra atoms in perpendicular-type loops/cm^3

$$= m_i N_l\left(P_\perp - \frac{1}{3}\right)$$

Following the lines of the argument leading to Eq. 19.198, the creep strain due to these extra loops in planes perpendicular to the stress is

$$\frac{\delta X}{X} = \epsilon_x = m_i \Omega N_l\left(P_\perp - \frac{1}{3}\right)$$

Or, using Eqs. 19.223 and 19.222,

$$\epsilon_x = \frac{2}{9}(\pi R_l^2 N_l b)\frac{m_{ic}\Omega\sigma}{kT} \qquad (19.224)$$

If the critical loop nucleus is known (m_{ic} is probably about 3 but can be as large as 10) and experimental information on loop size and density during irradiation are known, Eq. 19.224 determines the creep rate. Alternatively, the fluence dependence of R_l and N_l can be obtained theoretically from the point-defect balances, the void and loop growth laws, and the nucleation rates of these two defect clusters (Secs. 19.4 and 19.5). This approach is used in Ref. 40. Consideration of all the equivalent set of $\{111\}$ planes in the fcc lattice, rather than simply an orthogonal set of three, reduces the above creep rate expression by a constant factor of 2.5 (Ref. 38).

Attempts have been made to connect the creep strain to the void swelling. This is done by assuming that the number of interstitials contained in loops is equal to the number of vacancies in voids. A bit of consideration shows that the parenthetical term in Eq. 19.224 is equal to the fractional swelling of the solid due to the loops, and if this volume increase is equal to that due to the voids ($\Delta V/V$), we have

$$\epsilon_x = \frac{2}{9}\left(\frac{\Delta V}{V}\right)\frac{m_{ic}\Omega\sigma}{kT} \qquad (19.225)$$

There is no theoretical justification for the assignment of equal numbers of interstitials in loops and vacancies in voids. Excess interstitials can be absorbed by the network dislocations in the solid provided that the latter are free to climb. Interstitial loops disappear from the microstructure above about 500°C (Fig. 19.7), but the voids persist to above 600°C. Consequently, Eq. 19.224 is preferred to Eq. 19.225 if information on the fluence and temperature dependence of loop size and density is available. However, Eq. 19.225 can be modified by multiplication by the fraction of the total dislocation density contained in loops (i.e., one minus Eq. 19.15) and in this way be rendered a reasonably accurate predictor of the creep rate even when the loops and voids do not contain equal numbers of point defects.[40]

The model of irradiation creep just described is unique in that the stress affects only the nucleation process. Thus, if the specimen is unloaded after loop nucleation has occurred (and perturbed by the stress), the creep persists during stress-free growth. Conversely, application of the stress after nucleation has been completed should not produce this sort of irradiation creep.

*The same result is obtained by proceeding through homogeneous nucleation theory with the formation energy of a loop reduced by the right term of Eq. 19.219. The exponential terms in Eqs. 19.77 and 19.78 would be increased by the term containing the stress.

19.7.4 Climb-Controlled Dislocation Glide

The effect of irradiation on creep controlled by diffusion of point defects to sinks in the solid was discussed in Sec. 16.10 in connection with the fuel. It was shown that radiation-produced point defects do not accelerate the normal creep rate when the sinks are grain boundaries. The same conclusion is reached when the sinks are dislocations and creep is entirely due to climb of the dislocations. However, the class of creep mechanisms constructed by Weertman (Refs. 24 and 25 in Chap. 16) are susceptible to enhancement by irradiation. It will be recalled from Sec. 16.8 that this type of creep involves climb of mobile dislocations either over obstacles in the glide plane or toward a dislocation of opposite sign in an adjacent parallel slip plane. Creep occurs in the first type when the mobile dislocation reaches the top of the barrier and quickly glides to the next obstacle, and, in the second type, when the pileup expands by glide to replenish one of its members that has been annihilated by an opposing dislocation from the adjacent slip plane. The separation of the rate controlling process (climb) from the strain controlling step (glide) in these mechanisms is essential to the existence of an irradiation effect on the creep rate.

The effect of irradiation on diffusional creep processes (which include the climb-controlled glide variant) has long been the subject of dispute (see Refs. 38 to 43 in Chap. 16). On the basis of recent investigations (Refs. 21, 39, and 41 to 44), irradiation enhancement of Weertman-type creep requires an imbalance in the rates at which dislocations absorb interstitials and vacancies produced by fast-neutron bombardment of the metal. In the sections on void swelling in this chapter, we showed that absorption of excess interstitials by the intrinsically biased dislocations can occur only if another sink that consumes excess vacancies is also present. At high temperatures the vacancy sinks fulfilling this role are undoubtedly the voids, but at low temperatures depleted zones can perform the same function.

Irradiation creep by the climb-controlled glide mechanism is due to the climb velocity $(v_c)_{irr}$ with which the dislocation is endowed by virtue of capturing excess interstitials. For irradiation creep to be of significance, $(v_c)_{irr}$ must be at least comparable to the climb velocity $(v_c)_{th}$ induced in the blocked mobile dislocation by the stress arising from interaction with obstacles (Sec. 16.8). Irradiation simultaneously serves to reduce the creep rate because the obstacles that the mobile dislocation must climb over and glide between are either the voids and interstitial loops in the temperature range where swelling occurs or the depleted zones at low temperatures. The size and density of these clusters increase with fluence. These obstacles are responsible for the increased strength of irradiated metals (Secs. 18.5 to 18.7). They are also the cause of decreased creep rates in postirradiation tests, which should not be confused with in-pile irradiation creep. The former is a structural effect since the creep mechanisms are the same as in an irradiated metal, and only the nature and density of the obstacles to dislocation motion are affected by irradiation. In-pile, or irradiation, creep, which contains the additional element of enhanced climb by absorption of point defects, is sometimes called dynamic creep to emphasize the importance of the neutron flux as well as the neutron fluence.

Creep due to climb-controlled glide of mobile dislocations in an irradiated solid can be analyzed by starting from the general formula relating strain rate and dislocation velocity (Eq. 8.21):

$$\dot{\epsilon} = \rho_m b v_d \tag{19.226}$$

where ρ_m is the density of mobile dislocations in the solid, which is generally less than the total dislocation density ρ_d. Part of ρ_d may consist of unfaulted interstitial loops that are sessile (i.e., not mobile), or are pinned by voids or enmeshed in dislocation tangles. The b is the Burgers vector of the mobile dislocation; and v_d is the average velocity of the moving dislocation, which is the ratio of the average distance that a mobile dislocation glides between obstacles and the time required for it to climb over the obstacle:

$$v_d = \frac{l}{(h/v_c)} \tag{19.227}$$

Here, l is the glide distance, h is the distance perpendicular to the glide plane which the mobile dislocation must climb in order to surmount the obstacle, and v_c is the climb velocity; h/v_c is the average time required for the dislocation to overcome the barrier by climb.

We imagine the obstacles to be arranged on the glide plane in a square array with the spacing given by Eq. 18.25:

$$l = \frac{1}{(2RN)^{1/2}} \tag{19.228}$$

where R and N are the radius and density, respectively, of the obstacles, which may be depleted zones, voids, or interstitial loops. The applied stress is assumed to be less than that at which the dislocation can pass through the array by cutting through the obstacles or by bowing around them and pinching off. In the present case the dislocation line must climb to a critical height perpendicular to the slip plane at which point the applied stress is sufficient to permit slip to continue. A two-dimensional view of the process is shown in Fig. 19.32. Rows of obstacles are viewed end-on. The separation of the spherical obstacles in the direction perpendicular to the drawing is the same as the distance between rows in the glide plane, namely l. If the obstacles in the real solid were arranged in the perfect square pattern used in the analysis, climb of a blocked dislocation over one row would be sufficient for the dislocation to slip past all the subsequent rows. However, this deficiency of the idealized model should not be taken too seriously since in an actual irradiated solid the random arrangement of obstacles ensures that a mobile dislocation will be stopped by obstacles after gliding from its previous pinning position a distance given, on the average, by Eq. 19.228.

Determination of the creep rate is reduced to calculating the obstacle height h and the climb velocity v_c.

We first consider the situation proposed by Harkness et al.[43] in which the obstacles to be overcome by climb are voids. Inasmuch as voids attract dislocation lines (Sec. 18.6), the first dislocation approaching the row of voids is trapped by them, in a sequence of events similar to

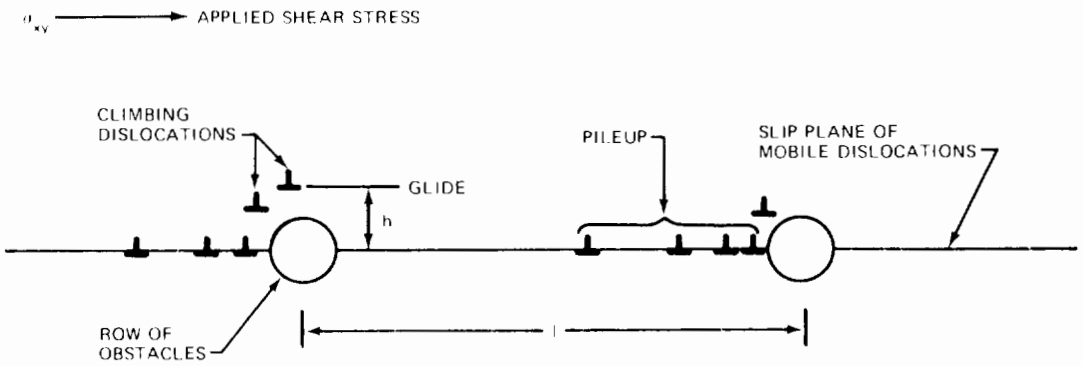

Fig. 19.32 Dislocation motion over irradiation-produced obstacles in the climb-controlled dislocation glide model of irradiation creep.

that shown in Fig. 18.22(b) except for the final pinching off (which does not occur here because the stress is less than the yield stress for this process). Succeeding mobile dislocations, however, are repelled by the first dislocation that has been sucked into the void row. They must climb over the trapped dislocation to continue on their way.

In the absence of irradiation, the climb process is identical to that analyzed in Sec. 16.7 (climb-to-escape model). The probability per unit time that a dislocation climbs over the pinned dislocation is given by Eq. 16.73, which can be used to define an average thermal climb velocity by

$$p = \frac{1}{C\tau_c} = \frac{(v_c)_{th}}{h} \tag{19.229}$$

where the barrier height h is given by Eq. 8.35 in which, to account for a dislocation pileup behind the trapped dislocation, σ_{xy} is multiplied by the intensification factor n of Eq. 8.39:

$$h = \frac{K}{4n\sigma_{xy}} = \frac{Gb}{8\pi(1-\nu)n\sigma_{xy}} \tag{19.230}$$

In Eq. 19.229 C is a coefficient that arises from averaging the climb process over all impact parameters separating the slip planes of the trapped dislocation and the impinging mobile dislocation (Eq. 16.72), and τ_c is a characteristic time for dislocation climb. When the climb velocity is based on the jog density of the line (i.e., Eq. 16.55), τ_c is given by Eq. 16.67. If, on the other hand, the entire dislocation line maintains the equilibrium vacancy concentration appropriate to the stress acting on it, the climb velocity is given by Eq. 16.58, and τ_c becomes

$$\tau_c = K\left[\frac{\ln(\mathscr{R}/r_d)}{2\pi}\right]\frac{kTb}{D_{vol}\Omega n^2\sigma_{xy}^2} \tag{19.231}$$

Substituting Eqs. 19.230 and 19.231 into Eq. 19.229 and using Eq. 8.39 for n yields

$$(v_c)_{th} = \frac{\pi^2(1-\nu)}{2C\ln(\mathscr{R}/r_d)}\frac{D_{vol}b\sigma_{xy}^2}{kTG} \tag{19.232}$$

where the length of the pileup in Eq. 8.39 has been taken as the spacing between obstacle rows.

Under neutron irradiation the velocity of dislocation climb is no longer governed by the thermal processes inherent in the value given by Eq. 19.232. Instead, it is determined by the flow of interstitials and vacancies to the dislocations. Let J_i^d and J_v^d be the fluxes of interstitials and vacancies, respectively, to a unit length of dislocation line (Eq. 13.89). The net rate at which interstitials arrive at the line is $J_i^d - J_v^d$, and, since each interstitial contributes a volume Ω, the rate at which the half-sheet of atoms comprising the edge dislocation gains volume is $(J_i^d - J_v^d)\Omega$ cm^3 sec^{-1} cm^{-1} of line. In Δt sec, each unit length of line gains a volume of $(J_i^d - J_v^d)\Omega\ \Delta t$, which is equal to the product of the width of the half-sheet of atoms, b, and the distance climbed in Δt, which is $(v_c)_{irr}\Delta t$. Thus, the climb velocity due to the net flow of irradiation-produced interstitials to the line is

$$(v_c)_{irr} = \frac{(J_i^d - J_v^d)\Omega}{b} \sim (J_i^d - J_v^d)\,b^2 \tag{19.233}$$

Equation 19.233 demonstrates that the climb of dislocations caused by irradiation is due to precisely the same phenomenon that is responsible for void growth, namely, the bias of dislocation lines for interstitials.

The irradiation creep rate is obtained by combining Eqs. 19.226 and 19.227 and using Eq. 19.230 for h and Eq. 19.233 for v_c, which yields

$$\dot{\epsilon}_{irr} = \rho_m b\frac{8\pi(1-\nu)n\sigma_{xy}}{G}(J_i^d - J_v^d)b^2 \tag{19.234}$$

Now we note that the product of $(J_i^d - J_v^d)$ and the total dislocation density of the solid, ρ_d, is the difference in the volumetric sink strengths of the dislocations for interstitials and vacancies, or

$$\rho_d(J_i^d - J_v^d) = Q_i^d - Q_v^d \tag{19.235}$$

where Q_i^d and Q_v^d are given by Eqs. 19.101 and 19.102, in which the notation N (representing the network dislocations) is replaced by d (representing all dislocations). For the present analysis the distinction between dislocation lines and dislocation loops is neglected. The irradiation creep rate can be related to void swelling by using the point-defect balances given by Eqs. 19.134 and 19.135. As before, we combine network dislocations and interstitial loops into the total dislocation density. Subtraction of one of the point-defect balances from the other shows that

$$Q_i^d - Q_v^d = Q_v^{void} - Q_i^{void} \tag{19.236}$$

which states that, in the absence of sinks other than voids and dislocations, the net flow of interstitials to dislocations is just equal to the net flow of vacancies to voids. Finally, the swelling rate is given by

$$\frac{d}{dt}\left(\frac{\Delta V}{V}\right) = \left(\frac{\dot{\Delta V}}{V}\right) = (Q_v^{void} - Q_i^{void})\Omega \qquad (19.237)$$

Combining the preceding four equations and expressing the number of dislocations in the pileup by Eq. 8.39 yields the irradiation creep rate according to this model:

$$\dot{\epsilon}_{irr} = \left(\frac{\rho_m}{\rho_d}\right)\left[\frac{8\pi^2(1-\nu)^2}{G^2}\right]\frac{l^2 b}{\Omega}\left(\frac{\dot{\Delta V}}{V}\right)\sigma_{xy}^2 \qquad (19.238)$$

which shows the direct connection between the swelling rate and the irradiation creep rate.

The creep rate under irradiation is less stress dependent than is the thermal creep rate. If Eq. 19.232 had been used in place of Eq. 19.233 in the foregoing derivation, the stress exponent would have been 4 instead of 2. If the mobile dislocation density is low or if the swelling rate is large, the mobile dislocations can climb over the dislocations trapped by the voids so quickly that pileups do not have time to develop. In this case we set n = 1 wherever it appears, with the result that the irradiation and thermal creep rates are proportional to σ_{xy} and σ_{xy}^2, respectively. In any case the exponent of the stress is lower in irradiation creep than in thermal creep, and this prediction is confirmed by experiment.

The irradiation creep rate has a somewhat narrower temperature range than does the swelling rate. When the temperature is low, a substantial part of the total dislocation density is present as faulted loops, which cannot glide; so ρ_m/ρ_d is low. In addition, $(\dot{\Delta V}/V)$ is small at low temperatures, and the irradiation creep rate is reduced by both these factors. At the high-temperature extreme, irradiation creep by this mechanism ceases when the voids do not grow (i.e., when $\dot{\Delta V}/V \to 0$ at $T \sim 600°C$ in stainless steel). At sufficiently high temperature, the rapidly increasing thermal climb velocity given by Eq. 19.232 overtakes the irradiation-induced climb velocity, and normal Weertman thermal creep supplants irradiation creep as the principal deformation mechanism. Similarly, the σ_{xy}^2 dependence of the thermal climb velocity implies that, at any temperature, thermal creep dominates irradiation creep if the applied stress is sufficiently high (but not high enough for the dislocations to cut through or bypass the voids by bowing and pinching off).

Equation 19.238 implies that the irradiation creep rate decreases with increasing fluence because the size and perhaps the density of voids increases during irradiation. According to Eq. 19.228, the obstacle separation is decreased accordingly.

The most difficult term in Eq. 19.238 to predict is the fraction of the total dislocation population which is mobile. Harkness et al.[43] identify the mobile dislocations with the line length of unfaulted loops in the microstructure. They assume that Frank loops unfault when R = 500 Å and consider that when the average loop radius exceeds this value, $\rho_m/\rho_d = 1$. When the average loop size is less than 500 Å, they employ the approximation

$$\frac{\rho_m}{\rho_d} = \frac{R_l(\text{Å})}{500}$$

where R_l is a function of fluence as determined by solution of the loop-growth law, which is obtained in the course of solving the void swelling (by the method shown in Fig. 19.23).

In addition to the voids, interstitial loops provide barriers to dislocation motion of strength comparable to that of the voids. Wolfer et al.[39] have formulated the climb-controlled glide model described above with loops instead of voids as obstacles. The loops directly repel mobile dislocations that approach them. The applied stress necessary to force a dislocation line past a row of loops of radius R_l separated by a distance l is given by combining Eqs. 18.54 and 18.58:

$$\sigma_{xy} = \frac{\alpha G b_l}{2(1-\nu)}\frac{R_l^2}{ly^2}$$

where y is the distance between the row of loops and the glide plane of the mobile dislocation. If the row of loops lies in the glide plane of the approaching dislocation and if the applied stress is too low for the line to penetrate the row (i.e., if $\sigma_{xy} < \sigma_s$ of Eq. 18.61), the line has to climb by a height y in order to continue slip. Therefore, y can be written as the barrier height h. If we allow for dislocation pileup behind the row of loops by replacing σ_{xy} by $n\sigma_{xy}$, the above formula can be solved for the barrier height in terms of the applied stress:

$$h = \left[\frac{\alpha G b_l}{2(1-\nu)}\frac{R_l^2}{nl\sigma_{xy}}\right]^{1/2} \qquad (19.239)$$

If the previous derivation is repeated using Eq. 19.239 instead of Eq. 19.230 for h, the irradiation creep rate is found to be

$$\dot{\epsilon}_{irr} = \left(\frac{\rho_m}{\rho_d}\right)\left[\frac{2\pi(1-\nu)}{\alpha G^2}\right]^{1/2}\frac{l^2}{R_l b}\left(\frac{\dot{\Delta V}}{V}\right)\sigma_{xy} \qquad (19.240)$$

which, when compared with Eq. 19.238 for void obstacles, shows a lower stress dependence (linear instead of squared) and a greater penalty due to fluence because of the factor R_l in the denominator.

As a final example of climb-controlled glide models of irradiation creep, Duffin and Nichols[44] have advanced a mechanism in which the obstacles are depleted zones. In this model the swelling rate does not appear because depleted zones and voids do not coexist in an irradiated metal.

19.8 NOMENCLATURE

- a_o = lattice constant
- $\mathcal{A}$ = area swept out by bowing of pinned dislocation segment
- A,B,C = constants in creep formula, Eq. 19.176
- b = length of Burgers vector
- B = binding energy of a diinterstitial
- C = point-defect concentration (particles per unit volume); constant given by the right side of Eq. 16.72

C^* = point-defect concentration at the surface of a coherent precipitate
D = point-defect diffusion coefficient
D_{vol} = volume self-diffusion coefficient
E_{loop} = energy of a loop
E_{void} = energy of a void
$f(R,\mathscr{R},l)$ = function defined by Eq. 19.157
F = force on a dislocation
$F(1/\mathscr{R})$ = function defined by Eq. 19.199
$F(\eta)$ = function defined by Eq. 19.142
g = gibbs free energy of a cluster
G = shear modulus; total Gibbs free energy
h = climb height for a dislocation to overcome a barrier; enthalpy of a cluster
$h(m)$ = function defined by Eq. 19.43
H = coefficient of M in Eq. 19.56
I = nucleation current or void current
j = gas atoms in a cluster
J = flux of point defects to a cluster
J^d = flux of point defects to a unit length of dislocation
k = Boltzmann's constant; rate constant
k_{iv} = vacancy–interstitial recombination rate constant
K = coefficient of $m^{1/2}$ in Eq. 19.6; given by Eq. 8.30
l = distance between dislocation pinning points
$\mathscr{l}$ = length of a bowed dislocation segment
m = vacancies per void or per vacancy loop; interstitials per interstitial loop
M = total helium concentration in metal
M_j = density of helium atom clusters containing j helium atoms
n = number of dislocations in a pileup; number of point defects in a region of solid
N = total number of voids per unit volume
$N(R)$ = void distribution function
N_l = number of faulted dislocation loops per unit volume
N_p = number of precipitate particles per unit volume
N_s = number of lattice sites per unit volume
p = helium pressure
P = probability of nucleating a loop of a particular orientation
Q_k^j = rate of absorption of a point defect of type k by all the defect clusters of type j in a unit volume of solid
r_d = radius of a dislocation core
R = rate of reaction; radius of a void
$\dot{R}$ = void growth rate
$\dot{R}_e$ = negative of void-shrinkage rate due to vacancy emission
$\dot{R}_0$ = void-growth rate in the absence of recombination and thermal emission of vacancies
R_0 = size of defect clusters created by collision cascade
R_l = radius of a faulted dislocation loop
$\mathscr{R}$ = radial extent of the stress field around a dislocation; radius of curvature of a bowed dislocation line
s = entropy of a cluster; distance between opposite faces of a vacancy platelet
S = supersaturation of point defect
t = time
T = temperature, °K
v_c = climb velocity of a dislocation
v_d = glide velocity of a dislocation
V = volume
ΔV = volume increase
w = jump frequency
W = combinatorial number
x = defined by Eq. 19.146
X,Y,Z = dimensions of a crystal
Y = defined by Eqs. 19.129 and 19.130
z = combinatorial number
Z = combinatorial number for dislocations, Eqs. 19.99 and 19.100

Greek Letters

α = point-defect emission rate from a cluster
β = point-defect arrival rate at a cluster
ϵ = creep strain; energy of formation
$\dot{\epsilon}$ = creep rate
ϵ_g = heat of solution of helium in metal
ϵ^* = energy of migration of a point defect
η = dimensionless parameter, Eq. 19.143a
γ = surface tension
γ_{sf} = stacking-fault energy
γ^* = defined by Eq. 19.122
μ = chemical potential
ν = vibration frequency; point defects produced per PKA
Ω = atomic value
Φ = total fast-neutron flux
ρ_d = total dislocation density
ρ_l = dislocation density as faulted loops
ρ_m = density of mobile dislocations
ρ_N = dislocation density due to perfect loops and the network dislocations
σ = hydrostatic stress (positive in tension)
σ_{xy} = shear stress
Σ_s = macroscopic neutron-scattering cross section
τ = time
τ_d = line tension of a dislocation
θ = fraction of sites on trapping interface occupied by point defects; T=623, °K
ξ = defined by Eq. 19.34

Subscripts and Superscripts

c = in critical embryo or critical-size vacancy platelet
eq = equilibrium
f = forward reaction
homo = homogeneous nucleation
i = interstitial
irr = due to irradiation
m = containing m point defects
nucl = nucleation
p = precipitate particles
r = reverse reaction
th = due to thermal process
v = vacancy

⊥ = edge dislocation with extra half-sheet of atoms perpendicular to applied stress; loop perpendicular to stress

|| = edge dislocation with extra half-sheet of atoms parallel to the applied stress; loop parallel to the stress

19.9 REFERENCES

1. C. Cawthorne and E. Fulton, *Nature*, **216**: 576 (1967).
2. D. J. Mazey, J. A. Hudson, and R. S. Nelson, *J. Nucl. Mater.*, **41**: 257 (1971).
3. F. S. Ham, *J. Appl. Phys.*, **30**: 915 (1959).
4. A. L. Bement, *Advan. Nucl. Sci. Technol.*, **7**: 1 (1973).
5. D. I. R. Norris, *Radiat. Eff.*, **14**: 1 (1972); **15**: 1 (1972).
6. J. W. Corbett and L. C. Ianniello (Eds.), *Radiation-Induced Voids in Metals*, Albany, N. Y., June 9–11, 1971, AEC Symposium Series, No. 26 (CONF-710601), 1972.
7. *Voids Formed by Irradiation of Reactor Materials*, Conference Proceedings, British Nuclear Energy Society, Reading, England, 1971.
8. J. I. Bramman et al., Void Formation in Cladding and Structural Materials Irradiated in DFR, in *Radiation-Induced Voids in Metals*, Albany, N. Y., June 9–11, 1971, J. W. Corbett and L. C. Ianniello (Eds.), AEC Symposium Series, No. 26 (CONF-710601), p. 125, 1972.
9. P. Murray, *Reactor Technol.*, **15**: 16(1972).
10. H. R. Brager and J. L. Straalsund, *J. Nucl. Mater.*, **46**: 134 (1973).
11. E. E. Bloom, Nucleation and Growth of Voids in Stainless Steels During Fast-Neutron Irradiation, in *Radiation-Induced Voids in Metals*, Albany, N. Y., June 9–11, 1971, J. W. Corbett and L. C. Ianniello (Eds.), AEC Symposium Series, No. 26 (CONF-710601), p. 1, 1972.
12. J. O. Stiegler, Void Formation in Neutron-Irradiated Metals, in *Radiation-Induced Voids in Metals*, Albany, N. Y., June 9–11, 1971, J. W. Corbett and L. C. Ianniello (Eds.), AEC Symposium Series, No. 26 (CONF-710601), p. 292, 1972.
13. D. W. Keefer and A. C. Pard, *J. Nucl. Mater.*, **45**: 55 (1972/1973).
14. J. L. Katz and H. Wiedersich, *J. Chem. Phys.*, **55**: 1414 (1971); a somewhat shorter version of this analysis appears in Ref. 6, p. 825.
15. K. C. Russell, *Acta. Met.*, **19**: 753 (1971); calculations based on the theory are reported in *Radiat. Eff.*, **12**: 127 (1972).
16. J. L. Katz and H. Wiedersich, *J. Nucl. Mater.*, **46**: 41 (1973); also in *Defects and Defect Clusters in bcc Metals and Their Alloys*, R. J. Arsenault (Ed.), p. 530, National Bureau of Standards, Washington, 1973.
17. K. C. Russell, *Acta Met.*, **20**: 899 (1972); also in *Defects and Defect Clusters in BCC Metals and Their Alloys*, R. J. Arsenault (Ed.), p. 545, National Bureau of Standards, Washington, 1973.
18. K. C. Russell and R. W. Powell, *Acta Met.*, **21**: 187 (1973).
19. G. J. Dienes and A. C. Damask, *Point Defects in Metals*, Gordon and Breach, Science Publishers, Inc., New York, 1963.
20. M. R. Hayns, *J. Nucl. Mater.*, **56**: 267 (1975).
21. S. D. Harkness, J. A. Tesk, and Che-Yu Li, *Nucl. Appl. Technol.*, **9**: 24 (1970); also, *Met. Trans.*, **2**: 1457 (1971).
22. H. Wiedersich, *Radiat. Eff.*, **12**: 111 (1972).
23. A. D. Brailsford and R. Bullough, *J. Nucl. Mater.*, **121**: (1972).
24. A. D. Brailsford and R. Bullough, British Report AERE-TP-538, 1973.
25. A. D. Brailsford and R. Bullough, *J. Nucl. Mater.*, **48**: 87 (1973).
26. J. L. Straalsund and G. L. Guthrie, *Nucl. Technol.*, **16**: 36 (1972).
27. F. A. Garner et al., The Effect of Stress on Radiation-Induced Void Growth, in *Radiation-Induced Voids in Metals*, Albany, N. Y., June 9–11, 1971, J. W. Corbett and L. C. Ianniello (Eds.), AEC Symposium Series, No. 26 (CONF-710601), p. 841, 1972.
28. S. D. Harkness and Che-Yu Li, Theoretical Study of the Swelling of Fast-Neutron-Irradiated Materials, in *Radiation-Induced Voids in Metals*, Albany, N. Y., June 9–11, 1971, J. W. Corbett and L. C. Ianniello (Eds.), AEC Symposium Series, No. 26 (CONF-710601), p. 798, 1972.
29. J. L. Straalsund, *Scr. Met.*, **4**: 459 (1970).
30. H. Wiedersich and K. Herschbach, *Scr. Met.*, **6**: 453 (1972).
31. J. R. Willis and R. Bullough, in *Voids Formed by Irradiation of Reactor Materials*, Conference Proceedings, British Nuclear Energy Society, Reading, England, 1971, p. 133.
32. V. F. Sears, *J. Nucl. Mater.*, **39**: 18 (1971).
33. E. R. Gilbert, *Reactor Technol.*, **14**: 258 (1971).
34. R. V. Hesketh, *Phil. Mag.*, **8**: 1321 (1963).
35. G. W. Lewthwaite and K. J. Proctor, *J. Nucl. Mater.*, **46**: 9 (1973).
36. R. V. Hesketh, in Proceedings of the International Conference on Solid State Research and Accelerators, A. N. Goland (Ed.), USAEC Report BNL-50083, pp. 389-401, 1967.
37. R. V. Hesketh, *Phil. Mag.*, **7**: 1417 (1962).
38. B. W. Lewthwaite, *J. Nucl. Mater.*, **46**: 324 (1973).
39. W. G. Wolfer, J. P. Foster, and F. A. Garner, *Nucl. Technol.*, **16**: 55 (1972); W. G. Wolfer and A. Boltax, in Conference on Irradiation Embrittlement and Creep in Fuel Cladding and Core Components, London, 1972, British Nuclear Energy Society, 1973.
40. A. D. Brailsford and R. Bullough, *Phil. Mag.*, **27**: 49 (1973); British Report AERE-TP-512, 1972.
41. G. W. Lewthwaite, *J. Nucl. Mater.*, **38**: 118 (1971).
42. G. Martin and J. P. Poirier, *J. Nucl. Mater.*, **39**: 93 (1971).
43. S. D. Harkness, R. Grappel, and S. G. McDonald, *Nucl. Technol.*, **16**: 25 (1972).
44. W. J. Duffin and F. A. Nichols, *J. Nucl. Mater.*, **45**: 302 (1972/1973).

19.10 PROBLEMS

19.1 Using Fig. 19.4, estimate the fraction of the vacancies created in an irradiation of fluence 5×10^{22} neutrons/cm^2 which is in voids.

19.2 Prove that Eq. 19.44 is the solution to Eq. 19.43 by using the fact that the logarithm of a product of terms is

the sum of the logarithms of each term and by carefully examining the behavior of h(m) and $N^{eq}(m)$ as $m \to 0$.

19.3 Determine the critical cluster size and the nucleation rate in classical nucleation theory (i.e., when $\beta_i/\beta_v = 0$).

19.4 Derive the void distribution function N(m) for the nonequilibrium case with steady-state nucleation.

19.5 At the beginning of irradiation of stainless steel at 500°C with a flux of 10^{14} neutrons cm^{-2} sec^{-1}, use the point-defect balances to compute:

(a) The vacancy and interstitial supersaturations S_v and S_i.

(b) The arrival-rate ratios $(\beta_v/\beta_i)_{disl}$ and $(\beta_i/\beta_v)_{void}$.

(c) The void and loop nucleation rates. For void nucleation, make a rough estimate from Fig. 19.10.

Take point-defect migration and formation energies from problem 19.11. Use a dislocation density of 10^9 cm^{-2}. The steel contains no precipitates and is unstressed. Assume that the combinatorial number for vacancy interstitial recombination is 100. For dislocations, assume $Z_i/Z_v = 1.02$.

(d) How are the results of (b) and (c) changed when the steel contains 4×10^{12} incoherent precipitate particles/cm^3 of radius equal to 100 Å?

19.6 Apply homogeneous nucleation theory (as developed in Sec. 13.8 for fission gases in the fuel) to predict the nucleation time (or fluence) for helium bubbles in the cladding. The nucleation time is defined as the time at which the concentration of di-atoms passes through a maximum. Use the simplified method described in Sec. 13.8 (i.e., invoking Eq. 13.137). The fast-neutron flux is monoenergetic ($E_n = 0.5$ MeV) and is equal to 10^{15} neutrons/cm^{-2} sec^{-1}. Assume a re-solution parameter of 10^{-6} sec^{-1} (problem 17.14) and make reasonable estimates of the other parameters needed in the calculation. Assume that the diffusion coefficient of helium in stainless steel is $\sim 10^{-16}$ cm^2/sec. Compare the fluence Φt_c for helium-bubble nucleation with the observed incubation fluence of $\sim 10^{22}$ neutrons/cm^2 needed for void formation in stainless steel.

19.7 Incorporate re-solution into the theory of loop nucleation by chemical-reaction-rate theory. Use the microscopic picture of re-solution, in which the probability per second of any atom in an interstitial loop being redissolved by radiation is b. Include re-solution as a term of the form nbN_n in the balance on clusters of n interstitials. Assume that the combinatorial numbers z_{ni} and z_{nv} are equal to 10n.

19.8 We wish to determine the equilibrium vacancy concentration C_v in a solid in which a void of radius R and internal gas pressure p is embedded. The system (solid plus void) is subject to hydrostatic (compressive) stress σ. To determine C_v, we use the technique applied to obtain the equilibrium vacancy concentration at a dislocation loop (Sec. 19.5). The Gibbs free energy of a system containing the void and the solid with vacancy concentration C_v and interstitial concentration C_i ($C_vC_i = C_v^{eq}C_i^{eq}$) is given by

$$G = G_0 + g(m_v) + n_v\mu_v + n_i\mu_i$$

where G_0 is the free energy of the stress-free solid without the void; $g(m_v)$ is the reversible work required to create a void containing m_v vacancies against the external pressure (stress) σ with constant internal gas pressure p in the cavity; n_v and n_i are the number of vacancies and of interstitials, respectively, in the matrix of the block; and μ_v and μ_i are the chemical potentials of the point defects when the solid is under stress.

The value of μ_v is equal to $kT \ln (C_v/C_v^{eq})$ where C_v^{eq} is the equilibrium vacancy concentration in the stressed solid:

$$C_v^{eq} = (C_v^{eq})_0 \exp\left(-\frac{\sigma v}{kT}\right)$$

where $(C_v^{eq})_0$ is the equilibrium vacancy concentration in the stress-free solid, and v is the volume change that occurs when one atom is moved from the interior of the matrix to the surface. In the text, v has been identified with the atomic volume Ω, but this neglects the contraction of the lattice around the vacant lattice site. If the volume contraction around the vacant lattice site is ψ_v, then v is $\Omega - \psi_v$.

Determine C_v, the vacancy concentration for which the system described above is in thermodynamic equilibrium. In nonequilibrium situations (such as stress-induced void growth), this concentration is assumed to apply at the surface of the void.

19.9 Removal of point defects by grain boundaries in the solid adds a term (assuming C_v^{eq} is small)

$$Q_v^{gb} = k_{gb}^2 D_v C_v \qquad (1)$$

to the vacancy balance of Eq. 19.134 and a similar term to the interstitial balance. The value of k_{gb}^2 is computed by the following method. The solid far from the grain boundary is assumed to be a homogeneous medium wherein the vacancy-balance equation, Eq. 19.136, applies. For simplicity, recombination is taken into account by defining an effective vacancy-production rate:

$$G' = \nu\Sigma_s\Phi - k_{iv}C_iC_v \qquad (2)$$

Terms involving C_v^{eq} are neglected, and Eq. 19.136 is written as

$$G' = k^2 D_v C_v \qquad (3)$$

where

$$k^2 = Z_v\rho_d + 4\pi RN + 4\pi R_p N_p \qquad (4)$$

Because the grain boundary acts to maintain the equilibrium point-defect concentrations ($C_v^{eq} \simeq 0$ in this calculation), Eq. 3 is not valid close to the grain boundary. Here, the vacancy balance must contain a term representing diffusion of vacancies toward the grain boundary.

(a) Assuming that the concentration drop occurs very close to the grain boundary, the vacancy-diffusion equation in this region can be written for a semiinfinite medium in Cartesian coordinates. By solving this diffusion equation, determine the vacancy concentration profile in the vicinity

of the grain boundary and the vacancy flux to the grain boundary.

(b) Now consider the grain as a sphere of diameter d. Compute the total rate of removal of vacancies by the grain boundary from the flux computed in (a). From this result, determine Q_v^{gb} and hence k_{gb}^2.

19.10 Calculate and plot the relative void-growth rate $\dot{R}/R_0$ for molybdenum (melting point $T_m = 2900°K$) as a function of T/T_m. Use the following parameters:

$\epsilon_v = 190$ kJ/mole
$\epsilon_v^* = 190$ kJ/mole
$\rho_d = 10^{10}$ cm^{-2}
$\Sigma_s = 0.3$ cm^{-1}
$\Phi = 10^{14}$ neutrons cm^{-2} sec^{-1}
$\nu = 100$
$z_{iv} = 30$
$Z_i = 1.02$
$Z_v = 1.0$

Neglect voids as sinks ($N = 0$) and precipitates ($N_p = 0$) and loops as sinks ($\rho_l = 0$). Assume the vacancy diffusion coefficient (in cm^2/sec) is given by $D_v = 10^{13} a_0^2 \exp(-\epsilon_v^*/kT)$. Assume that the voids are 300 Å in radius.

Compare the plot for molybdenum with Fig. 19.18 for stainless steel, taking the melting point of steel as 1750°K.

Would replacement of stainless steel by molybdenum avoid void swelling at the peak cladding temperature of 650°C?

19.11 Show that the recombination properties of coherent precipitates are virtually nil when this type of sink is introduced into a solid containing equilibrium concentrations of vacancies and interstitials (i.e., C_v^{eq} and C_i^{eq}). The migration and formation energies of interstitials and vacancies can be taken as

$\epsilon_i^* = 13$ kJ/mole
$\epsilon_i = 420$ kJ/mole
$\epsilon_v^* = 125$ kJ/mole
$\epsilon_v = 160$ kJ/mole

The temperature is 500°C.

19.12 Because of image dislocations in the voids, Eqs. 19.95 and 19.96 are multiplied by W_v and W_i, respectively. What is the growth law in the absence of recombination and thermal emission (i.e., the analog of Eq. 19.140)? Neglect the terms representing absorption by coherent precipitates.

19.13 (a) In problem 18.1a, replace the condition that the vacancy concentration is maintained at a value C_v^{eq} in the bulk solid by the condition that the only sinks for vacancies in the solid are the dislocations; the dislocation density is ρ_d and the void concentration is N. Determine the void radius as a function of time if the initial radius of all voids was R_0.

(b) Repeat problem 18.1a as stated but with the proviso that each void initially contains j helium atoms.

19.14 (a) Derive a growth law for interstitial loops (analogous to Eq. 19.138 for voids).

(b) Derive the analog of Eq. 19.140 for loops. Assume $N_p = 0$.

(c) Convert the loop-growth law to the time rate of change of the dislocation density of the solid.

(d) Define a dimensionless void size by Eq. 19.146 in which the dislocation density is replaced by ρ_{d0}, the value at the start of the growth period (t_0). By choosing appropriate dimensionless dislocation density and time, convert Eq. 19.140 to a totally dimensionless equation. Integrate this equation with the initial condition $R(t_0) = R_c$. The void and dislocation loop densities, N and N_l, can be assumed constant. For this integration, assume that the dislocation density remains constant at its initial value. Take $Z_i = Z_v$ except where the difference in these two quantities appears.

(e) Convert the result of part c to the same dimensionless quantities used in part d. Numerically integrate the dimensionless void- and loop- (or dislocation density) growth laws starting with the initial conditions:

$R_c = 10$ Å

and the cluster densities:

$N = 10^{14}$ voids/cm^3
$N_l = 10^{15}$ loops/cm^3
$\rho_{d0} = 10^9$ cm^{-2}

Choose the initial loop radius (R_{lc}) such that the number of vacancies in the void nuclei at t_0 is equal to the number of interstitials in the embryo loops.

(f) The incubation period corresponds to a fast-neutron fluence of 10^{22} neutrons/cm^2. Plot the results of the integrations in parts d and e. Compute the swelling at a fluence of 5×10^{22} neutrons/cm^2. This solution is applicable near the peak swelling temperature where recombination has become insignificant and the shrinkage term has not yet become important.

19.15 At some time t_0 during irradiation, nucleation of voids occurs. For $t > t_0$, growth of the voids continues. Assume the growth is diffusion-limited and that the concentrations of vacancies and interstitials at the void surface are zero.

Neglect the changing sink concentrations due to void and loop growth for $t > t_0$, and assume that the concentrations of vacancies and interstitials in the matrix are constant in time.

Calculate the swelling at some time $t > t_0$, neglecting swelling at t_0, for the following two void distributions at t_0.

(a) At t_0 all voids are of the same size, R_0. The total void density is N.

(b) At t_0, the voids are distributed in size according to the function $N_0(R_0)$.

(c) Show that the result of part b reduces to that of part a when the initial void distribution is described by a delta function.

19.16 Consider a segment of a circle of radius $\mathscr{R}$ which has an arc length $\mathscr{L}$ and a chord distance of l.

(a) Prove that $d\mathscr{L}/d\mathscr{A} = 1/\mathscr{R}$, where $\mathscr{A}$ is the area of the segment.

(b) Derive the equation for $d\mathscr{N}/d(1/\mathscr{R})$.

(c) Repeat part a when the ends of the chord are the centers of smaller circles of radius R.

19.17 Solve Eqs. 19.191 to 19.193 using the approximations of Eqs. 19.194 to 19.196.

19.18 In the Hesketh model of irradiation creep by stress-enhanced vacancy-loop collapse, depleted zones with less than $m_c \sim 200$ vacancies remain in the solid as vacancy platelets. For $m < m_c$, the volume per platelet of size m is $m\Omega$. Using the inverse-square distribution function for vacancy platelet (or depleted zone) sizes produced by a neutron collision, compute the swelling due to uncollapsed platelets in the absence of applied stress at a fast fluence of 10^{20} neutrons/cm^2. Assume $\Sigma_s = 0.2$ cm^{-1}, $\Omega = 12$ Å^3, and $\nu = 500$ Frenkel pairs per fast-neutron collision.

19.19 The Lagrangian formulation of the void continuity equation is to be applied to a case of simultaneous growth and nucleation of voids in an irradiated metal. It is assumed that the vacancy and interstitial constants and the void nucleation rate are time-independent.

(a) What is the void distribution function N(R,t) for this model?

(b) What is the swelling as a function of time for specified values of C_v, C_i, and I_{nucl}?